EUMETSAT NWC SAF
SUPPORT TO NOWCASTING AND VERY SHORT RANGE FORECASTING

Validation report of the Convection Product Processors of the NWC/GEO MTG-I Day 1

NWC/CDOP4/MTG/MFT/SCI/VR/Convection, Issue 1, Rev. 0.1

30th May 2025

Applicable to
GEO-CI v.3.0 (NWC-057)
GEO-RDT-CW v.6.0 (NWC-090)

Prepared by METEO-FRANCE Toulouse (MFT) / Direction des Opérations – Prévision Immédiate

REPORT SIGNATURE TABLE

Function	Name	Signature	Date
Prepared by	Météo-France MFT (R. Houël and M. Claudon)	Signed, M. Claudon Signed, R. Houel	*30th May 2025*
Reviewed by	Météo-France MFT (J.-M. Moisselin)	Signed, J.-M. Moisselin	*30th May 2025*
Authorised by	P. Ripodas NWC SAF Project Manager		*30th May 2025*

DOCUMENT CHANGE RECORD

Version	*Date*	*Changes*
1.0.0	*31st March 2025*	*First edition of the document*
1.0.1	*30th May 2025*	*Updated after ORR2 first round*

Table of Contents

1 INTRODUCTION 9

1.1 SCOPE OF THE DOCUMENT 9
1.2 SOFTWARE VERSION IDENTIFICATION 9
1.3 REQUIREMENTS 9
1.4 DEFINITIONS, ACRONYMS AND ABBREVIATIONS 10
1.5 REFERENCES 10
1.5.1 Applicable documents 10
1.5.2 Reference documents 10

2 CONVECTION INITIATION (GEO-CI) VALIDATION 13

2.1 OVERVIEW 13
2.1.1 General objectives of the validation 13
2.1.2 Methodology outline 13
2.2 SPECIFICITIES OF CI VERIFICATIONS 13
2.3 OBJECTIVE VALIDATION 14
2.3.1 Context 14
2.3.2 Data and methods 14
2.3.2.1 *Data* 14
2.3.2.1.1 Case studies overview 14
2.3.2.1.2 Ground truth used for the validation 15
2.3.2.1.3 NWC SAF CI product description and transformation into CI objects 17
2.3.2.2 Method 18
2.3.3 Results 19
2.3.3.1 Radar ground truths 19
2.3.3.2 CI objects 20
2.3.3.3 Statistical scores 21
2.3.3.4 General CI features 22
2.3.3.5 Summary 23
2.3.4 Assumptions and limitations 24
2.4 CASE STUDIES 24
2.4.1 20250311 MTG Case Study 24
2.4.2 20210621 MSG Case Study 25
2.4.3 20210207 MSG-IODC Case study 28
2.4.4 20210914 GOES16 Case Study 30
2.4.5 20250311 GOES18 Case study 32
2.4.6 20210215 HIMAWARI Case Study 32
2.4.7 Synthesis of case studies regarding limitations of CI 34
2.5 MSG/MTG CONTINUITY REGARDING CI 35
2.5.1 20250325 case 35
2.5.2 20250503 case 36
2.5.2.1 Case study description 36
2.5.2.2 Parisian supercell case study 37
2.5.2.3 MTG/MSG CI comparison 38
2.5.2.4 Objectives scores 39
2.5.3 Conclusions about MSG/MTG continuity 40
2.6 END-USERS' FEEDBACKS 40
2.7 CONCLUSION AND COMPLIANCE REQUIREMENTS 41

3 RAPIDLY DEVELOPING THUNDERSTORM – CONVECTION WARNING (GEO-RDT-CW) VALIDATION 43

3.1 OVERVIEW 43
3.2 VALIDATION OF GEN DISCRIMINATION DIAGNOSIS 43
3.2.1 Context 43
3.2.2 Data and methods 43

3.2.3 Results *44*
3.2.4 Conclusion *44*
3.3 THE VALIDATION OF CAL DISCRIMINATION SCHEME 45
3.3.1 Context *45*
3.3.2 Validation and Cases study *45*
3.3.2.1 RDT-CW discrimination using MSG in FDSS mission 45
3.3.2.1.1 Objective validation 45
3.3.2.1.2 Case Study 20180621 over Europe 48
3.3.2.1.3 Case study 20180702 over Europe 50
3.3.2.1.4 Case study 20190419 over Africa 52
3.3.2.2 RDT-CW discrimination using MSG - 9.5E° RapidScan mode 53
3.3.2.2.1 Objective validation 53
3.3.2.2.2 Case study 20180703 over Europe 53
3.3.2.3 RDT-CW discrimination using MSG1 - 41.5°E 55
3.3.2.3.1 Objective validation 55
3.3.2.3.2 20190221 over South-west part of Indian Ocean 56
3.3.2.4 RDT-CW discrimination using MTG-I1 0° 57
3.3.2.4.1 Objective validation of Yes/No convection decision 57
3.3.2.4.2 Test data set in September 2024 57
3.3.2.4.3 20250421 case 58
3.3.2.4.4 Case studies 59
3.3.2.5 RDT-CW applied to GOES16 61
3.3.2.5.1 Objective validation 61
3.3.2.5.2 Case study 20200919 62
3.3.2.5.3 Case study 20201123, Caribbean Sea 64
3.3.2.6 RDT-CW discrimination using Himawari-8 65
3.3.2.6.1 Case study 20210326 over Micronesia region 66
3.3.2.6.2 Case study 20180117 over Indonesia 67
3.3.2.6.3 Case study 20180702 over East Asia 68
3.3.2.7 RDT-CW applied to GOES17 ABI 70
3.3.2.8 RDT-CW applied to GOES-18 ABI 71
3.3.3 Conclusion about RDT-CW convection diagnosis validation *72*
3.4 OVERSHOOTING TOP DETECTION 74
3.4.1 Overview *74*
3.4.2 Objective validation vs expert CHMI OT database *74*
3.4.2.1 Context 74
3.4.2.2 Methodology 74
3.4.2.3 Example 75
3.4.2.4 Results of quantitative comparison 76
3.4.2.5 Synthesis 78
3.4.2.6 MTG-I1/FCI case 78
3.5 LIGHTNING JUMP DIAGNOSIS 81
3.5.1 Case study 20180529 over France and Benelux *81*
3.5.2 Case study 20190809 over France *84*
3.5.3 Applicability to GLM *84*
3.5.4 Synthesis *85*
3.6 FORECAST OF CLOUD SYSTEMS 86
3.7 MSG/MTG CONTINUITY, ADDITIONAL CASES AND MAIN CONCLUSION 89
3.7.1 20250421 over Italy *89*
3.7.2 20250429 over the full disk *90*
3.7.3 Conclusion about MSG/MTG continuity *90*
3.8 END-USERS FEEDBACKS 91
3.9 CONCLUSION AND COMPLIANCE REQUIREMENTS 92

4 CONCLUSION 94

List of Tables and Figures

Table 1: List of Applicable Documents....10

Table 2: List of Referenced Documents....11

Table 3: RDT v2011 Discrimination skill table....44

....16

Figure 1: Table of the various case studies with their sub-domains and the time period considered for the evaluation. Situations without RSS available have been excluded....16

Figure 2: 20220905 SO_France situation. Red polygon represents the study domain. CI pixels, RDT contours and lightning strokes with MSG true color RGB below....16

Figure 3: Example of RadCells and RadTrajs over two hours during the 5th September situation. The table presents the five ground truths categories. "ALL" ground truth is the less strict GT while "Storm_Trigg" is the strictest one. 17

Figure 4: Example of CI validation method. *F*or a given slot CI 30 minutes interval is in green. The beginning of a radar trajectory (blue) match CI signal....17

Figure 5: Example of the transformation of CI pixels into CI objects for the 1440 UTC slot (20220905 SO_France domain). 1) CI pixels to CI clusters 2) CI clusters to CI objects. Note that, in this example, the contours of CI objects correspond to the dominant probability of the CI pixels that compose them (and not the maximum). Observations from the 0.8 µm visible (MSG_RSS) channel are also displayed in the background. TObs corresponds to the estimated time of the *scan* passage over France....18

Figure 6: Diagram illustrating the methodology used to validate CI objects with radar ground truth and contingency table. FA: false Alarm, M:Miss and H:Hit....19

....20

Figure 7: Left: Distribution of RadCells and RadTrajs for each ideal case studies and as a function of GT categories. Right: Distribution of some properties of RadCells objects as a function of their GT categories....20

....21

Figure 8: Distribution of number of CI objects for each ideal case studies and as a function of CI objects maximum probability for both MSG and MSG_PS....21

Figure 9: Distribution of the 20 ideal cases studies scores for both satellites and for the five different ground truths. 23

Figure 10: Presentation of various CI properties considering ALL GT and MSG_RSS considering all ideal case studies. From left to right: 1) CI objects maximum probability distribution for CI objects that overlap or do not overlap the radar GT. 2) Earliness (precocity) of CI objects for well-forecasted radar trajectories. The lead time is calculated by taking the difference between the time of the first RadCell intercepted within a trajectory and the time of the very first CI overlapping this RadCell. 3) Distribution of the number of well-detected trajectories as a function of the number of different CI objects that have overlapped them during their lifetime....24

Figure 11: 20250311 MTG case study over Southern Nigeria from 1340 UTC to 1440 UTC. Sandwich image (VIS+IR) superimposed with v2025 RDT cells (polygons), LI lightning flashes (small dots) and v2025 CI pixels with standard colours (yellow, orange, red and magenta for the 4 levels of probability)....26

Figure 12: NWC SAF CI superimposed on SEVIRI IR10.8µm MSG data. Radar-derived convective objects (32 dBZ contours) are represented with black hatches. Ground truth is represented with red (birth within the next [0;30] minutes time interval) or green contours (birth within the last [0;30] minutes time interval....28

Figure 13: Same as Figure 12 with MSG Rapid scan data (CI product and IR10.8µm)....29

Figure 14: Same as Figure 12 for 20210207 case study and MSG-IODC data....30

Figure 15: 20210914 case study over Guyane. Cloud type superimposed with radar convective objects (radar echos over 32 dBZ, in blue) and v2021 CI product with standard colours (yellow, orange, red and magenta for the 4 levels of probability).....32

Figure 16: 20250311 GOES18 case study over southern Mexico and northern Guatemala from 2050 UTC to 2200 UTC. Visible image superimposed with v2025 RDT cells (polygons), GLM lightning flashes (small dots) and v2025 CI pixels with standard colours (yellow, orange, red and magenta for the 4 levels of probability).....33

Figure 17: Same as Figure 12 applied to 20210215 case study with Himawari data.....34

Figure 18: 20250325 case. Visible imagery and CI output for MSG_FDSS (1415 UTC). Sandwich imagery and CI output for MTG (1420 UTC).....36

Figure 19: 20250325 case. POD and FAR for CI operated with SEVIRI (MSG_PS/MSG_FDSS) or FCI (MTG). « ALL » radar ground truth (ref section 2.3.2.1.2) is used as reference. CI output are transformed into objects before score computation as explained in REF. DBSCAN and buffer parameters are adapted to FCI higher spatial resolution (20 km DBSCAN and 10 km buffering for CI operated with MTG, 30 km DBSCAN and 15 km buffering for MSG).....37

Figure 20: 20250503 case. Sandwich image and CI output at 1000, 1200, 1500 and 1700 UTC. CI operated with MTG/FCI.....38

Figure 21: 20250503 Parisian supercell case. Sandwich imagery, CI output and radar reflectivity composite (above 35 dBZ) at 1110, 1140, 1310 and 1420 UTC. CI operated with MTG/FCI.....39

Figure 24: 20250503 case. POD and FAR for CI operated with SEVIRI (MSG_PS/MSG_FDSS) or FCI (MTG). « ALL » radar ground truth (ref section 2.3.2.1.2) is used as reference. CI output are transformed into objects before score computation as explained in REF. DBSCAN and buffer parameters are adapted to FCI higher spatial resolution (20 km DBSCAN and 10 km buffering for CI operated with MTG/FCI, 30 km DBSCAN and 15 km buffering for MSG/SEVIRI).....41

Figure 25: Objective validation scores and scores ranges for EUMETSAT operational status requirement (see PRD). 43

Figure 26: Early-diagnosis (precocity) of RDT v2011 discrimination for moderate (black) and low (red marks) ground truths.....45

Figure 27: METEORAGE and partners network coverage area taken into account for objective validation.....47

Figure 28: MSG4 case study for 12h00-15h00Z on 20180621. 15h00Z IR image (top left), 30min accumulated METEORAGE impacts around 15h00Z (top right), v2018 (bottom left) and v2021 (bottom right) results for 15h00Z.....49

Figure 29: MSG4 case study for 20180621 15h00Z, zoom on South of France. v2018 (plain blue cells) and GEN (orange dashed) on the left, v2021 on the right. One can note a miss near Bordeaux (top left cloud) in any configuration, and a non-electric cloud system ignored by v2021.....50

Figure 30: MSG4 case study for 20180621 15h00Z, zoom on Central Europe. v2018 (blue cells) and GEN (orange dashed) on the left, v2021 on the *right*. One can note with v2021 the suppression of False Alarms seen by v2018 on the edge of cloud systems.....50

Figure 31: MSG4 case study for 20180621 15h00Z, large view. False Alarms suspicion in the North of the domain with v2018 (left), correctly rejected with v2021 release (right), in an area which is out of lightning coverage area.. 51

Figure 32: MSG4 case study for 20180702. 15h00Z, 16h00Z, 17h00Z and 18h00Z from top left to right bottom. RGB images with METEORAGE impacts, RDT-CW v2021 cells.....52

Figure 33: MSG4 case study for 20180702. Zoom over France, with accumulated Lightning and RDT data from 14h00Z to 18h00Z.....52

Figure 34: MSG4 case study for 20190419 17h00Z over Africa. IR image (top left) with RDT-CW black-dashed cells (top right), with WWLLN data as yellow stars (bottom left), all data overla*id* (bottom right).....53

Figure 35: Zoom of MSG4 case study for 20190419 zoomed. 17h00Z IR image overla*id* with synchronous RDT-CW black-dashed contours and electric data (yellow stars). Left: adding previous 2h WWLLN data (green crosses). Right: adding following 2h of WWLLN data (orange dots).....54

Figure 36: MSG3-RSS case study for 20180703 14h15Z. Top: IR image overla*id* with METEORAGE (magenta circles) and WWLLN strokes (yellow stars). Bottom: same with MSG3-RSS RDT-CW v2018 cells (green) and MSG3-RSS RDT-CW v2021 cells (magenta dashed).....55

Figure 37: Coverage area of GLD360 for Météo-France, and reduced domain (dashed red) to focus on land area....56

Figure 38: MSG1-41.5E case study for 20190221, 18h00Z slot. MSG1-IR image (top left), overla*id* with WWLLN data (top right), with GLD360 data (bottom left, coverage area grey shaded), and with RDT-CW cell contours (black dashed contours).....58

Figure 39: RDT coverage when operated on the Full Disk Scan Service (black line), MTG-LI Field-of-View (orange shading), coverage of the validation of the RDT convective trajectories with MTG-LI flashes as as reference (orange rectangle) and with EUCLID lightning network over Europe as a reference (green rectangle).....60

Figure 40: RDT cell South of Victoria Lake 20241029 13:30. RDT is operated with FCI, LI and WWLLN data. Trajectory in yellow, coldest region of the RDT in dark blue, overshooting top (reversed teardrop in blue/white), forecast outline (up to +1h) in grey. The *gauge* indicates several attributes of RDT.....61

Figure 41: Un-smoothed RDT outlines during the whole Valencia (Spain) MCS trajectory (20241029). RDT operated with FCI, period 1240Z-2350Z.....62

Figure 42: Sub-domain taken into account for replays and objective validation.....63

Figure 43: GOES16 case study for 20200919 at 20h00Z. RGB image (top left) *overlaid* with synchronous GLM (top right, orange dots), with RDT-CW (bottom left, dark shaded contours), and RDT-CW overla*id* with GLM (bottom right).....64

Figure 44: GOES16 case study for 20200919 at 20h00Z, over land. RGB image *overlaid* with synchronous GLM (top left , orange dots), with RDT-CW + next following 30min GLM data (top right, yellow dots), then with cumulated RDT-CW+GLM between 19h50 and 20h30Z (bottom left).....65

Figure 45: GOES16 case study for 20200919 at 20h00Z, over sea. RGB image *overlaid* with 40min cumulated GLM (left, orange/yellow dots), with RDT-CW (right).....65

Figure 46: GOES16 case study for 20201123 at 20h00Z. RGB image superimposed with synchronous GLM (left, red diamonds), and with RDT-CW (right, dark shaded contours). Blue circles are supposed false alarms.....66

Figure 47: GOES16 case study for 20201123 at 20h00Z. RGB and RDT-CW , superimposed with synchronous GLM flashes (red diamonds), following 30 minutes GLM (green diamonds), following 60 minutes (yellow diamond) and 90 minutes (pink diamonds). Misses (red circles) and confirmed early detections (green circles) highlighted.....66

Figure 48: Himawari-8 case study for 06h00Z on 20210326. RGB image with 1h-accumulated WWLLN impacts around 06h00Z *overlaid* with RDT-CW v2021 black dashed contours (top), and with RDT-CW v2018 light green cells (bottom).....68

Figure 49: Himawari-8 case study for 06h00Z on 20180117. RGB image (top left), 30min-accumulated WWLLN impacts around 06h00Z (top right), RDT-CW *overlaid* with WWLLN (bottom right) and all data superimposed (bottom left). *S*upposed false alarms (blue circle), good detections (green circles), misses (red circles) are indicated 69

Figure 50: Himawari-8 case study for 20180702 06h00Z. Northern inner land Est Asian domain. RDT-CW v2021 black dashed contours with WWLLN strokes as yellow stars (top left), same *overlaid* with RGB (top right), RDT-CW v2018 blue cells (bottom right).....70

Figure 51: Himawari-8 case study for 20180702 06h00Z. Southern oceanic Est Asian domain. RDT-CW v2021 black dashed contours with WWLLN strokes as yellow stars (top left), same *overlaid* with RGB (top right), RDT-CW v2018 blue cells (bottom right).....71

Figure 52: GOES17 case study for 20201123. 20h30Z IR image over French Polynesia with RDT-CW Left panel: v2021 cells in magenta, dashed. Right panel: same, *overlaid* with cells from previous version in green, cells detected by both versions appear in green and dashed. Tahiti Island in orange. Absence of electrical activity from GLM-GOES17.....72

Figure 53: GOES17 case study for 20210418. *RGB* image with synchronous WWLLN data (left), and with RDT-CW black dashed contours (*right*).....72

Figure 54: 20250309T220000Z. RDT-CW operated with to GOES18 ABI (colours of the RDT cells depending on the severity), GOES18 GLM (grey circles).....73

Figure 55: Synthesis of POD (X-axis) and FAR (Y-axis) values for several experiences described in previous sub-chapters. Scores with large *domain* over Indian Ocean are not shown. One point for one day.....74

Figure 56: Sandwich image (HRV+IR10.8) with expertised OT for 16h40Z on 20/06/2013 (top). IR image with RDT-MSG cells from 16h30Z slot (+11minutes for exact radiometer date) and OTDs as green triangles (bottom). .77

Figure 57: scores of RDT-CW OTD vs CHMI expert OTs for the two periods 20/06/2013 (top left) , 29/07/2013 (top right) and both day together (bottom).....79

Figure 58: *evolution of several RDT attributes for Valencia case (20241029, X-axis time scale relative to the lif of MCS detected by each RDT). RDT operated (from top to bottom) SEVIRI (FDSS), SEVIRI (RSS), FCI. OT in green triangles, minimum temperature of the cell in blue (Y-Axis), other curve non relevant for the analysis*.....80

Figure 59: box-plot (median, 1st and last quartiles, first and last deciles and outliers) of BTD4 top of RDT cells during Valencia case.....81

Figure 60. 20180529 Case study. Left: cumulated [15h30-16h00] RDT-CW cells *overlaid* with [16h00-16h15] HYDRE product. Right: filter on RDT-CW cells with *LJ* and on hail diagnosis with HYDRE (red pixels for small/medium/large hail classes).....83

Figure 61. 20180529 Case study. RDT-CW cells with *LJ*s (left column) , consecutive ESWD severe weather reports (right column).....84

Figure 62: 20190809 16h-19hZ case study. Accumulated RDT-CW cells with LJ (magenta contours), and accumulated medium/large hail pixels from HYDRE (red pixels).....85

Figure 63: 20210222 case study with GOES16. RDT-CW cell over Bolivia at 15h00Z (left) with 190 paired flashes (here simulated as WWLLN) and OTD (yellow triangle). [06h30-16h00Z] cumulated RDT-CW cells with diagnosis of lightning jump during the period.....86

Figure 64: 20210222 case study with GOES16. [06h30-16h00Z] Time series of GLM-flashes paired with RDT-CW cell over Bolivia. Top: 10 minute flash count and diagnosed LJ with FR>10 (red bars). Middle: 1 minute FR and 2 minutes-average FR. Bottom: LJ algorithm parameters, and "corrected" LJ (red triangles) taking into account new threshold FR>20.....87

Figure 65: v2013 vs v2016 illustration of RDT motion vectors improvement.....88

Figure 66: RDT-CW v2016 advection products (forecast contours in Magenta) from slot 2010-06-28T15:00:00Z (Observed contours in yellow).....89

Figure 67: RDT-CW v2016 advection products (green forecast contours) from previous slots valid for slot 2010-06-28T15:00:00Z (yellow observed contours).....90

Figure 68: RDT operated with MSG/SEVIRI (left) and MTG/FCI (right) over Italy (20250421 at 1300). Style of outlines style depends of life-phase of the cell. Overlay: General RGB image, METEORAGE and LI flashes.....91

1 INTRODUCTION

The EUMETSAT "Satellite Application Facilities" (SAF) are dedicated centres of excellence for processing satellite data, and form an integral part of the distributed EUMETSAT Application Ground Segment (http://www.eumetsat.int). This documentation is provided by the SAF on Support to Nowcasting and Very Short Range Forecasting, NWCSAF. The main objective of NWCSAF is to provide, further develop and maintain software packages to be used for Nowcasting applications of operational meteorologica satellite data by National Meteorological Services. More information can be found at the NWCSAF webpage, http://nwc-saf.eumetsat.int. This document is applicable to the NWCSAF processing package for geostationary meteorological satellites, NWC/GEO.

1.1 SCOPE OF THE DOCUMENT

This document is the convection product validation report applicable to NWC/GEO software package v2025. The accuracies of the convection products (GEO-CI, Convection Initiation and GEO-RDT-CW, Rapidly Developing Thunderstorm Convection Warning) are discussed.

1.2 SOFTWARE VERSION IDENTIFICATION

This document describes the products obtained from the GEO-CI v3.0 (Product Id NWC-057) and from GEO-RDT-CW v6.0 (Product Id NWC-090) implemented in the release 2025 of the NWC/GEO software package.

1.3 REQUIREMENTS

Skill requirements had been expressed in PRD Table for RDT and CI (see [AD.4.]).

- CI:
  - Accuracy: FAR<0.6 POD>0.4 for +30' ahead
  - Target FAR<0.5 POD>0.5 for +30' ahead
  - Optimal: FAR<0.4 POD>0.7 for +30' ahead
- RDT:
  - Accuracy
    - 1) early detection (before first lightning occurrence) 10%
    - 2) 30 minutes after first lightning occurrence 30%
    - 3) overall thunderstorm detection skill 50%
  - Target
    - 1) early detection (before first lightning occurrence) 25%
    - 2) 30 minutes after first lightning occurrence 50%
    - 3) overall thunderstorm detection skill 70%
  - Optimal
    - 1) early detection (before first lightning occurrence) 50%
    - 2) 30 minutes after first lightning occurrence 75%
    - 3) overall thunderstorm detection skill 90%

1.4 DEFINITIONS, ACRONYMS AND ABBREVIATIONS

See [AD.5.]for a complete list of acronym for the NWC SAF project.

1.5 REFERENCES

1.5.1 Applicable documents

The following documents, of the exact issue shown, form part of this document to the extent specified herein. Applicable documents are those referenced in the Contract or approved by the Approval Authority. They are referenced in this document in the form [AD.X]

For dated references, subsequent amendments to, or revisions of, any of these publications do not apply. For undated references, the current edition of the document referred applies.

Current documentation can be found at the NWC SAF Helpdesk web: http://nwc-saf.eumetsat.int.

Table 1: List of Applicable Documents

Ref	*Title*	*Code*	*Vers*	*Date*
[AD.1.]	*Proposal for the Fourth Continuous Development and operation Phase (CDOP) march 2022 – February 2027*	*/NWC/SAF/AEMET/MGT/ CDOP4Proposal*	*1.0*	*12/03/2021*
[AD.2.]	*Project Plan for the NWCSAF CDOP4 phase*	*NWC/CDOP4/SAF/AEMET/MGT/ PP*	*3.0.0*	*21/10/2024*
[AD.3.]	*Configuration Management Plan for the NWCSAF*	*NWC/CDOP4/SAF/AEMET/MGT/ CMP*	*1.2.0*	*29/3/2024*
[AD.4.]	*NWCSAF Product Requirement Document*	*NWC/CDOP4/SAF/AEMET/MGT/ PRD*	*3.0*	*21/102024*
[AD.5.]	*The Nowcasting SAF glossary*	*NWC/CDOP4/SAF/AEMET/ MGT/GLO*	*1.0.0*	*31/10/2023*
[AD.6.]	*System and Components Requirements Document for the NWC/GEO MTG-I day-1*	*NWC/CDOP2/MTG/AEMET/SW/ SCRD*	*1.3.1*	*31/3/2025*
[AD.7.]	*Interface Control Document for Internal and External Interfaces of the NWC/GEO*	*NWC/CDOP3/MTG/AEMET/SW/ICD/1*	*1.4.0*	*31/3/2025*
[AD.8.]	*Interface Control Document for the NWCLIB of the NWC/GEO*	*NWC/CDOP2/MTG/AEMET/SW/ICD/2*	*1.4.0*	*31/3/2025*
[AD.9.]	*Data Output Format for the NWC/GEO*	*NWC/CDOP2/MTG/AEMET/SW/DOF*	*1.4.0*	*31/3/2025*
[AD.10.]	*Architecture Design Document for the NWC/GEO v2025*	*NWC/CDO2/MTG/AEMET/SW/ ACDD*	*1.3.0*	*31/3/2025*
[AD.11.]	*User Manual for the tools of the NWC/GEO*	*NWC/CDOP3/MTG/AEMET/SCI/ UM/Tools*	*1.2.0*	*31/3/2025*

1.5.2 Reference documents

The reference documents contain useful information related to the subject of the project. These reference documents complement the applicable ones, and can be looked up to enhance the information included in this document if it is desired. They are referenced in this document in the form [RD.X]

For dated references, subsequent amendments to, or revisions of, any of these publications do not apply. For undated references, the current edition of the document referred applies

Current documentation can be found at the NWC SAF Helpdesk web: http://nwc-saf.eumetsat.int.

Table 2: List of Referenced Documents

Ref	Title	Code	Vers	Date
[RD.1.]	Best Practice Document, 2013, for EUMETSAT Convection Working Group, Eds J.Mecikalski, K. Bedka and M. König »	Available on CWG Website		2013
[RD.2.]	Scientific Report on verification of RDT forecast	NWC/CDOP3/GEO/ MFT/SCI/RP/01	1.2	5/9/2018
[RD.3.]	Lenk, S., Senf, F., Deneke, H., Final Report on the Associated Scientist Activity for the Validation of the Convection Initiation (CI) product of NWCSAF v2018	NWC/CDOP3/SAF/MF-PI/SCI/RP/ CI_Improv_Tropos available on NWCSAF Website	1.0	November 2018
[RD.4.]	Karagiannidis, A., 2016, Final Report on Visiting Scientist Activity for the validation and improvement of the Convection Initiation (CI) product of NWC SAF v2016 and v2018, Visiting Scientist Activity followed in Nowcasting Department of Météo France, Toulouse, France Period June-December 2016 »	available on NWCSAF Website		2016
[RD.5.]	Scientific Report on Extended Validation of RDT	SAF/NWC/CDOP/MFT/ SCI/RP/1		7th December 2012
[RD.6.]	Haberlie, A. M., Ashley, W., S., Pingel, T. J., 2014, The effect of urbanisation on the climatology of thunderstorm initiation, QJRMS, https://doi.org/10.1002/qj.2499			2014
[RD.7.]	Walker, J. R., W. M. MacKenzie, Jr., J. R. Mecikalski, and C. P. Jewett, 2012: An enhanced geostationary satellite-based convective initiation algorithm for 0/2-h nowcasting with object tracking. J. Appl. Meteor. Climatol., 51, 1931-1949"			2012
[RD.8.]	Autonès, F., Moisselin, J.-M., **2019**, Validation Report for Convection Products, available on http://nwc-saf.eumetsat.int	NWC/CDOP3/GEO/ MFT/SCI/VR/Convection	1.0	2019
[RD.9.]	https://www.vaisala.com/fr/products/data-subscriptions-and-reports/data-sets/gld360			
[RD.10.]	Brenguier, J.-L., Bouttier, F., Moisselin, J.-M., 2015, Les nouveaux services météorologiques pour l'aviation, La Météorologie 91, Novembre 2015			2015
[RD.11.]	Moisselin, J.-M., 2017, Scientific report on on future verification of CI product, available on http://nwc-saf.eumetsat.int	NWC/CDOP2/GEO/ MFT/SCI/RP/08		2017
[RD.12.]	Setvák, M., Radová, M., Kaňák, J., Valachová, M., Bedka, K, Šťástka1, J., Novák, P., Kyznarová, H., 2014, Comparison of the MSG 2.5-minute rapid scan data and products derived from these, with radar and lightning observations, 2014 EUMETSAT Meteorological Satellite Conference, 22 - 26 September 2014, Geneva, Switzerland			2014
[RD.13.]	Celano, M., Campana, V., 2025, Analysis of the first stages of supercell storms occurred in Northern Italy in July 2023 with NWCSAF Convection Initiation and Rapid Developing Thunderstorms combined with radar and lightning data	NWCSAF Users Workshop February 2025		2025
[RD.14.]	Autonès, F., Moisselin, J.-M., Claudon M., 2022, Validation report of the Convection Products Processors of the NWC/GEO	NWC/CDOP3/GEO/ MFT/SCI/VR/Convection		2022
[RD.15.]	Towards a better characterization of the severity of thunderstorms by improving Cloud Top Features detection	NWC-CDOP4-GEO-MFT-VSA-CloudTopFeatures_v3.0	3.0	April 2025

Ref	Title	Code	Vers	Date
[RD.16.]	Expert Workshop on selected NWC SAF products with a focus on applications to convective storm forecasting, 29/11-1/12/202			12/12/2022

2 CONVECTION INITIATION (GEO-CI) VALIDATION

2.1 OVERVIEW

2.1.1 General objectives of the validation

The main objective of this section is to document Convection Initiation product accuracy. The method used has to compare POD and FAR scores to the threshold accuracies listed in the NWCSAF product requirements document [AD.4] : FAR<0.6, POD>0.4

2.1.2 Methodology outline

CI product verification is performed with both objective scores and case studies. The ground truth in objective scores is a radar-based product in object mode, providing key information about the birth of and the lightning activity of the cells. In addition, a new CI object approach is used for this validation.

The objective validation study focused on seventeen days with convection over France from August to October 2022 using both full disk and rapid scan service of MSG. The verification is rather strict depending on the definition of the various ground truths derived from a Météo-France radar-based product.

2.2 SPECIFICITIES OF CI VERIFICATIONS

The verification method will have also a high impact on scores (see [RD.11.])

- Case study for convective days or large period,
- Double penalty issue taken into account or not,
- Threshold above which CI is verified (0-25%, 25-50%, 50-75%, 75-100%),
- Day verification or day and night verification,
- Object or pixel-based verification,
- Verification of tracked clouds or verification of all clouds,
- CI below cirrus taken into account or not,
- Use of a rapid scan imager or not,

For example in [RD.7] the POD varies from 0.32 to 0.72 depending on the way CI is verified.

Additionally high FAR are often attributed to difficulties inherent to CI problem. For example one CI object can dominate all other CI objects in the surrounding, as low-level convergence and upper-level divergence suppress other up-drafts. Furthermore, not all clouds with cooling tops develop into thunderstorms (even less so on their first surge). Very large FAR values can be found in literature.

2.3 OBJECTIVE VALIDATION

2.3.1 Context

Tropos (Leibniz Institute for Tropospheric Research) performed in Autumn 2018 a verification of CI v2018 in the framework of an Associated Scientist activity [RD.3] with German radar data. On a few case studies, they obtained low CI performance scores with a POD between 20 and 50% and with high FARs (>60%). Following this study, they suggested creating CI objects from CI pixels to reduce false alarms.

The v2021 CI version validation was performed with radar-based convective objects over several territories [RD.14]. One of the main improvement of this version was the correction of the imbalance between the four different classes of CI probability. Using CI pixels, spatial tolerance and a rather strict ground truth, this work resulted in lower scores but highlighted the conditions in which the CI is more accurate. Indeed, day-time isolated convection with clear sky and without strong movement field are the best conditions for CI to operate. These ideal cases are the ones where the CI product should bring value to the forecasters.

In parallel, Arpae Emilia-Romagna and Arpae Piemonte evaluated the CI (v2021) for an early diagnosis of the initial phase of some supercells in July 2023 over North-Italy [RD.13]. They focused on cases studies without pre-existing convection taking radar data with spatial tolerance as ground truth. They showed a POD of 64% (with sometimes an anticipation of 30-60 minutes) in combination with numerous false alarms.

The CI product is validated by MFT in the continuity of the previous works but introducing some new approaches such as the CI-objects, the use of multiple ground truths radar-based convective objects and a focus on ideal cases studies. This new objective validation is performed with CI v2021. No major changes have been made in the CI algorithm between v2021 and v2025 that could influence the results of this objective validation. However, MTG case study in the next section is performed with the CI v2025.

Following sections describe this new fully object-based validation of the CI product.

2.3.2 Data and methods

The objective validation study focused on 20 ideal situations with convection over France in different sub domains spanning 17 days from August 18th to October 23th 2022. CI objects are considered instead of CI pixels and the various ground truths are derived from a Météo-France radar-based product. The verification is rather strict with only 30 minutes for a CI validation.

2.3.2.1 Data

2.3.2.1.1 Case studies overview

20 ideal cases situations spanning 17 days from August 18th to October 23th 2022 are used for the objective validation. As a reminder, ideal cases studies for the CI are day-time, clear-sky situations with isolated and unorganized convection and without strong movement field. Each case is defined by a domain and a period of study (Figure 1). All domains are included in the radar coverage area.

All these ideal case studies have been manually selected to represent a range of convective situations for the summer 2022 over France. Most of the cases are associated with convection with diurnal or relief evolution, but a few are associated with more dynamic situations with the passage of a low-pressure system, as in the case of September 2 or October 23. For example, Figure 2 shows the study domain and the evolution of convection for the September 5th SO_France situation. Between 1300Z

and 1600Z convection developed from clear satellite scene (almost no high altitude cirrus clouds) to multiple storms with high lightning activity. All CI pixels and radar ground truth inside the domains are taken into account for the validation of each situation.

Day	Name Domain	Slot Start Score	Slot End Score	
~~20220816~~	~~SE_France~~	~~1000~~	~~1400~~	No RSS
20220818	SE_France	1100	1400	
20220822	Corse_France	1000	1200	
20220824	Pyrenees_France	1300	1500	
20220825	SudOuest_France	1000	1500	
20220826	SudEst_France	1000	1500	
20220826	Corse_France	1200	1500	
20220828	ReliefE_France	1100	1700	
20220828	Pyrenees_France	1200	1500	
20220830	SudE_France	1000	1300	
20220831	NordE_France	1200	1400	
20220901	MC_France	1100	1500	
20220902	O_France	0900	1200	
20220903	MC_France	1000	1400	
20220905	CentreFrance	1000	1500	
20220905	SO_France	1300	1600	
20220906	CO_France	1200	1500	
~~20220914~~	~~SO_France~~	~~1200~~	~~1500~~	No RSS
20221008	SO_France	1000	1500	
20221009	Pyrenees_France	1100	1400	
~~20221012~~	~~MC_France~~	~~900~~	~~1400~~	No RSS
20221021	NO_France	1400	1700	
20221023	NO_France	1000	1400	

Figure 1: Table of the various case studies with their sub-domains and the time period considered for the evaluation. Situations without RSS available have been excluded.

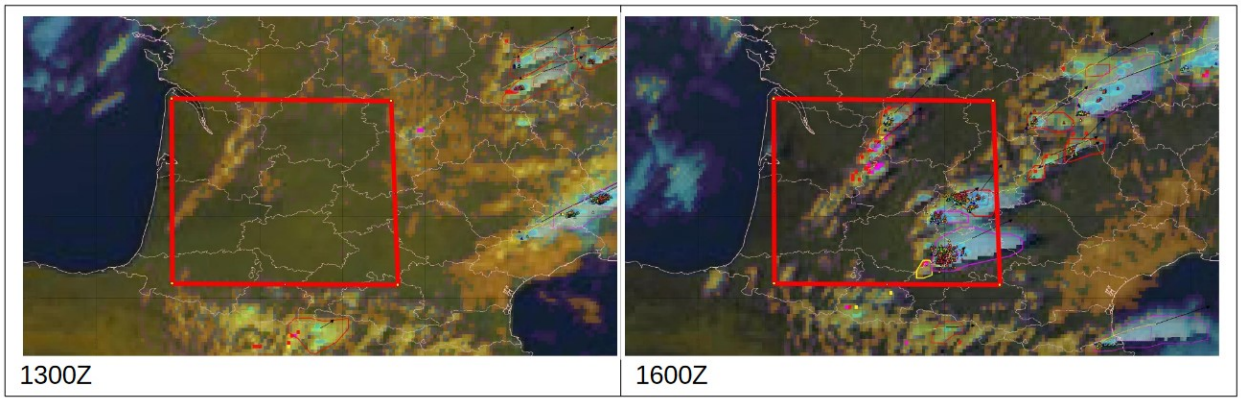

Figure 2: 20220905 SO_France situation. Red polygon represents the study domain. CI pixels, RDT contours and lightning strokes with MSG true color RGB below.

2.3.2.1.2 Ground truth used for the validation

Convective initiation is most of the time defined as the first occurrence of a radar precipitation echo of intensity reaching or exceeding 30 to 40 dBZ (RD.1), most often 35 dBZ (RD.7). Validation of CI follows this common approach, rather on the lower values of the various thresholds (32 dBZ outline with a condition for reaching at least the 35 dBZ), as explained hereafter

Météo-France produces routinely radar-based convective objects (RadCells) at the radar temporal frequency (5 minutes) and at the radar spatial resolution (1 km) over France. The radar objects

delineate convective cells with an outline at 32 dBZ radar echo. Thus, the product includes cell tracking, so the identification of trajectories of RadCells (RadTrajs) and lightning activity. All RadCells with a maximum reflectivity (Zmax) under 35 dBZ are discarded and all trajectories with a duration of less than 5 minutes (only two RadCells in the trajectory) are ignored.

Based on these RadCells and RadTrajs, we built five different ground truths (GTs), with various degrees of strictness, that are supposed to represent different phase of the convection. The figure 3 presents the five GT categories and illustrates the classification with an example. The two most representative GTs for the CI are *Storm_Trigg* and *Storm_30min*, since we want the CI to give signals for storm trajectories in their initial phase and not throughout their lifetime.

With *Storm_30min*, we consider only the RadCells in the first 30 min of a storm trajectory as the reference for the validation of a CI. Some of these GTs overlap by design, *ALL* GT includes all the other GTs, while *Storm* and *NoStorm* GTs have no RadCells in common. *Storm_30min* is included in *Storm* and *Storm_Trigg* is itself included in *Storm_30min*. With this classification, a CI object can be validated by all, some or none of these GTs.

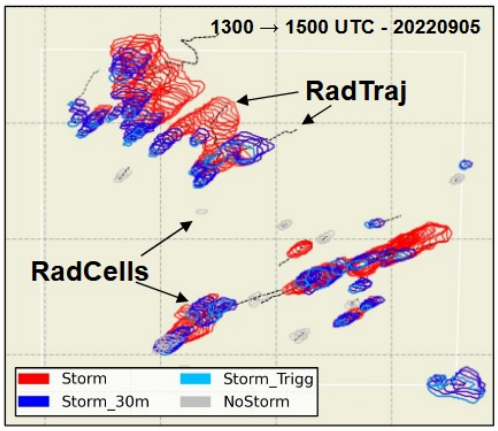

GT name	RadTrajectories	RadCells
Storm_Trigg	At least 1 lightning paired	**First** RadCell *
Storm_30m	At least 1 lightning paired	RadCells in the **first 30 min***
Storm	At least 1 lightning paired	All RadCells *
NoStorm	No lightning	All RadCells *
All	All trajectories	All RadCells*

*Of their respective RadTraj

Figure 3: Example of RadCells and RadTrajs over two hours during the 5th September situation. The table presents the five ground truths categories. "ALL" ground truth is the less strict GT while "Storm_Trigg" is the strictest one.

Validation method is also illustrated through a very simple example in the figure hereafter. In that example the CI signal (an interval 30 minutes ahead the current slot) matches with the beginning of a radar trajectory: it's a hit for the ground truth "Storm_Trigg" (and all the other ones).

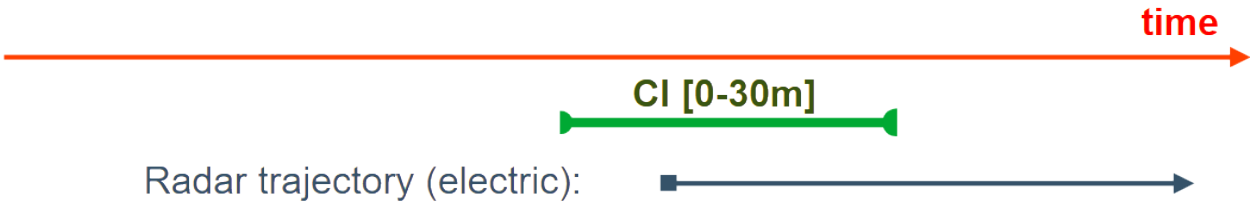

Figure 4: Example of CI validation method. For a given slot CI 30 minutes interval is in green. The beginning of a radar trajectory (blue) match CI signal.

2.3.2.1.3 NWC SAF CI product description and transformation into CI objects

It is operated with data from MSG Primary service mode (MSG4 satellite also called MSG_FDSS for MSG Full Disk Scan Service or MSG_PS) and from MSG Rapid Scan Service mode (MSG_RSS, MSG3 satellite). CI is operated in nominal configuration with v2021. Finally, CI is produced over quite a small domain covering France and the French meteorological radar coverage.

The product is originally in the form of pixels associated with a certain CI probability. Following advices from previous works to reduce false alarms, the pixels are transformed into CI Objects. The aim of this object approach is also to improve the visualization of convection initiation areas for users by representing elliptical regions that encompass neighbouring CI pixels.

For each satellite slot, CI pixels are grouped into clusters using a DBSCAN (Density-Based Spatial Clustering of Applications with Noise) algorithm. The maximum distance criterion for two pixels to belong to the same cluster is set at 30 km. In practice, pixels within the same cluster may have distances greater than 30 km if they have numerous neighbouring pixels in common. Polygons are then constructed from the contours formed by pixels in the same cluster, and a buffer of 15 km is applied to artificially increase the surface area of CI objects. These values were chosen after several visual inspections of ideal study cases and confirmed after a sensitivity study. The addition of the buffer results in more ellipsoidal objects, which better illustrate convection initiation areas. It also extends the CI signal into a region around the CI pixels, reducing uncertainties about 1) the spatial co-localization of the CI (satellite) signal and radar ground truth and 2) the advection of CI pixels thanks to the retrieved motion field. Figure 5 shows how a dozens of CI pixels are transformed into five distinct CI objects.

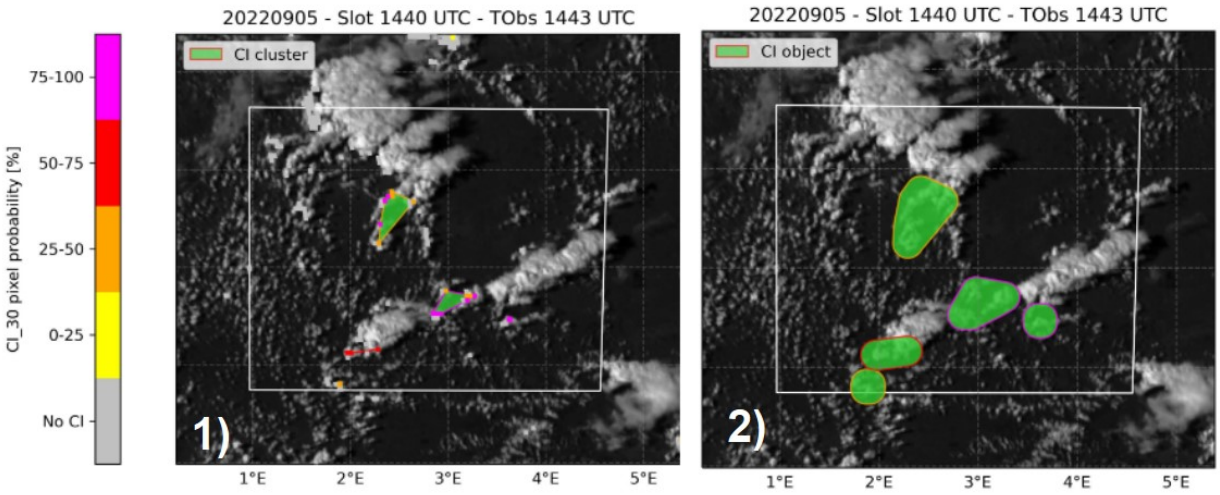

Figure 5: Example of the transformation of CI pixels into CI objects for the 1440 UTC slot (20220905 SO_France domain). 1) CI pixels to CI clusters 2) CI clusters to CI objects. Note that, in this example, the contours of CI objects correspond to the dominant probability of the CI pixels that compose them (and not the maximum). Observations from the 0.8 µm visible (MSG_RSS) channel are also displayed in the background. TObs corresponds to the estimated time of the scan passage over France.

CI objects are characterized by their contours, their identifiers and their maximum probability, which is associated with the maximum probability within CI objects. These CI objects, constructed from CI pixels, are therefore used in this validation as convection initiation areas for the next 30 minutes and the objects that need to be validated by the ground truth.

2.3.2.2 Method

As a reminder, the CI object defined at time T gives a convection initiation area that is valid for the following 30 minutes. To evaluate this product, one needs to check whether radar objects (RadCells) are actually observed in the area defined by the CI objects and within the given time (T+30 minutes).

To achieve this, one searchs for a spatial overlap (YES/NO) between the CI and RadTraj objects (through the RadCells contours that compose them). To ensure a balanced result, RadTraj are used to count missing events and good detections.

Figure 9 illustrates the methodology with one slot. In this case, two CI objects are observed and 4 different RadTrajs (emerging or already existing) are recorded in the next 30 minutes. After looking for spatial overlap, one CI object appeared to be a false alarm while the other CI gave two hits. Two RadTrajs are not detected (2 misses).

In order to objectively compare the CI product's performance in relation to different ground truths, scores are calculated thanks to a contingency table. The metrics most often used are POD and FAR Another indicator, the CSI (Critical Score Index) is also used.

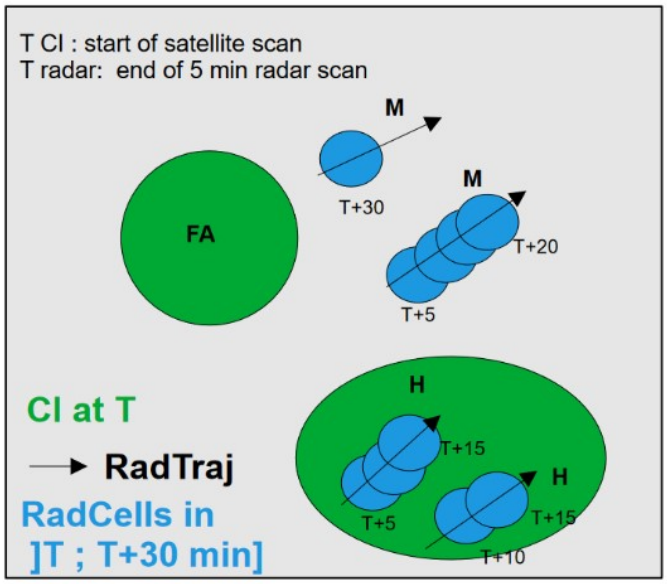

		CI Object	
		Yes	No
RadTraj	Yes	Hit	Miss
	No	False Alarm	X

Figure 6: Diagram illustrating the methodology used to validate CI objects with radar ground truth and contingency table. FA: false Alarm, M:Miss and H:Hit.

A few additional points to consider:

- To ensure better temporal correlation between satellite and radar observations, the reference times of the satellite slots have been shifted by 10 minutes for MSG_PS and 3 minutes for MSG_RSS to optimize the timing of the scan's passage over France (TObs in Figure 5).
- Scores are calculated per slot and/or per case study independently and there is no relation between CI objects from successive slots.
- A single RadTraj can be used to test the overlap with the CIs of several successive slots (as long as it is within the 30 min window) and can give multiple misses and/or multiple hits.

- CI objects maximum probability attribute is not used in this validation → Binary yes/no overlap validation.

2.3.3 Results

2.3.3.1 Radar ground truths

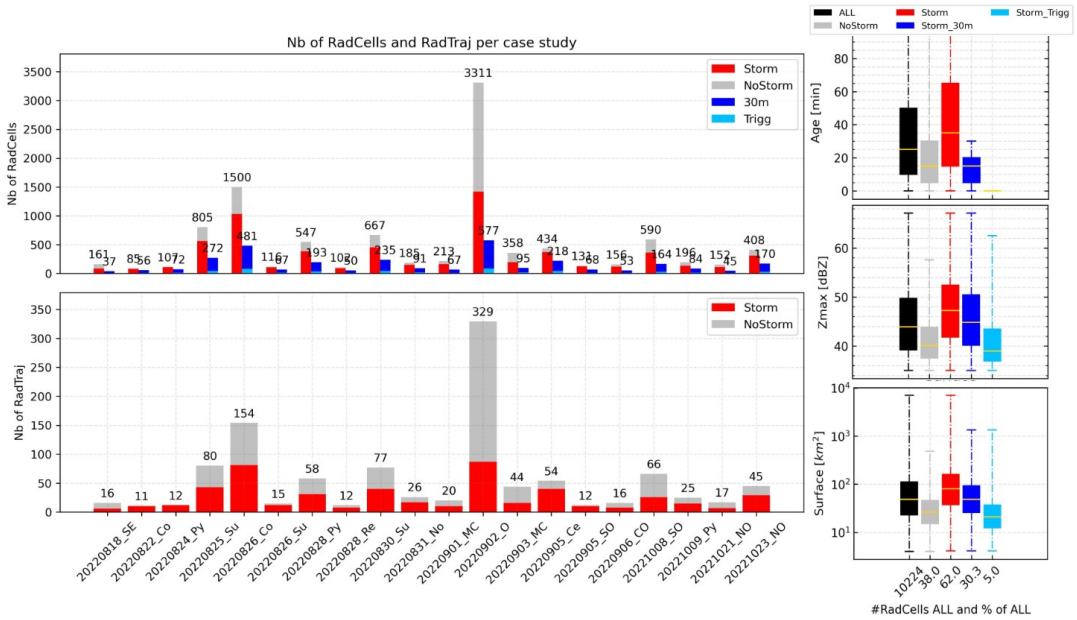

Figure 7: Left: Distribution of RadCells and RadTrajs for each ideal case studies and as a function of GT categories. Right: Distribution of some properties of RadCells objects as a function of their GT categories.

Over the 20 ideal cases studies, 1089 RadTraj have been observed with 47% of them associated to electrical activity. These trajectories are composed of 10 224 RadCells. The distribution of RadCells and RadTraj are quite unequal depending on the different situations as shown in Figure 7. The Figure also shows some properties of the different ground truths:

1) Looking at the distribution of object's age in their trajectory, maximum reflectivity and surface area of the different GTs, we can see that *NoStorm* GTs are well associated with lower reflectivity, shorter lifetimes and smaller surface than *Storm* GTs. Logically, we also see an increase in maximum reflectivity (from under 40 dBZ to over 45 dBZ), age and surface area as we advance from *Storm_Trigg* to *Storm_30min* and then *Storm* categories. The rapid evolution (less than 30 minutes) of surfaces and maximum reflectivities between *Storm_Trigg* and *Storm_30min* clearly shows the explosive nature of the convection, and indicates that these two GTs can be attributed to emerging convection.

2) *Storm_30min* GT represents about 30% of all GTs while *Storm_Trigg* only 5%, illustrating the scarcity of these GTs purely associated with emerging convection from the radar perspective.

2.3.3.2 CI objects

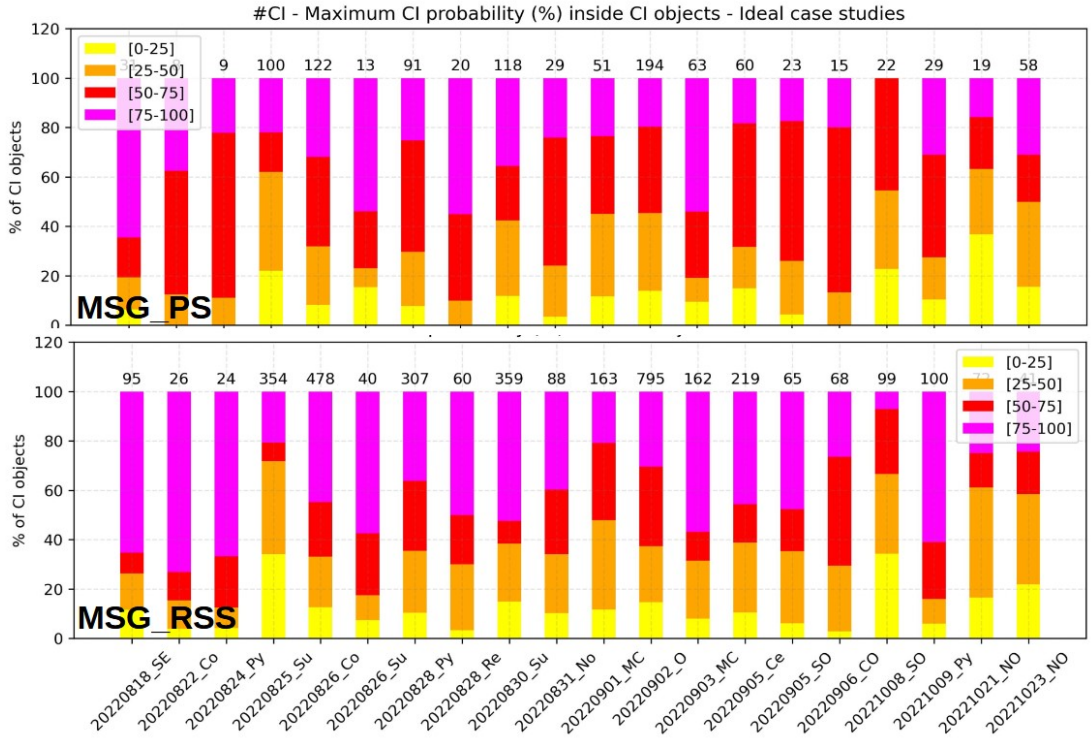

Figure 8: Distribution of number of CI objects for each ideal case studies and as a function of CI objects maximum probability for both MSG and MSG_PS.

Over the 20 ideal cases studies, with MSG_RSS satellite, 21 061 CI pixels were observed thanks to 822 satellite slots analysed (5 min duration). The CI-pixels-to-objects methodology gave 3615 CI objects with an average of 4.4 CI per slot and 5.8 pixels per CI object. For MSG_PS satellite, 289 slots were analysed (15 min duration) giving 4859 CI pixels, 1075 CI objects with an average of 3.7 CI per slot and 4.5 pixels per CI object.

The distribution of these CI objects with the different case studies is shown on Figure 8. As can be seen, the highest probabilities are logically favoured due to the selection of the maximum probabilities within objects as attribute. However, we note that MSG_RSS tends to have far more CI objects with very high probabilities [75-100%] than MSG_PS, as illustrated by 20220822_CO case.

This inter-satellite comparison shows that, in general, MSG_RSS produces more CI objects, which are composed of more CI pixels and associated with higher probabilities. Given the similarity of the channels used by the two satellites, the only difference in the CI algorithm lies in the analysis of certain BT and BTD trends. The better temporal resolution of MSG_RSS allows these trends to be recalculated every 5 minutes, thus increasing the probability of detecting the cloud cooling phase and of passing certain thresholds in the CI decision tree.

2.3.3.3 Statistical scores

As shown in Figure 7 and Figure 8, the 20220902_O case study represents almost one third of all the ground truth database and 22% of all the CI objects for MSG_RSS. To ensure that global scores are not too influenced by a particular situation, they are computed for each case study independently. As an example, the 20220905_SO case study, with MSG_RSS, gave quite good scores with a POD of 0.75, a FAR of 0.25 and a CSI of 0.6 taking *Storm_30min* as the ground truth. In contrast, the

20220902_O case study resulted in lower scores with a POD of 0.57 a FAR of 0.48 and a CSI of 0.38 using the same ground truth.

Figure 9 shows the distribution of daily scores for the 20 ideal case studies for MSG_PS and MSG_RSS. One of the first important results is the better overall performance of MSG_RSS compared to MSG_PS. For all ground truths, PODs are better and FARs are the same or slightly lower. This shows that the greater (compared with MSG_PS, see section 2.3.3.2) number of CI pixels and therefore number of CI objects observed for MSG_RSS is generally associated with good detections.

Focusing now on the MSG_RSS results, we can see that the median POD is just over 0.5, regardless of the ground truth. On the other hand, the FAR varies greatly according to ground truth, with a FAR of 0.15 for the *ALL* category and up to 0.65 for *No_Storm* and *Storm_Trigg* GTs. This disparity is also reflected in the CSI.

The results obtained with the different ground truths inform us several things:

- *ALL* GT gives better scores than *Storm*, indicating that the CI also anticipates certain non-storm trajectories (but with Zmax > 35 dBZ).
- The fact that the PODs are very similar between GT categories shows that if a trajectory overlaps with a CI, this is generally at the very beginning of the trajectory's life. However, the differences in FAR indicate that many CI objects continue to overlap on the already developed trajectory throughout its lifetime. For GT *ALL*, these CI objects give well-detected trajectories, whereas for *Storm_30min* or *Storm_Trigg* these CI objects are considered as false alarms.
- The CI predicts some starts but is also triggered by more mature stages of convection and shows a strong temporal persistence of the signal.

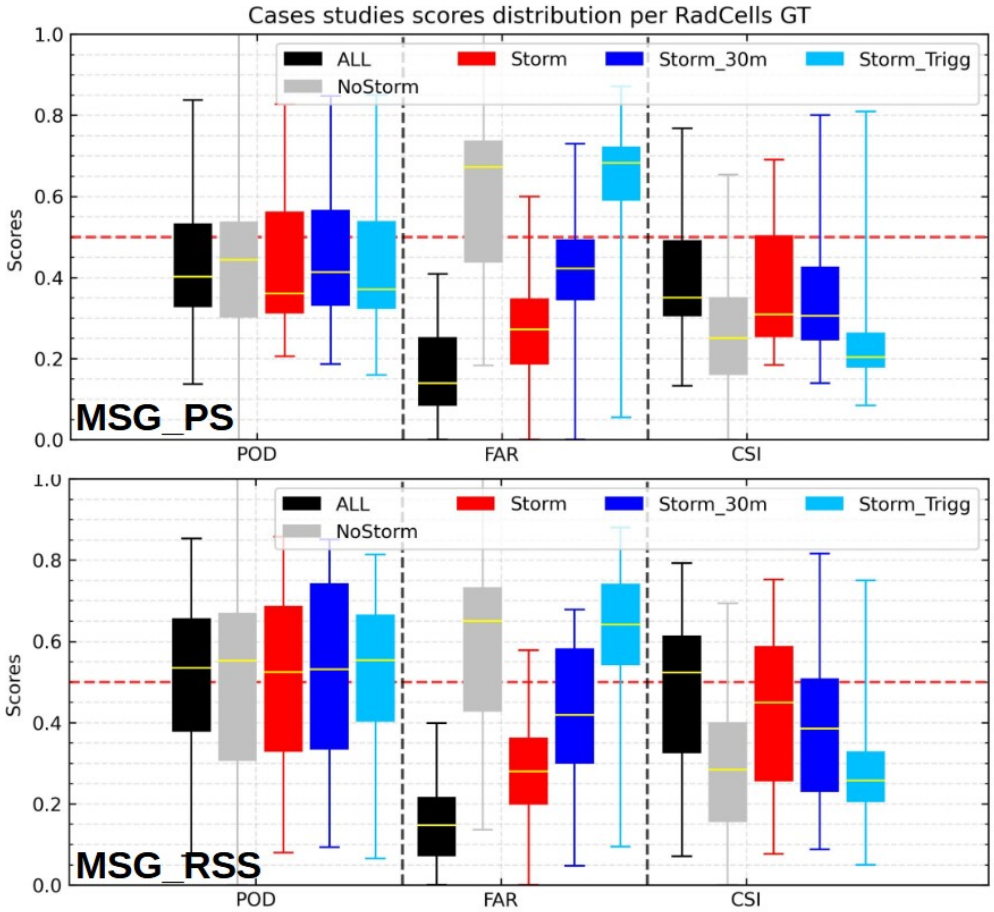

Figure 9: Distribution of the 20 ideal cases studies scores for both satellites and for the five different ground truths.

2.3.3.4 General CI features

Figure 10 shows various CI properties extracted from the objective validation of ideal case studies with *ALL* ground truth and with MSG_RSS. Here are the key points that can be learned from this Figure:

- As expected, the [75-100%] maximum probability category is the most common in the population of CI objects, representing almost 40%. The [50-75%], [25-50%] and [0-25%] categories account for 20%, 25% and 15% of CI objects respectively. As for the ratio of good detections by CI probability category, we note that the higher categories ([50-75%] and [75-100%]) have excellent ratios (75% and 85%), matching their respective probability levels. On the other hand, for the lower categories, the ratio of good detections is too high and does not correspond to their probability level (for example, there is 54% good detection for the [0-25%] probability category).
- Among the 1089 RadTrajs in the *ALL* ground truth, 918 were intercepted by at least one CI object. More than 60% of these trajectories were predicted/overlapped by a CI object, with a lead time of 20 to 30 minutes. In contrast, slightly less than 20% of trajectories had a lead time of 5 to 10 minutes. These results are positive, given that among all the trajectories well anticipated by CI, 87% overlap a CI object at the time of their birth (first RadCell of a RadTraj, not shown). No relationship could be established between CI maximum probability categories and CI precocity.

- Out of the 918 RadTraj intercepted by CI objects, just under 20% were overlapped by maximum 3 CI objects during their lifetime. 50% were overlapped by more than 5 CI and 20% by more than 10 CI. This shows that some trajectories had continually one or more CI objects superimposed throughout their lifetime, and confirms the observations made in the previous section 2.3.3.3 that the CI showed a strong temporal persistence. The results are quite different with MSG_PS (not shown), with far fewer objects superimposed on the same trajectory, due to the satellite's 3 times lower frequency.

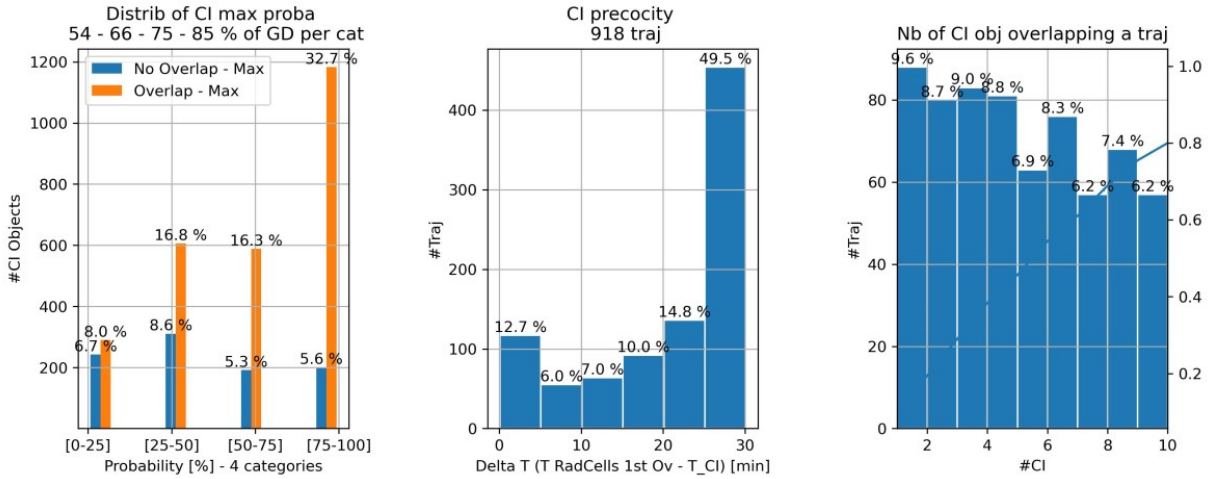

Figure 10: Presentation of various CI properties considering ALL GT and MSG_RSS considering all ideal case studies. From left to right: 1) CI objects maximum probability distribution for CI objects that overlap or do not overlap the radar GT. 2) Earliness (precocity) of CI objects for well-forecasted radar trajectories. The lead time is calculated by taking the difference between the time of the first RadCell intercepted within a trajectory and the time of the very first CI overlapping this RadCell. 3) Distribution of the number of well-detected trajectories as a function of the number of different CI objects that have overlapped them during their lifetime.

To resume, statistically, the CI gives signal with a rather high probability [75-100%] in a region where a radar trajectory with reflectivities > 35 dBZ is likely to initiate within the next 20 to 30 minutes. This CI signal is then expected to continue for the following satellite slots.

2.3.3.5 Summary

As it was already highlighted in the previous CI version, false alarms in CI are the main issue. In this objective validation, thanks to the transformation of CI pixels into CI objects and to the focus on ideal case studies, false alarms are significantly reduced without degrading POD. However, results are highly dependent on the type of ground truth considered (median FAR varies between 0.15 and 0.65).

The best scores are obtained by taking entire radar trajectories as GTs, indicating that the CI product is not only triggered by the initial phase of the convection, but also by more advanced stages. The median POD of 0.5 shows that there is still room for improvement to make CI diagnosis more sensitive to convection initiation phases.

This validation highlighted CI properties such as its high temporal persistence and its 20-30 minutes anticipation of the majority of radar trajectories. This work has also shown that MSG_RSS yields better scores due to his higher scan frequency.

2.3.4 Assumptions and limitations

As a reminder, this objective validation is performed only over small domains for ideal cases studies, meaning day-time and clear-sky situations with isolated and unorganized convection and without strong movement field. In case of high altitude thin cirrus clouds or night-time convection, for example, the CI product may perform badly and yields much lower scores.

The method assumes that satellite and radar convective initiation signals might be compared, even though they are intrinsically different. Spatial resolutions differ by a minimum factor of 3 (so 9 in surface) with MSG data (1km with radar data vs 3km with satellite data at satellite sub-point). Moreover, radar signal focuses on the convective core of the convective cell.

To mitigate these differences, pixel-to-object transformation with an additional buffer reduces spatial and temporal localization uncertainties. For ideal study cases, this works quite well, creating CI objects a few tens of kilometers in diameter, slightly larger than the radar objects associated with early convection. However, in the case of more complex and non-isolated convection, this method can sometimes create large CI objects that cover region of several hundred kilometers, artificially giving radar overlays (good detections) while losing the interest of the product.

The definition of the GTs is very dependent on the construction of the trajectories; the method does not distinguish between emerging cells coming from cell split or not. In addition, the CI can give signal on already mature convection because of small localized towering clouds at the edge of active cells. These CI signals are considered as false alarms for the strictest ground truths (*Storm_Trigg* or *Storm_30min*).

The study was restricted purely to the definition of the product CI, namely the probability of initiation of convection in the next 30 minutes. As can be seen in the results, a large part of the CI objects associated with good detections had a lead time of 20/30 minutes; it is possible that a fairly large number of CI objects with a lead time of 30 to 45/60 minutes were considered as false alarms, thus reducing the scores.

2.4 CASE STUDIES

Since no major changes have been made in the CI algorithm between v2021 and v2025 that could influence the results, all the case studies presented here after are realized with the v2021, except for case studies using MTG or GOES18 instruments that are realized with the v2025.

2.4.1 20250311 MTG Case Study

This first MTG case study relies on a verification of CI with LI lightning flashes and v2025 RDT cells over Africa (Southern Nigeria). The question of MSG/MTG continuity is discussed in detail in dedicated chapter 2.5

Figure 11 illustrates this 20250311 MTG case study. At the start of the period, the sky was fairly free of high-level clouds, with numerous small cumulus clouds over the area. Convective activity has already been detected, with RDT cells and LI flashes at sea and over Cameroon. Numerous CI pixels are observed in the centre of the domain, including a large cluster of CI pixels with probabilities of 75-100% (magenta).

20 minutes later (1400 UTC), at the same location, several RDT cells were detected along with numerous LI flashes. Further RDT cells were observed a few kilometers to the South-West, which also had early CI pixels (good detections). For some of these cells, CI pixels continued to appear despite the fact that convection had already developed. But 20 minutes later (1420 UTC), the pixels above these RDT cells completely disappeared as convection continued to grow.

Focusing on the coast, a majority of CI pixels gave good detections with a lead time of 20 to 40 minutes. In contrast, at the border with Cameroon, CI pixels were observed throughout the period without ever being validated by an RDT cell, demonstrating the presence of false alarms.

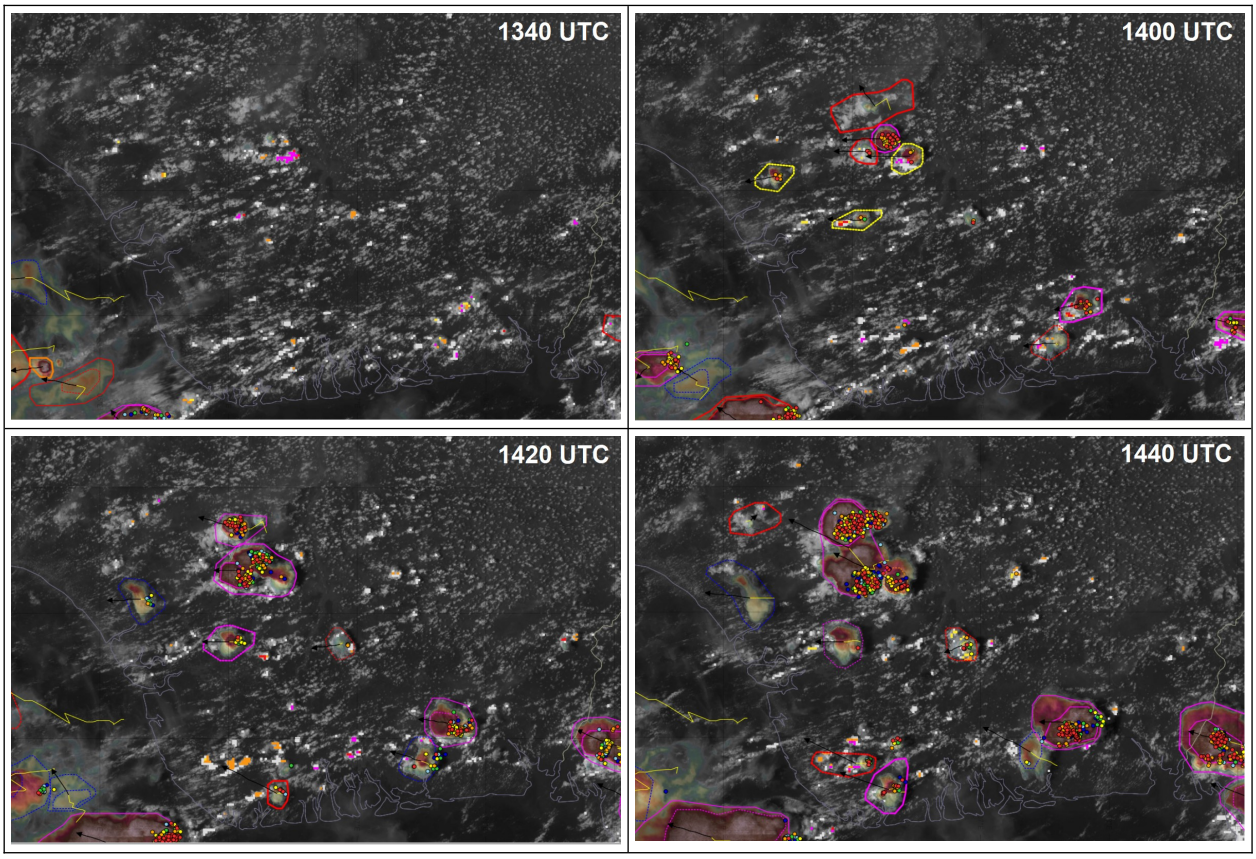

Figure 11: 20250311 MTG case study over Southern Nigeria from 1340 UTC to 1440 UTC. Sandwich image (VIS+IR) superimposed with v2025 RDT cells (polygons), LI lightning flashes (small dots) and v2025 CI pixels with standard colours (yellow, orange, red and magenta for the 4 levels of probability).

2.4.2 20210621 MSG Case Study

Figure 12 illustrates a MSG case study. Early in the morning (0530Z, top), already existing large-scale convective storms affect northern parts of France while small-scale cells hit southern part. New radar cells (ground truth) form in the southwestern part of France. Some CI good detections appear in the vicinity of them. CI false alarms are detected in the western part of France. Additional information about the meteorological context (trough at the edge of the Atlantic coast) may help the forecaster not to take into account those signals.

Later in the morning (0930Z, bottom), CI product offers good skill to detect diurnal evolution of convection over land. CI pixels are quite well collocated with new developing radar convective cells. False alarms are detected, especially over Spain (it is to note that radar data in the validation only marginally cover Spain). Over Spain, in a north-westerly flow (colder air mass), CI product may have difficulties to catch the quick displacement of low levels clouds, hence wrong values of growth parameters and an unexpected CI diagnosis. We may notice that CI pixels appear at the edge of cloud systems.

Figure 13 illustrates the same case study with MSG rapid scan data as the one with MSG data. Early in the morning (0530Z, top), the two CI products behave similarly. More false alarms appear on the edge of the cold large-scale convective system over northern part of France and United Kingdom.

Again, cloud movement tracking and then growth parameters' values are probably responsible for that. In contrast, later in the morning (0930Z, bottom), less false alarms are detected over Spain. With the diurnal evolution, good CI detections are observed over southern and western part of France.

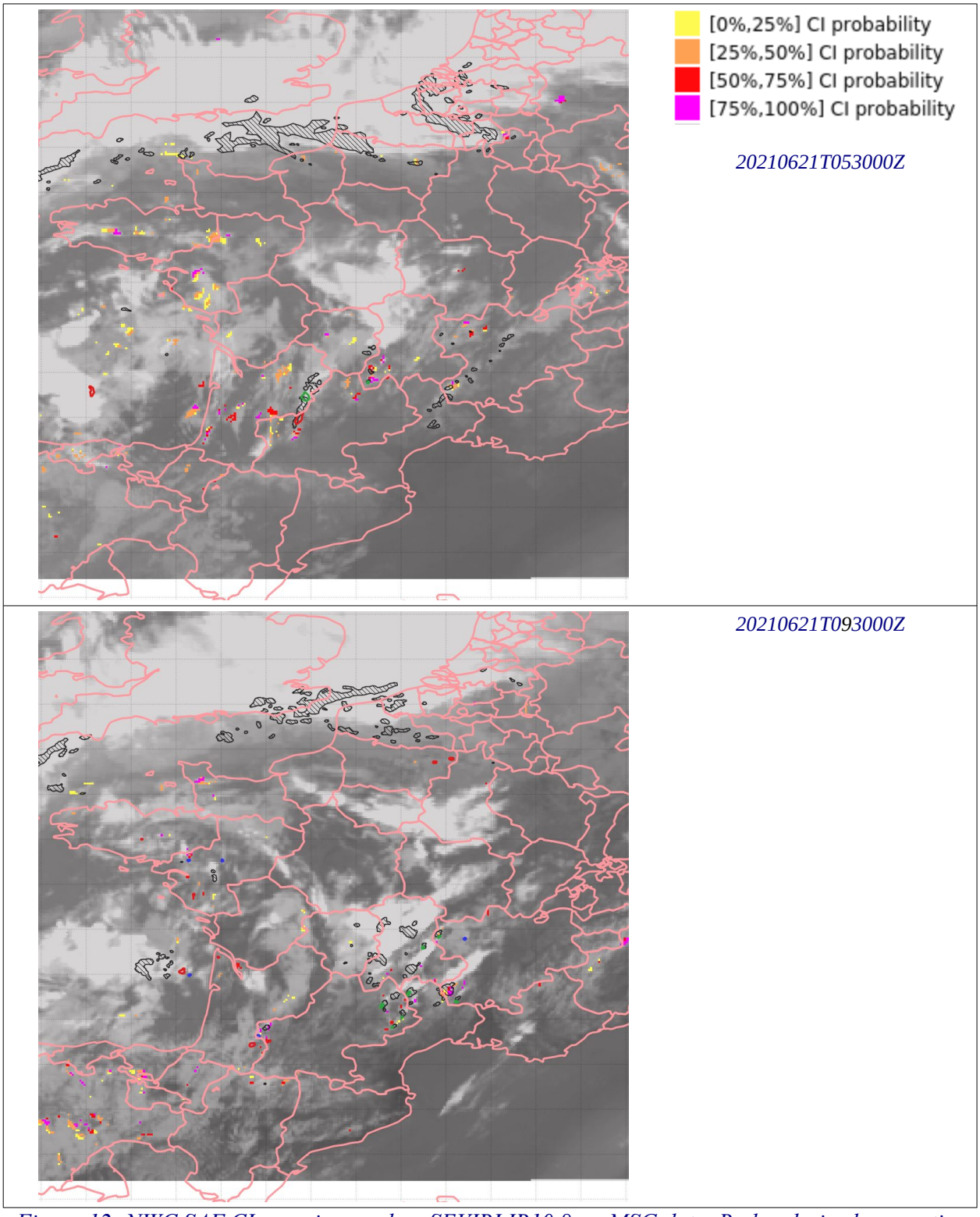

Figure 12: NWC SAF CI superimposed on SEVIRI IR10.8µm MSG data. Radar-derived convective objects (32 dBZ contours) are represented with black hatches. Ground truth is represented with red (birth within the next [0;30] minutes time interval) or green contours (birth within the last [0;30] minutes time interval.

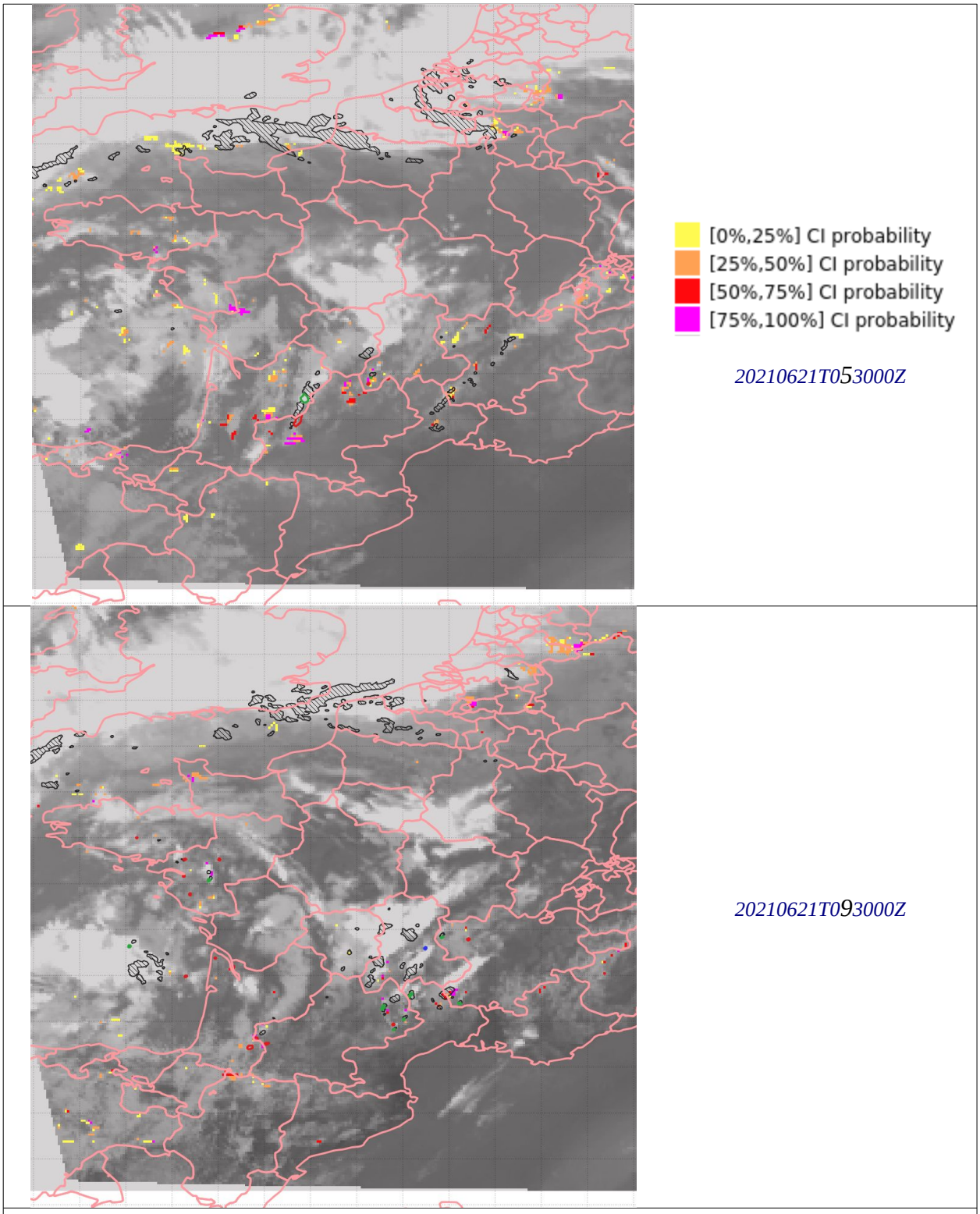

Figure 13: Same as Figure 12 with MSG Rapid scan data (CI product and IR10.8µm)

2.4.3 20210207 MSG-IODC Case study

Figure 14 illustrates a case study over the Indian Ocean, with a focus on La Reunion Island (located at the centre of the image, pink contour). It highlights the difficulty to gain information from CI product on some situations with ground truth embedded in cold convective systems. The appearance

and evolution of new Radar ground truth is already hard to grasp in such situations; CI pixels are not linked at all with the ground truth. Cloud movement is probably hard to track, giving a lot of CI false alarms. Some good detections may be noticed on the southern part of La Reunion Island, at 1400Z.

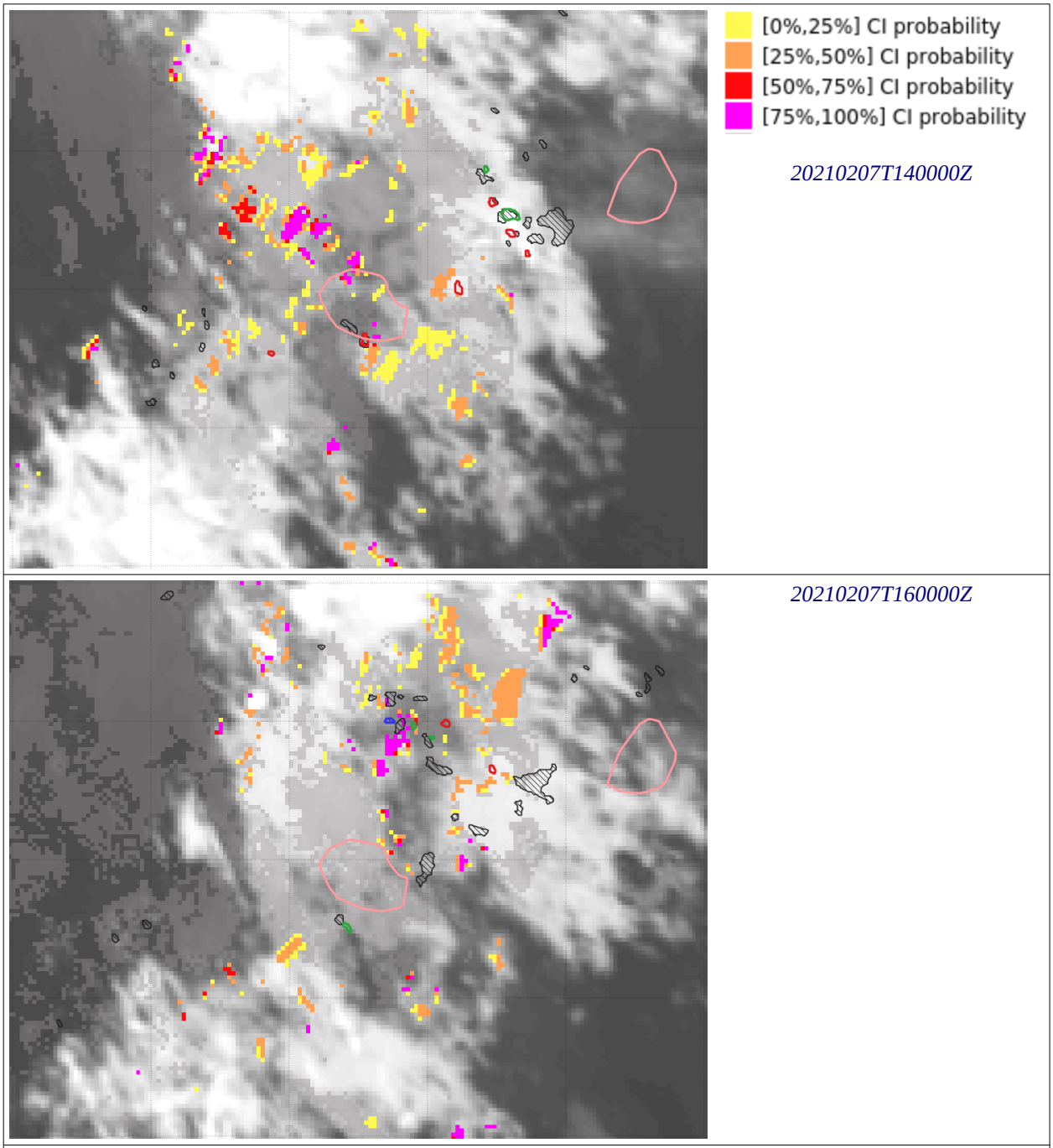

Figure 14: Same as Figure 12 for 20210207 case study and MSG-IODC data

2.4.4 20210914 GOES16 Case Study

Validation of GOES16 CI product relies on the analysis of 20210914 case study over French Guyane. Figure 15 depicts the diurnal evolution over French Guyane with the forecaster workstation. First radar convective cells (radar echos above 32 dBZ) are concomitant with the first CI signals at 1430Z if we accept a 2-3 pixel tolerance. The convective cells evolve first in low clouds. Lightning flashes occur one hour and a half after the first CI signals (1600Z). When the storm south of Cayenne becomes mature, CI pixels appear downstream, in the convergence area between the density current of the storm and the environment, where thunderstorm is about to move forward (1630Z to 1800Z). Subjectively, it looks like a good detection even if in the objective validation, it would have been considered as a false alarm.

GOES19 being committed at the beginning of April 2025, it was not possible to showcase CI applied to GOES19 ABI. However, the results for GOES19 should be similar to those of GOES16 since they are of the same generation and located at the same position.

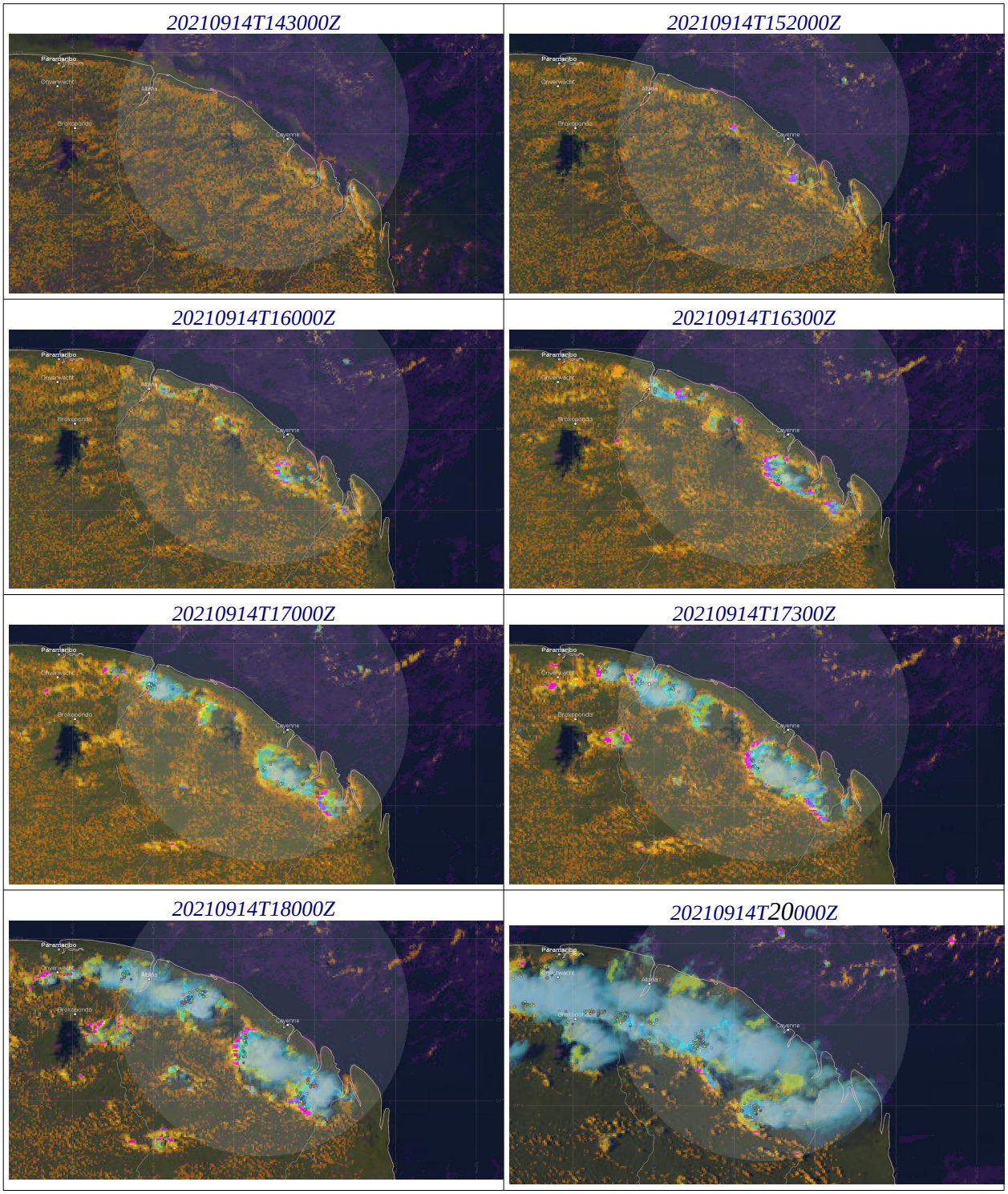

Figure 15: 20210914 case study over Guyane. Cloud type superimposed with radar convective objects (radar echos over 32 dBZ, in blue) and v2021 CI product with standard colours (yellow, orange, red and magenta for the 4 levels of probability)

2.4.5 20250311 GOES18 Case study

For GOES18 satellite, at the moment of the validation, no convective systems were observed over the territories where Météo-France operates weather radar. As a result, this case study relies on a verification of CI based on GLM lightning flashes and v2025 RDT cells over central America (Southern Mexico and northern Guatemala). Figure 16 illustrates this 20250311 GOES18 case study. At the start of the period (2050 UTC), numerous cumulus clouds were present over the area with only few CI pixels at the Eastern and Western ends of the domain.

The CI signals remain active for over an hour, with signal persistence on many slots before RDT cells and GLM flashes are detected around 2200 UTC, subjectively validating these CI pixels. However, in an objective validation, a large proportion of the first CI pixels in these areas would be considered false alarms, as they do not respect the maximum product lead time of 30 min. This case study shows that cumulus clouds in the process of cooling can take a long time and require several surge attempts before becoming a thunderstorm. For this case study, all RDT cells have been preceded at some point by at least one CI pixel.

GOES-W mission was previously performed by GOES17. GOES17 is still supported in reprocessing mode.

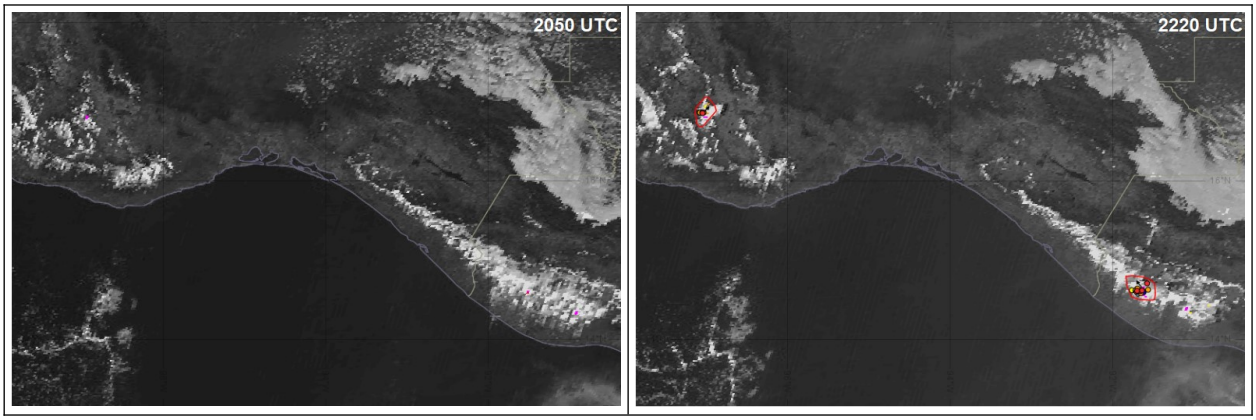

Figure 16: 20250311 GOES18 case study over southern Mexico and northern Guatemala from 2050 UTC to 2200 UTC. Visible image superimposed with v2025 RDT cells (polygons), GLM lightning flashes (small dots) and v2025 CI pixels with standard colours (yellow, orange, red and magenta for the 4 levels of probability).

2.4.6 20210215 HIMAWARI Case Study

Figure 17 gives a focus on this case study centred on New Caledonia, where Météo-France operates meteorological radars. At 1000Z (top), CI product gives interesting features near existing radar convective cells and ground truth. It is worth noting that over tropical regions, convective cells trigger with less cloud extension than in mid-latitudes.

1700Z picture (bottom) depicts an important feature of CI. North of New Caledonia over the Pacific ocean, CI pixels are diagnosed on the northern part of a large convective system, where it regenerates. Attention should be paid in the future to keep such signals when further trying to remove CI false alarms on the edge of low cloud systems, detected as CI because of bad-assessed cloud movement and then wrong growth parameters' values.

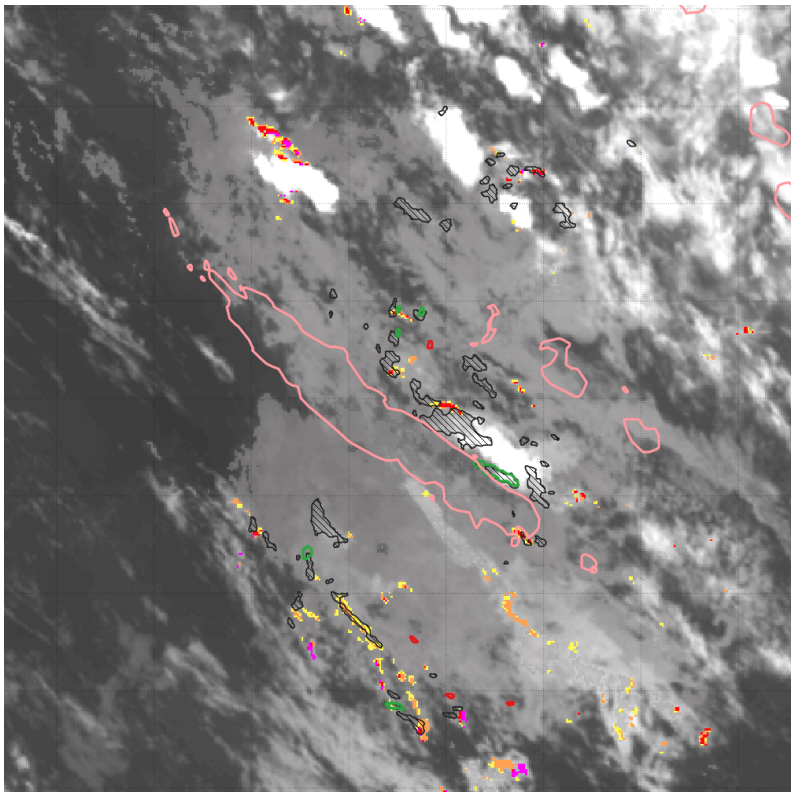

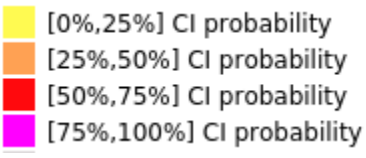

20210215T100000Z

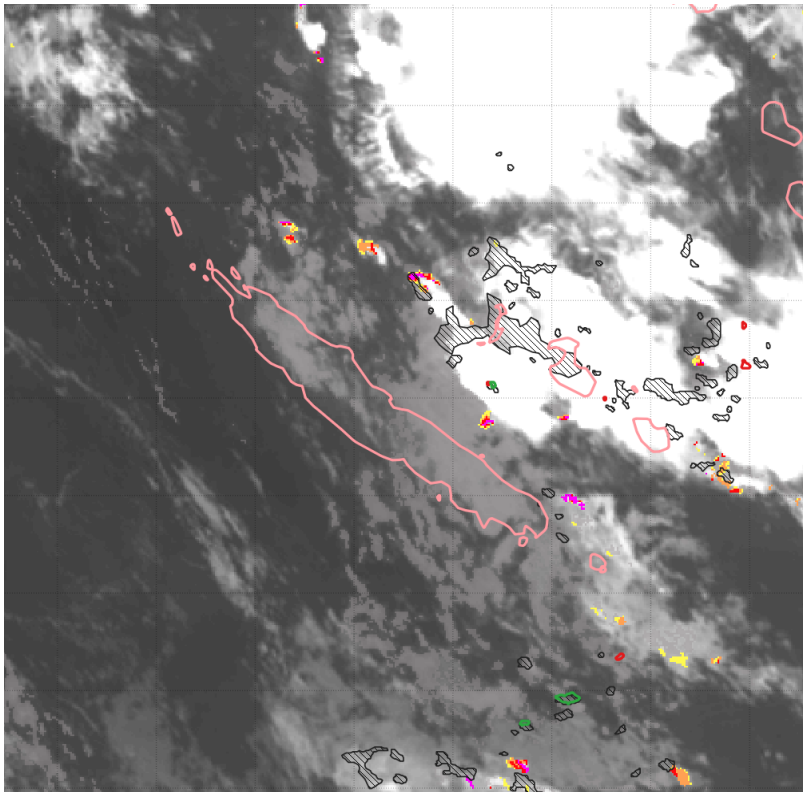

20210215T170000Z

Figure 17: Same as Figure 12 applied to 20210215 case study with Himawari data

2.4.7 Synthesis of case studies regarding limitations of CI

The different case studies have highlighted various limitations and situations where the CI performs poorly:

- In the case of a convective system, the CI gives numerous false alarms, as illustrated by the case over Réunion Island with MSG_IODC. The restitution of motion fields within cloud clusters is complex with also clouds being present at many levels.
- The case over French Guyane with GOES16 (e.g.) shows CI false alarms at the edge of convective clouds.
- Other false alarms can be observed in the case of a rapid flow that limits the proper restitution of the motion field. Pixel trends are then inaccurate, as is CI diagnosis, as shown by the case over Northern Spain with MSG_FDSS.
- The cases over French Guyane with GOES16 and over Mexico with GOES18 have shown that certain CI pixels can appear up to an hour before the ground truth and with strong persistence. These CI pixels are, objectively, false alarms.
- Some of these points confirm conclusions of the ESSL workshop in 2022 on SAF NWC products [RD.16], namely that the CI product is limited in the presence of medium to high clouds, or at night, and also in the presence of thin high-altitude clouds.

2.5 MSG/MTG CONTINUITY REGARDING CI

2.5.1 20250325 case

The 2025 March 25 case is concerned by a low-pressure system over the "Golfe du Lion" bringing instability in a north-easterly flow over southern France, with convection starting in clear skies in the late morning. Meanwhile the Northern and Western parts of France are covered by high-level clouds, with no sign of convection.

Figure 18 shows a comparison between the CI output for MTG and MSG_FDSS over Southern France. There are more CI pixels with MTG compared to MSG due to the increased spatial resolution, but overall the areas with CI pixels are well co-located and illustrate the continuity of the CI product regarding MSG/SEVIRI or MTG/FCI input data.

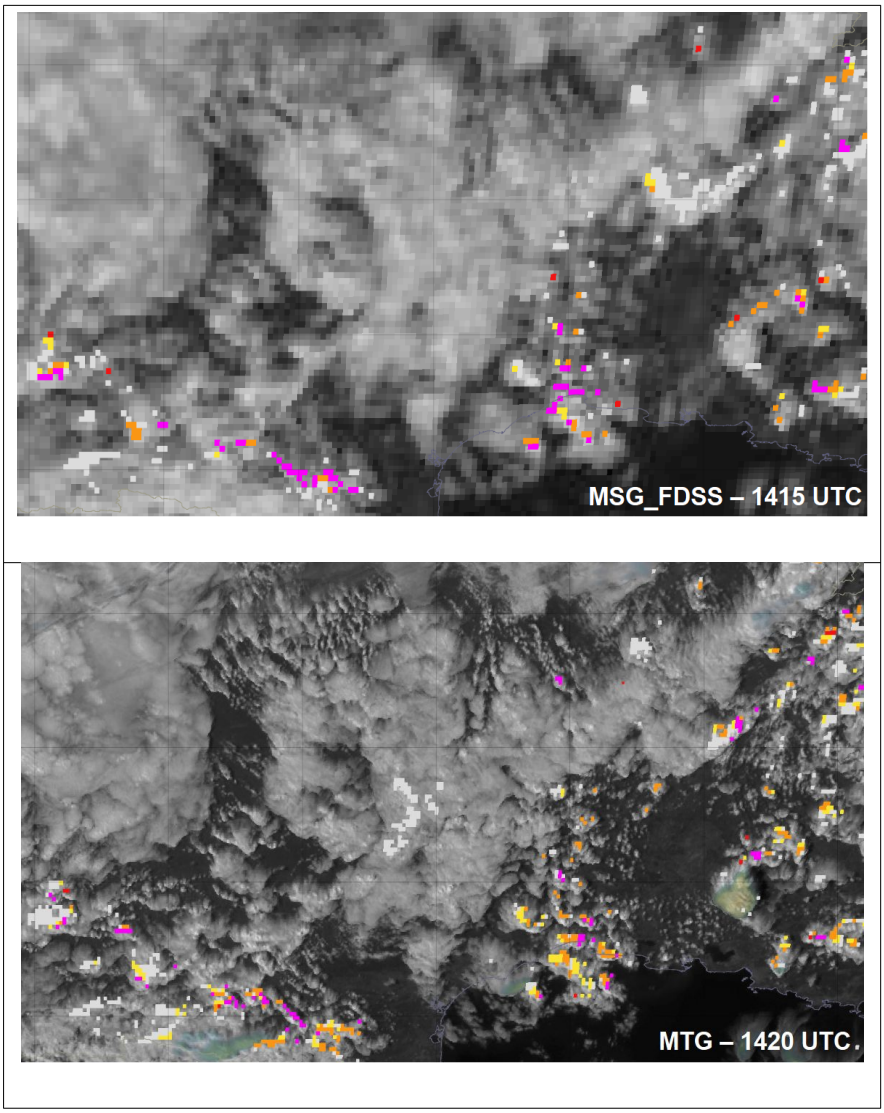

Figure 18: 20250325 case. Visible imagery and CI output for MSG_FDSS (1415 UTC). Sandwich imagery and CI output for MTG (1420 UTC)

For this case, scores are obtained using the same methodology as explained in previous section 2.3.2. The study area covers the entire French metropolitan weather radar network and the study period

ranges from 1000 UTC to 1700 UTC. Following graph Figure 19 indicates that the scores are very comparable and sometimes better for MTG (especially for the POD).

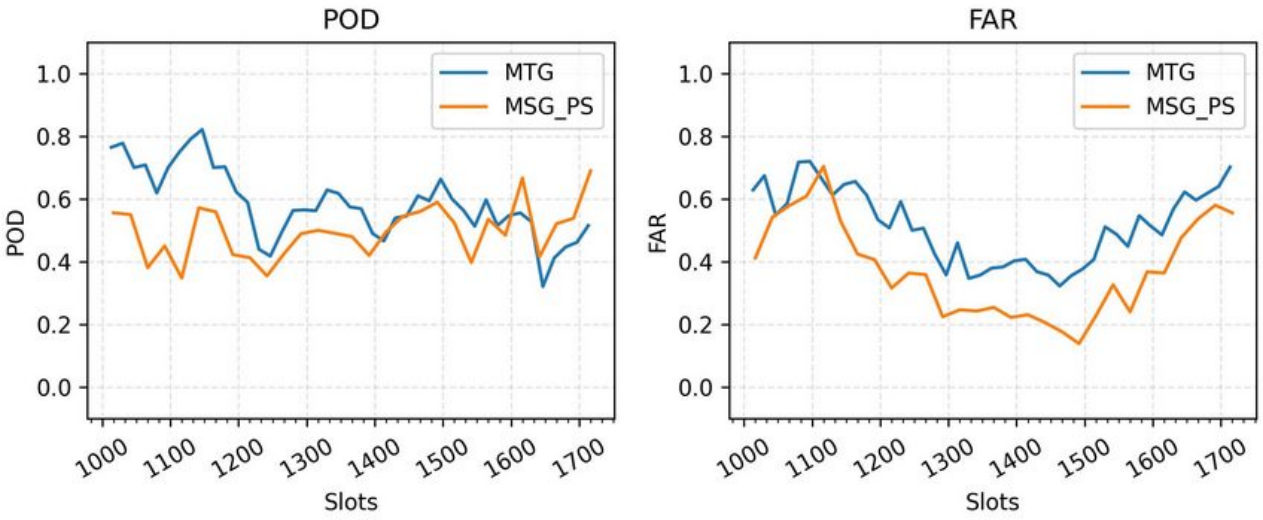

Figure 19: 20250325 case. POD and FAR for CI operated with SEVIRI (MSG_PS/MSG_FDSS) or FCI (MTG). « ALL » radar ground truth (ref section 2.3.2.1.2) is used as reference. CI output are transformed into objects before score computation as explained in REF. DBSCAN and buffer parameters are adapted to FCI higher spatial resolution (20 km DBSCAN and 10 km buffering for CI operated with MTG, 30 km DBSCAN and 15 km buffering for MSG).

2.5.2 20250503 case

2.5.2.1 Case study description

This case study is one of the first days of spring associated with convective activity affecting almost all of metropolitan France. A low pressure system situated off Portugal is bringing instability to the country, with warm, humid air in the lower layers in a south-westerly flow. At 1000 UTC (Figure 20), the sky was clear over most of the country, with only a band of high-level clouds in the far north and a few convective developments in the east at the Swiss border. A few clusters of CI pixels can be seen here.

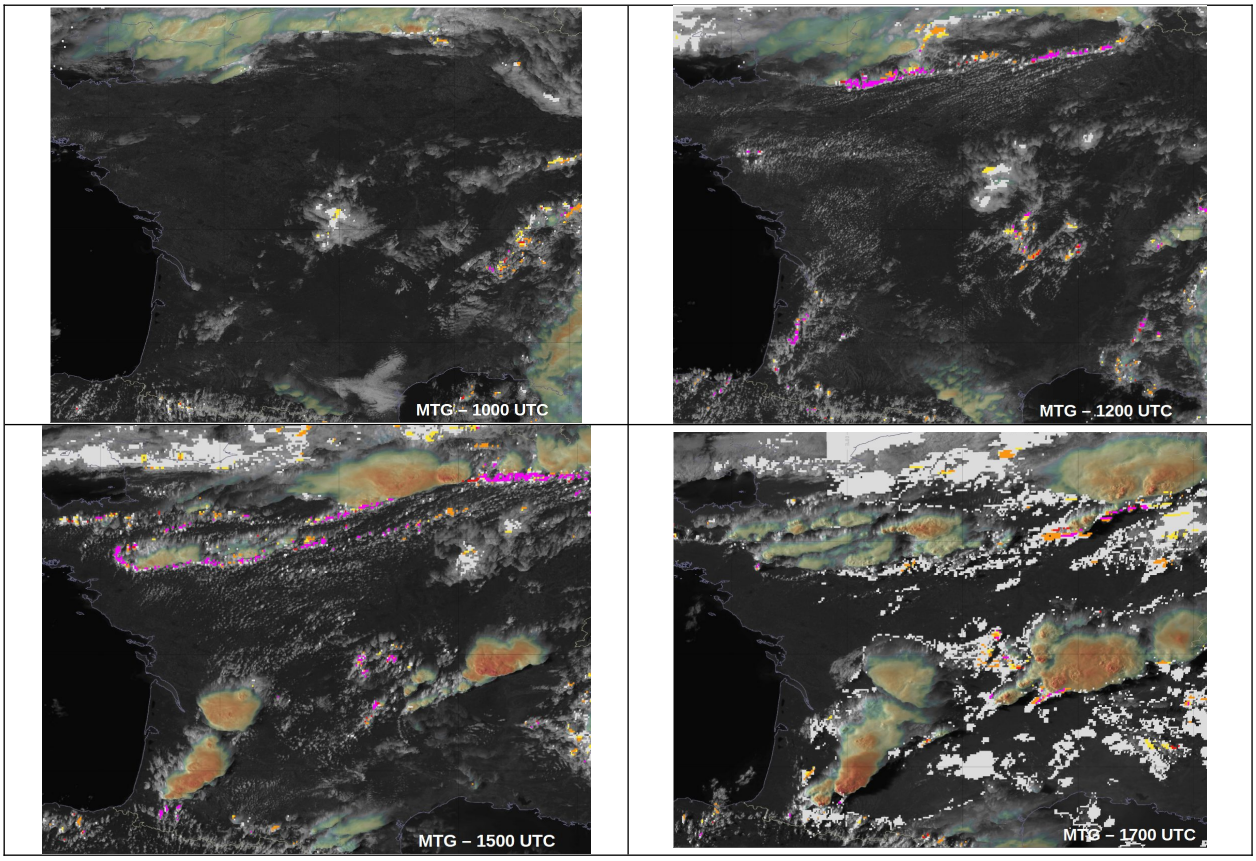

Figure 20: 20250503 case. Sandwich image and CI output at 1000, 1200, 1500 and 1700 UTC. CI operated with MTG/FCI.

Between 1100 and 1200 UTC, a widespread line of CI signals appeared over Paris area. Low clouds/cumulus also appear over the South-West, central West and central East of France, all accompanied by CI signals. The first radar echoes above 35 dBZ appear over these regions around 1215 UTC. A region of CI (yellow pixels) giving false alarms can be seen 150 km southward the Paris convective line. This area corresponds to mid-level clouds that will never evolve into deep convection, whereas CI captures cooling on these cloud tops.

Convective activity continues to develop throughout the afternoon, accompanied by CI signals upstream and/or on the periphery of convective cells (Figure 20, 1500 UTC).

At 1700 UTC one can note many grey CI pixels that correspond to eligible-CI pixels that fail the second step of the CI algorithm (decision tree). These pixels appear because CMIC output is not available at that time and thus the filter of eligible-CI pixels is less efficient. The more candidate you have the higher the chance to have a CI diagnosis>0 : this figure can also be seen as an illustration of the higher FAR of CI during night-time and one of the limitation of the product when we back away ideal conditions.

2.5.2.2 Parisian supercell case study

At around 1420 UTC, a supercell swept over Paris, bringing hail up to 4 cm in diameter. Figure hereafter [Figure 21] shows a few moments in the life of this cell. At 1110 UTC, the first CI signals appeared 100 km west of Paris, indicating a high risk (75-100%) of convection initiation in the next 30 minutes. In subsequent satellite slots, this CI signal remains persistent over the same area for around 1 hour. At 1140 UTC, the first radar echo above 35 dBZ corresponding to the supercell

appears. At 13:10 on Figure 21 we can note some CI signal on another cell backward the future Parisian cell, this kind of false alarms are relatively frequent for CI output but can be easily identified as false alarm by forecasters. The cell then propagates eastwards, strengthening and reaching Paris around 1400 UTC. During its path, CI signals were observed on its periphery and upstream. Finally, this event was well forecast by the CI product, with an earliness of 30 minutes and a strong persistence of the CI signal.

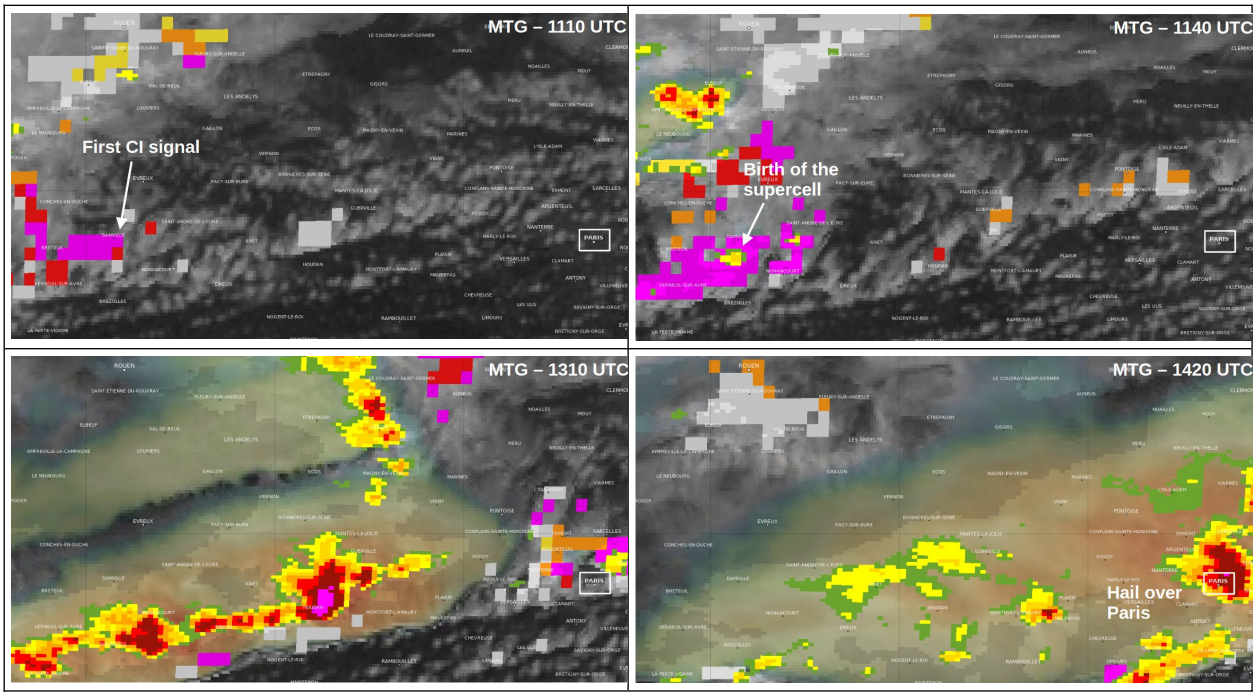

Figure 21: 20250503 Parisian supercell case. Sandwich imagery, CI output and radar reflectivity composite (above 35 dBZ) at 1110, 1140, 1310 and 1420 UTC. CI operated with MTG/FCI

2.5.2.3 MTG/MSG CI comparison

Following figures (Figure 22 and Figure 23) clearly show the continuity of the CI as an output of the MTG/FCI and MSG/SEVIRI data. Indeed, for these two slots, areas with CI signal are well collocated with similar patterns between the two outputs. As seen in the previous case study, MTG CI tends to produce more CI pixels relative to the total number of pixels in the frame.

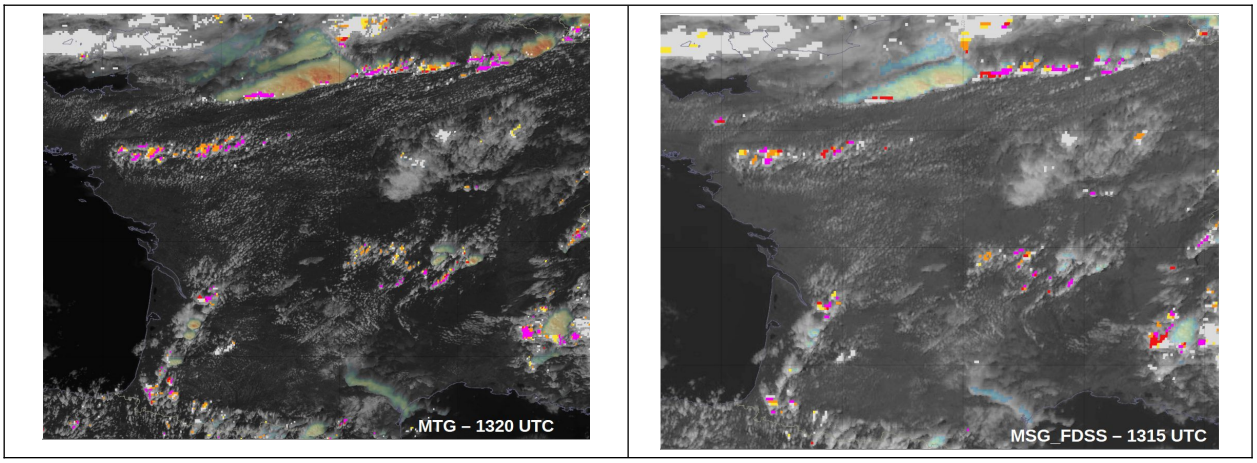

Figure 22: 20250503 case. Sandwich imagery and CI output for MTG_(1320 UTC) and MSG_FDSS (1315 UTC)

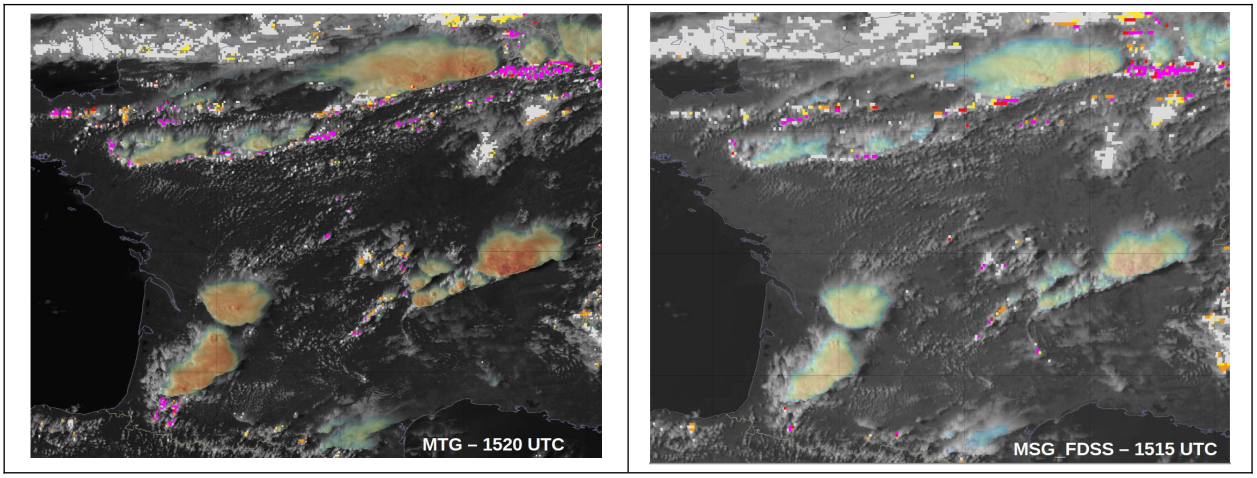

Figure 23: 20250503 case. Sandwich imagery and CI output for MTG (1520 UTC) and MSG_FDSS (1515 UTC)

2.5.2.4 Objectives scores

Objective scores were computed for this case study using the same methodology as explained above (section 2.3.2.2).

Following an approach similar to the previous case study, the domain covers the entire weather radar network in mainland France over the period 1000-1700 UTC. Figure 24 shows the evolution of these scores during the day, illustrating the continuity of MTG/FCI and MSG/SEVIRI with very similar scores. The greater number of CI pixels with MTG increases the POD but also the FAR. However, the overall score for the day with MTG CI is slightly better, reaching a CSI of 0.42 compared to 0.38 with MSG.

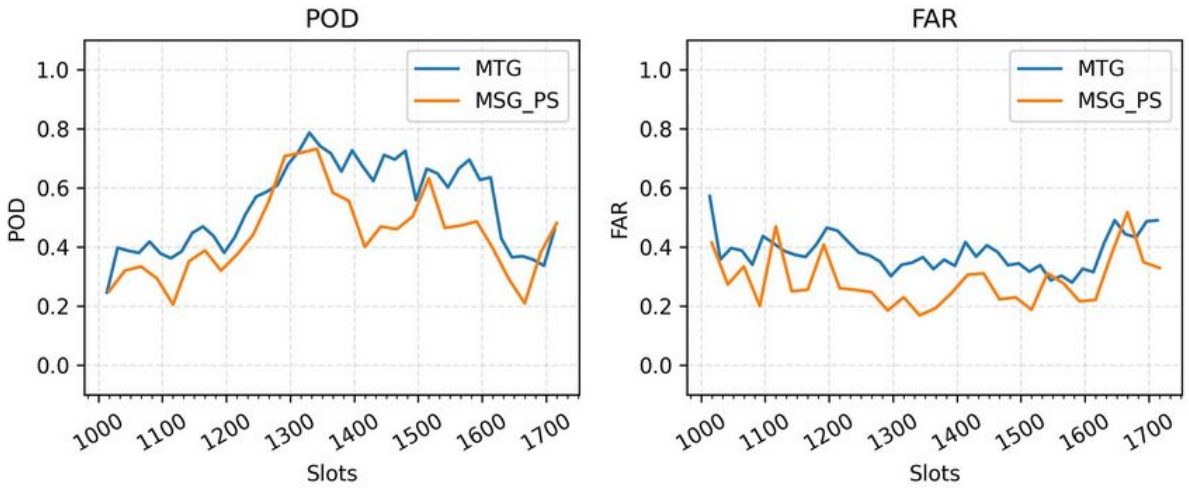

Figure 24: 20250503 case. POD and FAR for CI operated with SEVIRI (MSG_PS/MSG_FDSS) or FCI (MTG). « ALL » radar ground truth (ref section 2.3.2.1.2) is used as reference. CI output are transformed into objects before score computation as explained in REF. DBSCAN and buffer parameters are adapted to FCI higher spatial resolution (20 km DBSCAN and 10 km buffering for CI operated with MTG/FCI, 30 km DBSCAN and 15 km buffering for MSG/SEVIRI).

2.5.3 Conclusions about MSG/MTG continuity

Previous case studies taken in early convective 2025 season illustrate the good behaviour of CI product operated with FCI compared to SEVIRI: visual continuity, higher detection. Regarding the FAR scores are correct but one can note that FAR is higher for CI operated with MTG/FCI compared to CI operated with MSG/SEVIRI. Two main causes are identified:

- Higher sensitivity of CI operated with FCI : more pixels with a probability >0 (but this has a positive impact on POD)
- A lack of tuning in the transformation of CI pixels into objects for FCI.

Day-2 mitigation will concern a change in the CI algorithm (for example thresholds) and a dedicated MTG method for the transformation of CI into objects.

2.6 END-USERS' FEEDBACKS

2024 NWCSAF users' exhibits that

- 36.4% of users use CI repeatedly
- The usefulness is rated 7.4 (/10)

CI is mainly used for forecasting. It emphasizes the fact that the product needs expertise and difficult to integrate in automatic warning due to false alarms.

Several feedback have been received during NWCSAF users' workshop in February 2025. The study by ARPA [RD.13] with a validation method similar to the one implemented by Météo-France illustrates the benefit of CI: "for the analysed cases, CI […] shows a good capability to […] anticipate (in some case also of 30-60 minutes), with a POD of 64%."

A ESSL workshop [RD.16] exhibits in the conclusion that CI can add to forecasters an additional lead time of 15 minutes. The product "performs pretty good in clear scenes without mid to high level clouds being present and when the sun is high up". Limitations concern dusk/dawn, night-time, presence of thin cirrus on-top convective clouds

2.7 CONCLUSION AND COMPLIANCE REQUIREMENTS

After CI v2016 first delivery of the product, v2018 exhibited major improvement and an first effort on validation has been made. Improvements are illustrated in [RD.4] and the v2018 reached the status “pre-operational”. v2018.1 and v2021 brought new improvements of CI products and a larger set of committed satellite. v2025 is not associated with major changes of the CI algorithm but supports new satellites as MTG and GOES19.

The high sensitivity of CI validation scores to the method used has been quoted from the first stage of CI development [RD.11]. High FAR can be found in literature and are often attributed to difficulties inherent to CI problem.

Previous validations [RD.14] have shown, among other things, scores below the accuracy level, but have highlighted the conditions in which the CI brings value to forecasters. In fact, situations with day-time isolated and unorganized convection with clear sky and without strong movement field are the best conditions for CI to operate and can be considered as ideal situations. These CI properties are also mentioned in the end-users’ feedbacks [section 2.6] and put into evidence in the various case studies [section 2.4].

The new objective validation method based on ideal case studies, on CI objects and with various radar-based ground truths has shown promising results. Figure 25 shows the median scores obtained during this objective validation for the various ground truths, the two satellites as well as the scores ranges for EUMETSAT operational status requirements. It can be seen that the scores are just within the target zone for MSG_RSS and for certain ground truths, notably Storm_30min (the most representative of early convection). These results also demonstrate the benefits of using higher-frequency scans for better detection of convection initiation.

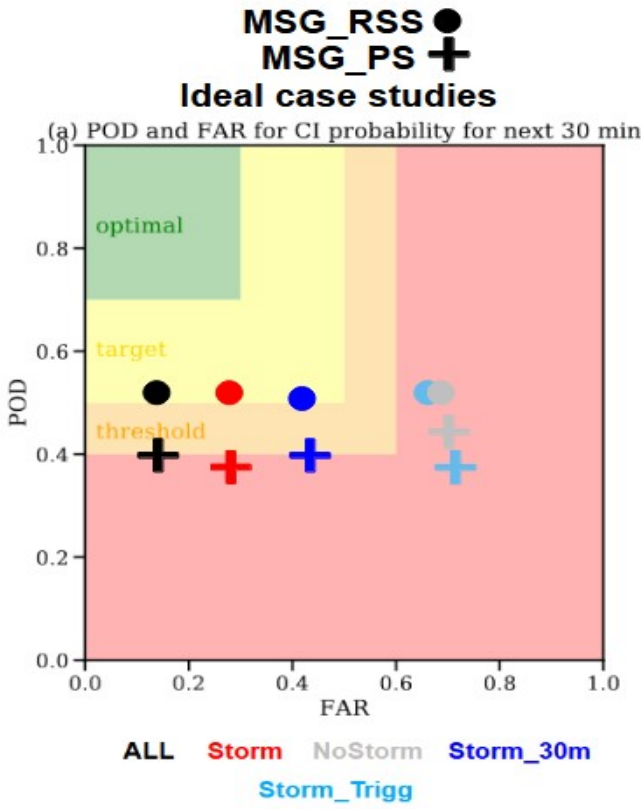

Figure 25: Objective validation scores and scores ranges for EUMETSAT operational status requirement (see PRD).

Case studies with isolated convection clearly help user to understand the behaviour of the product and exhibit some cases where CI can be useful with bad scores, sometimes for a too-early diagnosis. It illustrates also the difficulty for CI to provide behaviour in case of quick displacement (perturbation of trends computation). Lastly a case illustrates how a basic knowledge of the meteorological context helps to easily identify some false alarms pixels.

In conclusion, MFT considers that the strength and weakness of the product are identified.

- Strength :
  - CI provides as expected a 20-30 minutes anticipation of the majority of radar trajectories.
  - This analysis has also shown that MSG_RSS yields better scores due to its higher scan frequency.
- Weakness
  - More false alarms during night-time as CMIC is not available.
  - No diagnosis in case of thin cirrus layer
  - Dependency of movement fields retrieval
  - CI signal may persist on the edge of convective systems.

Situations with day-time isolated and unorganized convection with clear sky and without strong movement field are the best conditions for CI to operate. These situations are the ones where the CI performs best and brings the most value to users.

Regarding the recent works with selection of cases and transformation of output, CI now meets the requirements about scores for a future operational status.

3 RAPIDLY DEVELOPING THUNDERSTORM – CONVECTION WARNING (GEO-RDT-CW) VALIDATION

3.1 OVERVIEW

The main objective of this section is to document RDT convective discrimination accuracies and compare them to the threshold accuracies listed in the NWCSAF product requirements document [AD.4]. As the RDT discrimination scheme has been enriched with an additional calibrated scheme, new graphs and comments in this report will refer to this new approach (CAL). One still can refer to the previous validation of so-called generic (GEN) scheme over European areas, which can be still used in specific configurations (un-calibrated satellite, invalidated statistical model).

Concerning the forecast capabilities (forecast products) included in RDT-CW code (CW part) it is to note that thunderstorm conceptual models often show a rapid morphological evolution and intensity variability, for which satellite data doesn't bring enough information. A subjective evaluation based on cases study is undertaken for an analysis of the localization of extrapolated cloud cells, depending on moving speed estimate accuracy and morphological evolution of the cloud systems. An objective validation has been made in a scientific report [RD.2].

3.2 VALIDATION OF GEN DISCRIMINATION DIAGNOSIS

3.2.1 Context

The GEN discrimination diagnosis has been fully described in previous validation report and results are still available as this choice of validation is still proposed to end-users. Hereafter a summary of the validation.

3.2.2 Data and methods

The configuration of discrimination verification is following

- Domain Europe
- Ground truth given by EUCLID network
- Period including intermediate season: June-August 2008 + April-October 2009
- Section approach where trajectory is split in convective and non convective sections
- Trajectories with light electric activity suppressed of the sample
- H2 hypothesis where RDT-CW early diagnosis (before an electric section) and continued diagnosis (after an electric section) have a positive impact on scores. It meets the requirement of "30 minutes detection after first lightning occurrence"
- RDT v2011 operated without lightning data to force the discrimination process.
- Results applicable to this release with GEN discrimination option

3.2.3 Results

Table 3: RDT v2011 Discrimination skill table

POD	*77 %*
POFD	*4 %*
FAR	*28 %*
TS	*59 %*

The figure below points out that more than 50% of good detection are already classified at the time of the first lightning occurrence, 80 % thirty minutes after. Nevertheless, only 25% are classified before the first flashes stroke (15 min before).

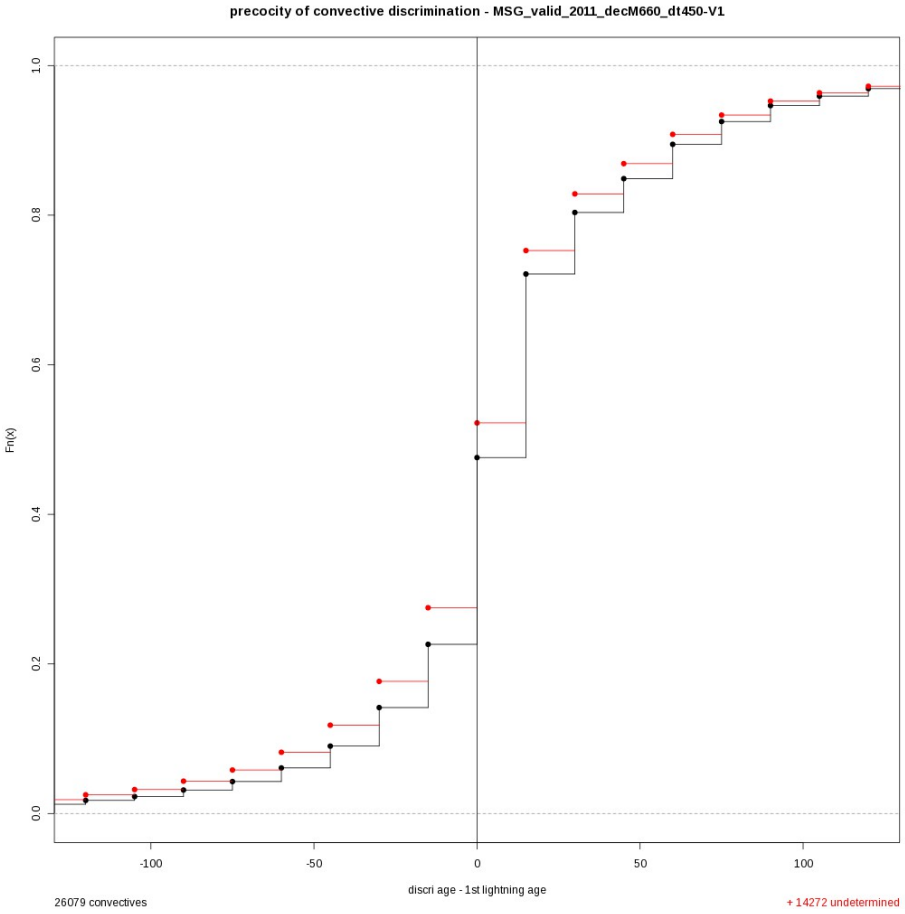

Figure 26: Early-diagnosis (precocity) of RDT v2011 discrimination for moderate (black) and low (red marks) ground truths.

3.2.4 Conclusion

Threat Score is above 50% (above threshold accuracy of overall thunderstorm detection skill of 50%) and POD of 77% (above target detection 30 minutes after first lightning occurrence 50%). For this option GEN, the early diagnosis is still of 25% (threshold of the target requirement).

We consider that RDT meets the requirement. The versions associated with GEN discrimination scheme are “operational” in EUMETSAT sense. Details and complete verification are in scientific report [RD.5] and previous verification report [RD.8]].

3.3 THE VALIDATION OF CAL DISCRIMINATION SCHEME

3.3.1 Context

The purpose of this release is to provide updated calibrated discrimination for each geostationary satellite at its nominal scan rate. As mentioned in ATBD, long series of operational runs have been taken into account for that purpose: MSG-FDSS (MSG4 at that time) and MSG-IODC (MSG1 at that time) / 15 minutes, MSG-RSS (MSG3 at that time) / 5 minutes, GOES16 / 10 minutes. Himawari-8 being taken into account at Météo-France every 20 minutes only, and GOES18 every 30 minutes only, no calibrated discrimination has been attempted for those satellites. GOES16 models will be used instead.

In this report, only the nominal default configuration for the latest release is analysed, it means that calibrated discrimination is used. For GOES and HIMAWARI satellites, the channel #15 is taken as main channel. For GOES18 and HIMAWARI satellites, only subjective validation is presented hereafter. For MSG satellites and GOES16, both objective and subjective validations have been undertaken.

Lightning data remain the ground truth used to tune and to validate (on objective or subjective basis) RDT-CW. Those data are usually provided by a ground lightning network. Meteorage lightning network data allow to get reliable information over Europe, providing a high-quality ground truth. GLD360 network is operationally used by Météo-France on a limited region in southern part of Indian Ocean including Madagascar and La Reunion island, and allows also a reliable verification for RDT operated with MSG-IODC. GLM data are used for the RDT operated with ABI radiometer data from GOES16 and GOES18. For HIMAWARI, WWLLN global network is available. Compared to other networks, the quality of detection and precision of localization are however limited in that case. The RGB image used in some figures of RDT-CW validation is a Météo-France production based upon channels 0.6 µm (day), 3.7 µm (night), 10.8 µm and 12.0 µm.

3.3.2 Validation and Cases study

Those cases study rely on RDT-CW processing whose discrimination scheme is based on satellite data only, after NWP filtering . Lightning data are paired with cloud cells on a passive "mode" (data not used for the convective diagnosis). Satellite image and lightning data will be hereafter visualized to synthesize ground truth.

3.3.2.1 RDT-CW discrimination using MSG in FDSS mission

Runs for MSG4 case have been undertaken over Europe, for several dates out of the period used for the tuning. Those dates range from May to October 2018.

3.3.2.1.1 Objective validation

3.3.2.1.1.1 Data

Only datasets included in extended Meteorage and partners network coverage area are taken into account (see Figure 27).

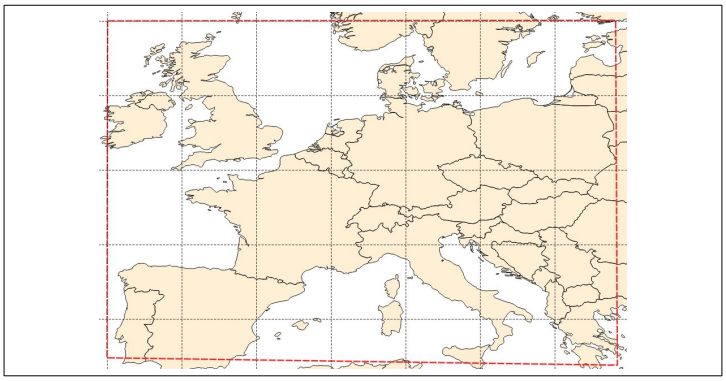

Figure 27: METEORAGE and partners network coverage area taken into account for objective validation

3.3.2.1.1.2 Methodology

RDT-CW was operated with lightning flashes as input data, but without changing the convective diagnosis. This diagnosis is evaluated against a "Ground Truth" based on electrical activity of the trajectory. Two "levels" of Ground Truth are considered: moderate and severe, regarding the electrical activity:

- Number of flashes per cloud cell of a given trajectory
- Total number of flashes during the trajectory
- Continuity of activity during the trajectory

For example moderate trajectories are assumed convective if they match with 5 flashes strokes at least. Moreover, non electric trajectories are defined if their minimum distance to nearest flash during lifetime is over 200km. This value is set to eliminate ambiguous cases and to take into account limited geographical extension of RDT-CW cell contours when focusing on a convective tower part of a larger convective cloud system.

Non electric trajectories helps to define correct rejection (CR). Hit (HI), False alarm (FA) and miss (MI) case are determined for the whole trajectory.

3.3.2.1.1.3 Results

Contingency tables scores are resumed hereafter and then scores for various satellites are plotted in Figure 54.

- Period from 20180513 to 20190618, 14 cases : POD ranges from 40,4 to 81,1% (median 68,7) and FAR ranges from 1,9 to 35,2% (median 6%) when moderate GT is considered
- Period from 20180513 to 20190618, 14 cases : POD ranges from 42,9 to 85,4% (median 75,13) and FAR ranges from 2,2 to 68,3% (median 7,6) when severe GT is considered

Scores against moderate ground truth below highlight the ability of RDT-CW updated discrimination scheme to limit false alarm ratio in most cases, keeping correct values for POD. Scores are of course dependent on the situation, generally better for most actives situations.

Those results become of course even better when lightning data is considered also for the diagnosis, when necessary. In this configuration (100% for POD by construction), FAR value is automatically reduced (not shown here). In that case the gain is limited, to few situations : FAR drops from 35% to 26% on the 15th June 2019, from 33% to 22% o the 6th August 2019).

Scores against severe ground truth implies a reduced dataset, and show very logically a strong decrease of misses. One can note a light increase for PODs and FARs, sometimes significant like in the less favourable situations. .

3.3.2.1.2 Case Study 20180621 over Europe

Following figures illustrate a convective situation in the Southern part of Europe. A cold front associated to a synoptic perturbation splits the region in two parts, convective systems developing in the warm air mass. Comparing the results for v2018 and v2021 releases, one can note that:

- Most electric phenomena are identified as convective clouds with RDT-CW, whatever the release.
- v2021 discrimination scheme does slightly lower the number of false alarms on this situation, when compared to v2018. This is illustrated at 15h00Z in Central Europe, but also in the Northern part of the perturbation.
- Some misses can be observed in embedded cloud systems especially in the cold front, but also with some isolated low active clouds.

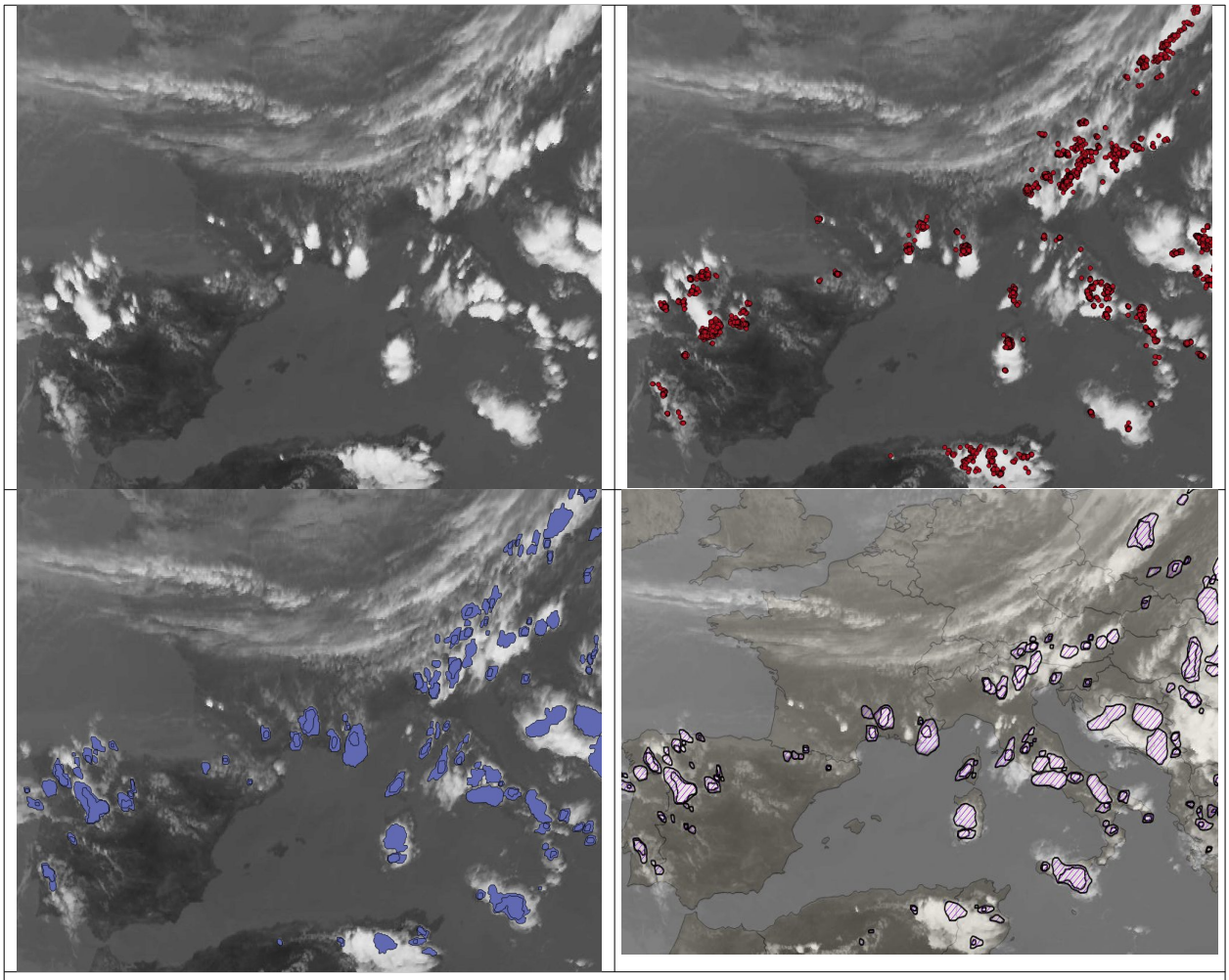

Figure 28: MSG4 case study for 12h00-15h00Z on 20180621. 15h00Z IR image (top left), 30min accumulated METEORAGE impacts around 15h00Z (top right), v2018 (bottom left) and v2021 (bottom right) results for 15h00Z.

Embedded cloud systems are difficult to distinguish, and lead either to numerous cloud cells among which some can be false alarms, either to limited cloud cells, at the risk of missing some apparent electric cells. This latest v2021 release is aimed to limit the number of false alarms, with the possibility to eventually use external lightning data to complement diagnosis.

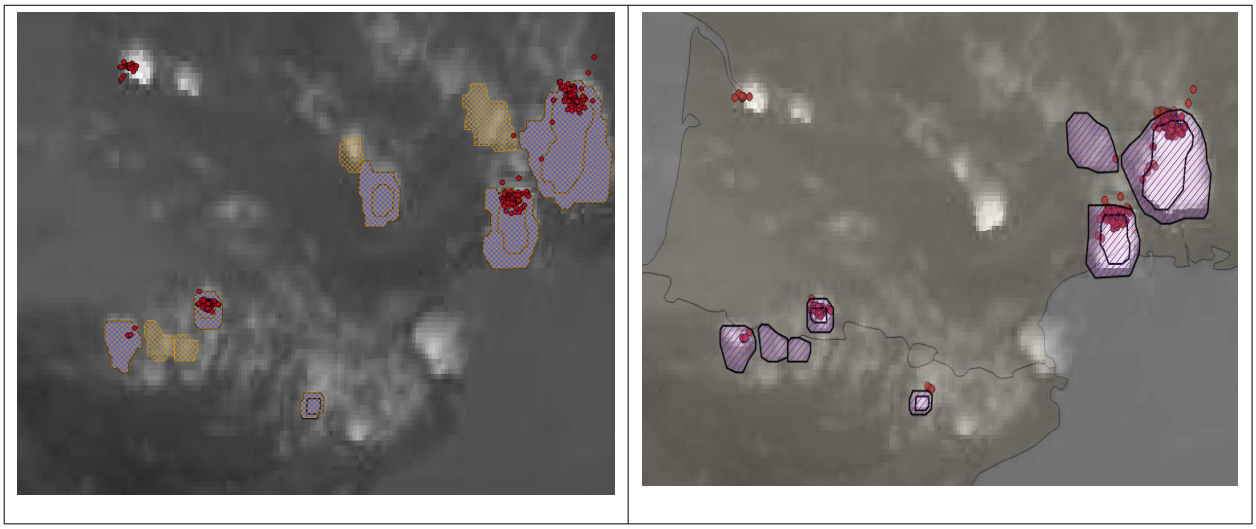

Figure 29: MSG4 case study for 20180621 15h00Z, zoom on South of France. v2018 (plain blue cells) and GEN (orange dashed) on the left, v2021 on the right. One can note a miss near Bordeaux (top left cloud) in any configuration, and a non-electric cloud system ignored by v2021.

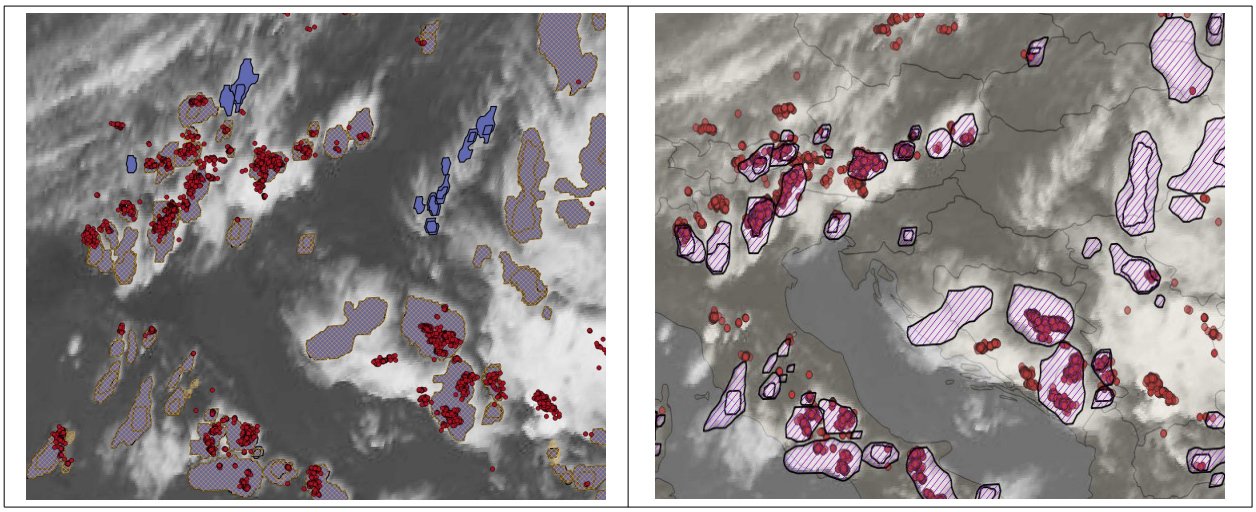

Figure 30: MSG4 case study for 20180621 15h00Z, zoom on Central Europe. v2018 (blue cells) and GEN (orange dashed) on the left, v2021 on the right. One can note with v2021 the suppression of False Alarms seen by v2018 on the edge of cloud systems

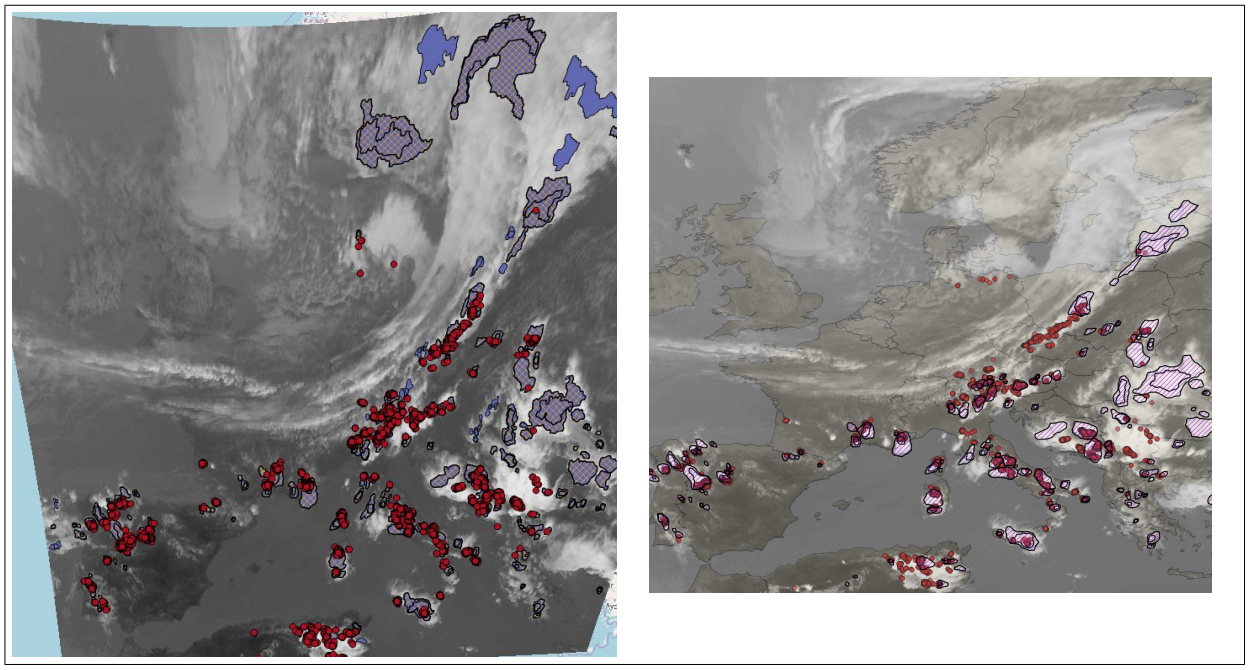

Figure 31: MSG4 case study for 20180621 15h00Z, large view. False Alarms suspicion in the North of the domain with v2018 (left), correctly rejected with v2021 release (right), in an area which is out of lightning coverage area.

3.3.2.1.3 Case study 20180702 over Europe

Figures hereafter illustrate a large and zoomed view of this situation.

Embedded and also isolated diurnal convective cells can be observed. The behaviour of RDT convective diagnosis appears here pretty efficient regarding electrical activity, especially if we have a look on the temporal evolution. Most of lightning strokes have been, are, or will be associated with a RDT-CW cloud cell diagnosed as convective.

In the middle part of France, RDT-CW cells appear sometimes prior to electrical activity. On the other hand, embedded cloud systems, as on the top left of the image, seem more difficult to separate and identify. Electrical activity is observed in several places, RDT-CW cells do not fully correspond at that time for this complex system. The focus of RDT-CW on the identification of cloud towers limits the representation of convective activity.

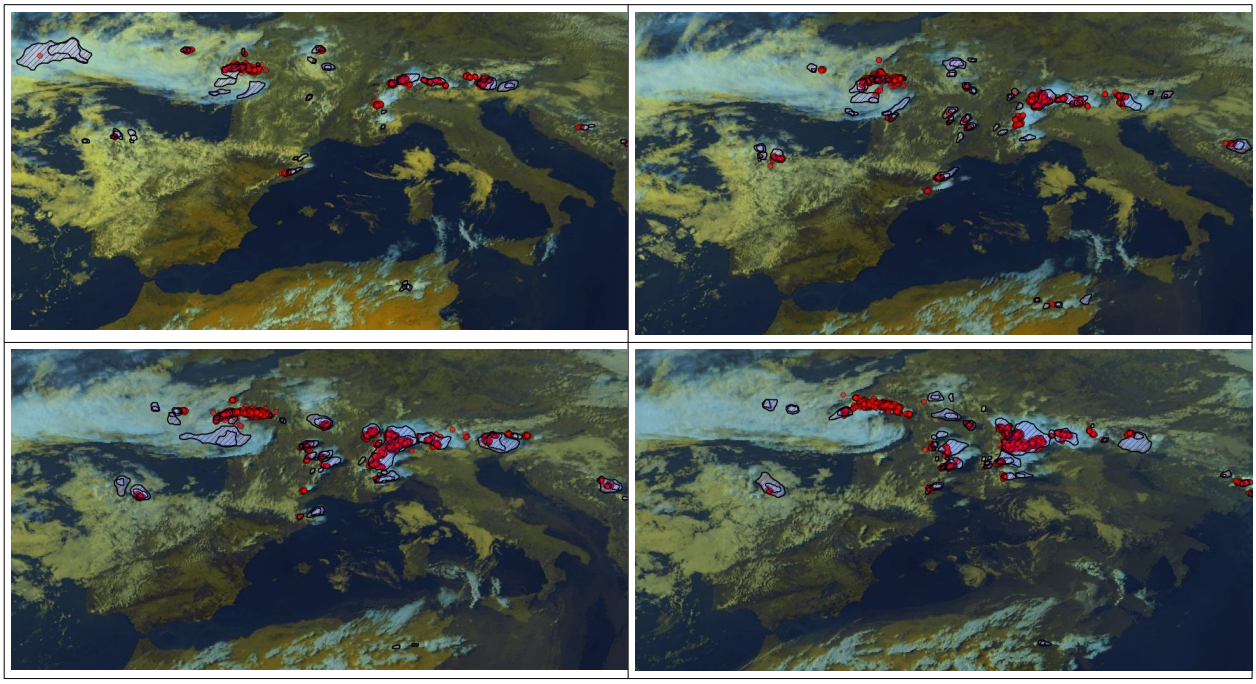

Figure 32: MSG4 case study for 20180702. 15h00Z, 16h00Z, 17h00Z and 18h00Z from top left to right bottom. RGB images with METEORAGE impacts, RDT-CW v2021 cells.

And if we consider RDT-CW from a temporal point of view, like in Figure 33, one can conclude that all electrical activity can be associated with a RDT-CW cloud systems, even if the flashes can be in the vicinity of the cells. Few false alarms are noted. Even an apparent miss at a given time (15h00Z on the French Alps) corresponds to a case where cells were diagnosed earlier (14h to 14h45Z) in the vicinity, and part of a larger system later on (17h00Z).

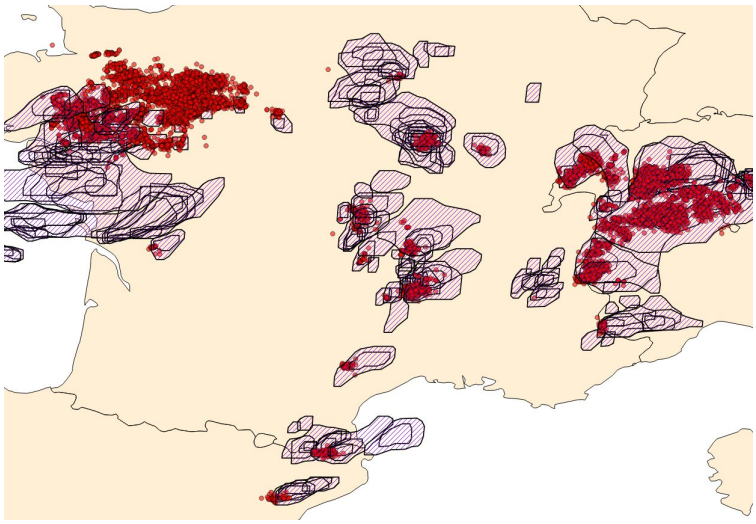

Figure 33: MSG4 case study for 20180702. Zoom over France, with accumulated Lightning and RDT data from 14h00Z to 18h00Z

3.3.2.1.4 Case study 20190419 over Africa

When regarding RDT-CW behaviour over Africa, one can note that lots of convective systems, even the smallest ones, are linked to strong signatures of predictors, and make the statistical models adapted and relevant.

For this region, WWLLN data are used to check a RDT-CW convective diagnosis based on satellite characteristics only. Following figures illustrate RDT-CW performances for a 20190419 situation in the end of afternoon.

A global overview show a good agreement between electrical activity and identification of convective cells by RDT-CW. both diurnal intensification of convection over land, and activity of ITCZ over ocean are highlighted, even if electrical activity over land is obviously stronger.

One can note rare misses (mainly around 40°S in a cold air mass behind synoptic perturbation, red circle). Few false alarms are suspected (blue circles). Most of them occur over sea surface. A deeper analysis looking at previous and following periods reveal that for some of those suspected false alarms, RDT-CW cells are located in areas where electrical activity was, or will be present.

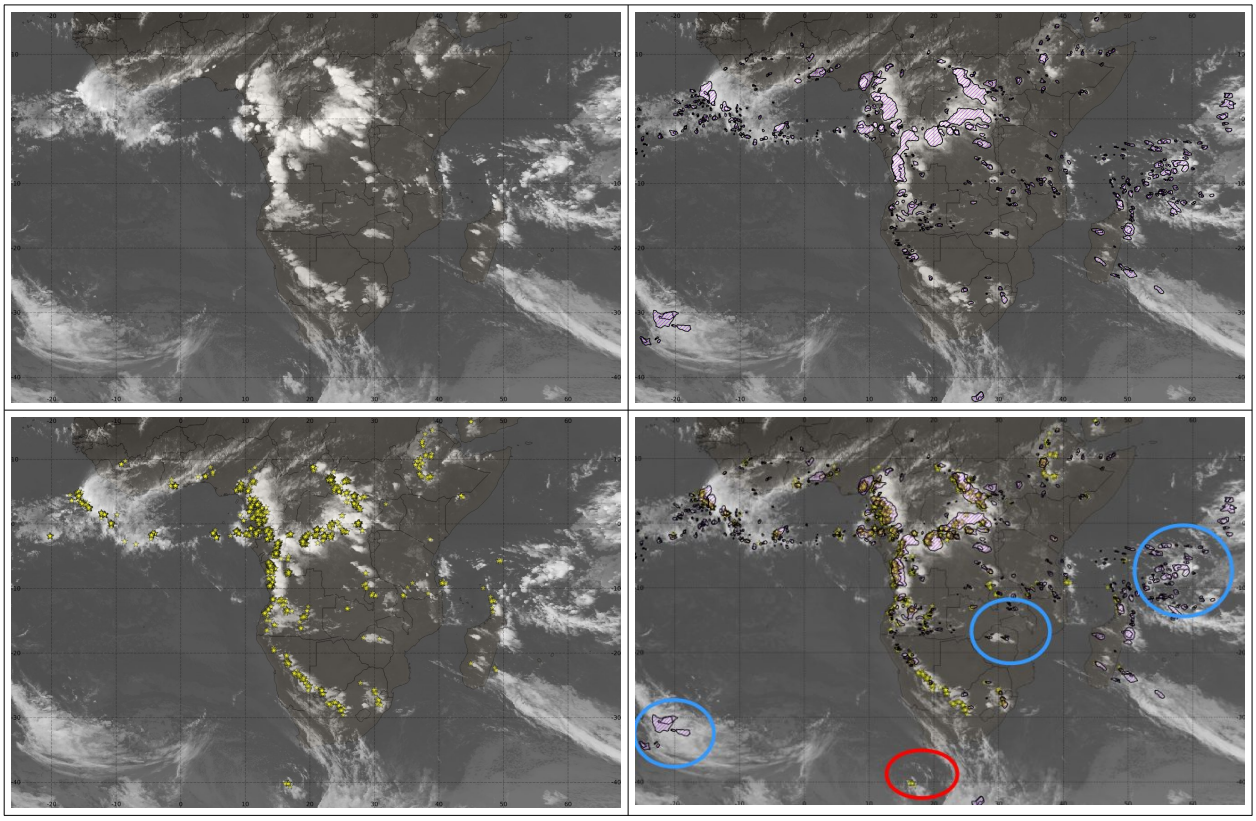

Figure 34: MSG4 case study for 20190419 17h00Z over Africa. IR image (top left) with RDT-CW black-dashed cells (top right), with WWLLN data as yellow stars (bottom left), all data overlaid (bottom right).

A detailed zoom over inland (Democratic Republic of Congo, Tanzania, Zambia), taking into account previous (H-2h) and following (H+2h) electrical dataset is illustrated in following figure. RDT-CW maintains the identification of cloud systems which have been electrically active (yellow circles), and identifies cloud system which will become electrically active (magenta circle). It highlights and confirms the fact that RDT-CW cells are located in active regions, even if not always synchronous with electrical activity.

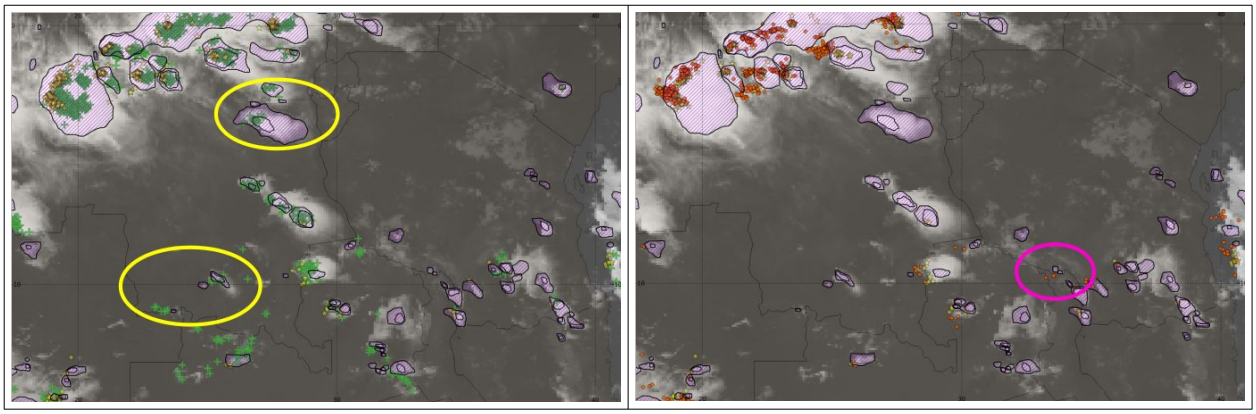

Figure 35: Zoom of MSG4 case study for 20190419 zoomed. 17h00Z IR image overlaid with synchronous RDT-CW black-dashed contours and electric data (yellow stars). Left: adding previous 2h WWLLN data (green crosses). Right: adding following 2h of WWLLN data (orange dots).

This coherence regarding a temporal tolerance is also found in Indian Ocean north-east of Madagascar, where RDT-CW points lots of convective cells. Finally we can consider the behaviour of RDT-CW relevant on those tropical / equatorial regions during a warm season.

3.3.2.2 RDT-CW discrimination using MSG - 9.5E° RapidScan mode

RDT runs with MSG3 have been undertaken over Europe, for 6 dates out of the period used for the tuning, common with but less numerous than for MSG4. Those dates range from May to August 2018.

3.3.2.2.1 Objective validation

The same methodology has been applied than for RDT-MSG4, for quantifying the results against Meteorage&Partners ground truth.

Contingency tables and corresponding scores are presented below. They are determined independently for each full day.

Two situations among six reveal higher false alarms with RDT-MSG-RSS compared to RDT-MSG-FDSS. PODs are sometimes much better than RDT-FDSS, sometimes slightly lower or equivalent. Scores are of course dependent on the situation, generally better for most actives situations.

- Period from 20180526 to 201900806, 6 cases : POD ranges from 61,3 to 68,3% (median 64,3) and FAR ranges from 5,9 to 42,9% (median 11,1%) when moderate GT is considered
- Period from 20180526 to 201900806, 6 cases : POD ranges from 67,9 to 74,5% (median 70,4) and FAR ranges from 7,2 to 50,3% (median 14,1%) when severe GT is considered

Regarding severe ground truth, one can note again an increase of PODs and FARs, more significant for the worse situations. AThe higher update rate of MSG-RSS implies a higher number of diagnosis attempted, which could bring an explanation to the higher number of false alarms compared to RDT-FDSS. But we also have to consider that a higher number of splits and merges can be diagnosed. Situations with embedded convection in particular do probably not benefit from a higher update rate.

3.3.2.2.2 Case study 20180703 over Europe

With this situation, we focus on the problematic of false alarms which could be observed in areas without any electrical activity, more frequently with the tuning for RapidScan mode.

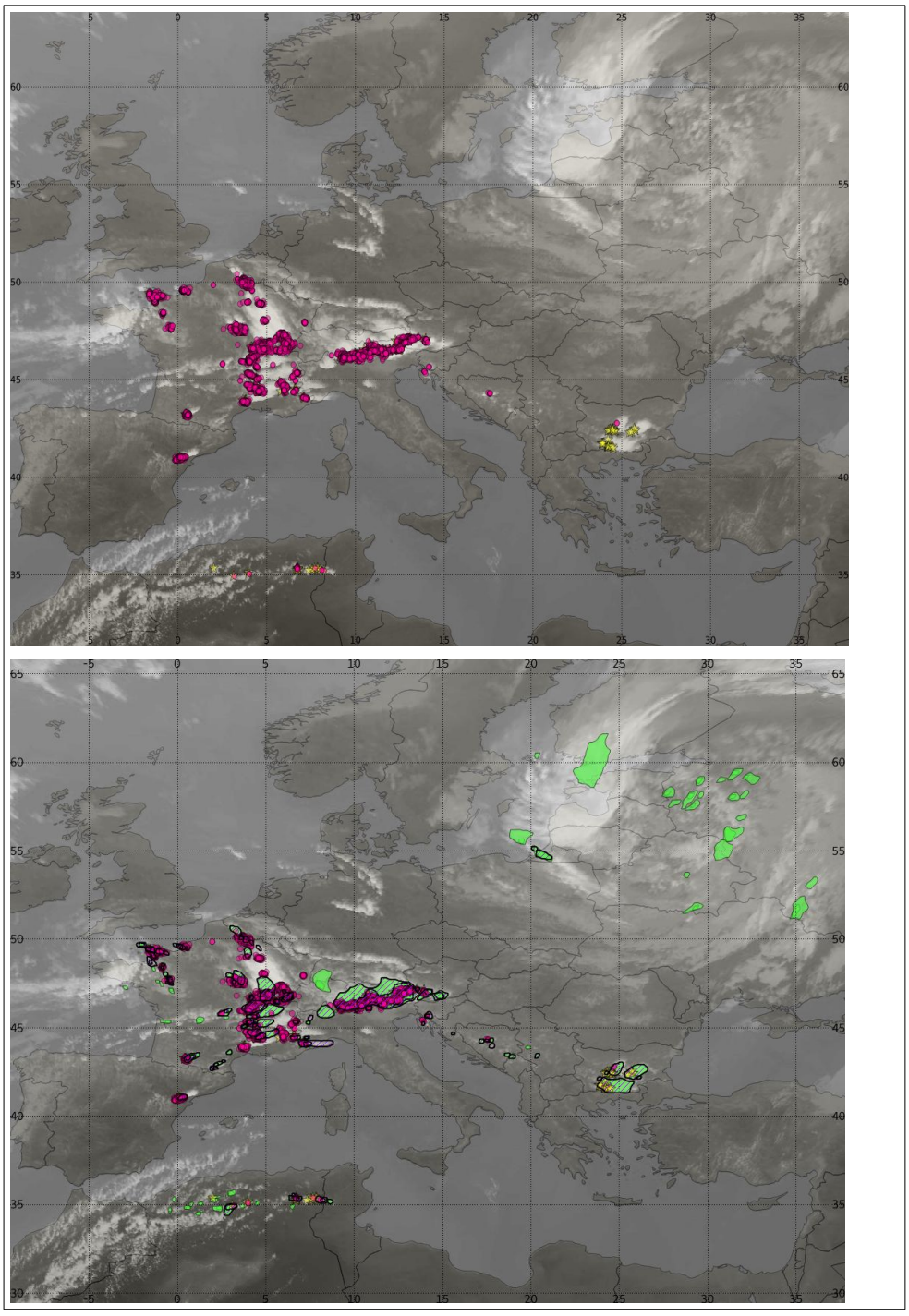

Figure 36: MSG3-RSS case study for 20180703 14h15Z. Top: IR image overlaid with METEORAGE (magenta circles) and WWLLN strokes (yellow stars). Bottom: same with MSG3-RSS RDT-CW v2018 cells (green) and MSG3-RSS RDT-CW v2021 cells (magenta dashed)

Despite a relative good agreement between v2018 and v2021 results over the central convective zone, v2021 tuning obviously improves this point, regarding tree different regions: North-east of Europe where almost all v2018 cells disappear with v2021 tuning, North Algeria where 2021 tuning seems more focused on active clouds, and in the central and west of France, where no convective cells appear in non electric areas with v2021 tuning.

As for other cases, RDT-MSG3-RSS with updated tuning shows improved performances.

3.3.2.3 RDT-CW discrimination using MSG1 - 41.5°E

RDT runs with MSG1-IODC have been undertaken for February 2019 over a limited domain, over which GLD360 data are operationally available at Meteo-France (see next figure). The period is representative of the warm and convective season, and has been extended to catch enough convective systems over the oceanic part of the domain.

3.3.2.3.1 Objective validation

The same methodology has been applied than for RDT-MSG4, for quantifying the results against a ground truth. But in that case GLD360 data have been taken into account in the area illustrated in Figure 37. This ground lightning network is considered to be reliable in this region. Full domain and a reduced domain limited mainly to land surfaces have been considered.

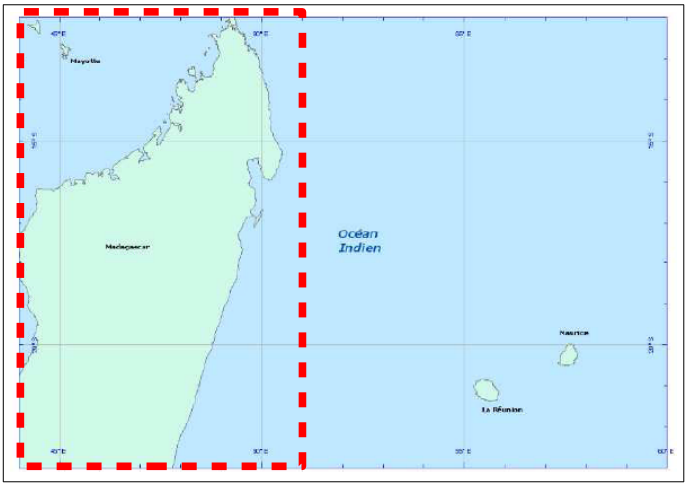

Figure 37: Coverage area of GLD360 for Météo-France, and reduced domain (dashed red) to focus on land area

- Period from 20190131 to 20190228, 29 cases : POD ranges from 64,5 to 92,5% (median 72,5) and FAR ranges from 5,3 to 78,4% (median 42,27%) when moderate GT and a large domain are considered
- Period from 20190131 to 20190228, 29 cases : POD ranges from 64,5 to 92,0% (median 77,0) and FAR ranges from 4,0 to 56,4% (median 18,5%) when moderate GT and a smaller terrestrial domain are considered

It is to note that, regarding the season, the number of convective systems is not so high. But the length of the period makes the results significant.

FARs are considerably reduced when the proportion of terrestrial surface increses in the validation dataset. It suggests that a large part of false alarms are located over ocean. Results appear much better over land. Case study below will confirm the fact that with a lower electrical activity, convective systems over ocean are difficult to assess. The tuning in particular is highly influenced by the electrical activity over land. And an unknown part of “false alarms” could probably be cancelled because obviously convective without electrical activity.

Regarding a severe ground truth lead to the same conclusions (not shown): higher POD, slightly higher FAR, with a more positive impact over land (high gain for POD, low loss for FAR).

As a consequence of RDT-MSG-OI objective validation, one can consider that the tuning phase of RDT-CW discrimination should take into account the nature of the surface (land or sea), with a kind of tolerance still to determine, in order to establish two different statistical approaches. This should also be the case for real-time RDT-CW processing. But the main difficulty will remain the adaptation of the ground truth to take into account over ocean.

3.3.2.3.2 20190221 over South-west part of Indian Ocean

This case study illustrated below in Figure 38 highlights two major features:

1) On one hand RDT-CW seems to be in good agreement with convective clouds as they appear in MSG1-OI IR image

2) On the other hand, this agreement is supported by lightning data over land than over ocean. Out of the GLD360 coverage area (grey shaded), WWLLN lightning data shows weak activity over ocean at latitudes closer to equator.

It confirms how difficult it is to consider a ground truth, depending on sensors (coverage area, detection efficiency), but also on the region concerned: land or ocean surface, equatorial / tropical / mid latitudes.

Nevertheless this RDT-CW discrimination scheme is considered to be satisfactory in most cases

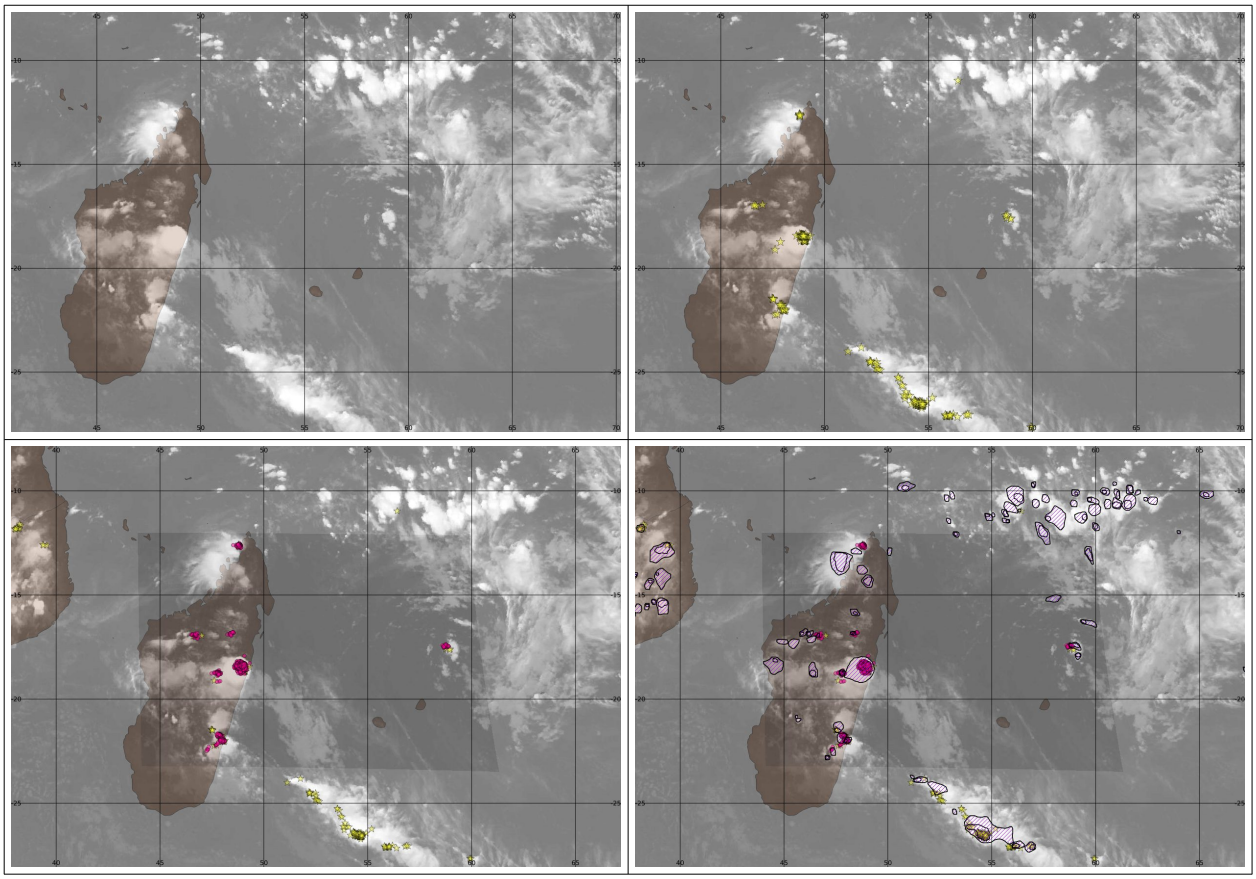

Figure 38: MSG1-41.5E case study for 20190221, 18h00Z slot. MSG1-IR image (top left), overlaid with WWLLN data (top right), with GLD360 data (bottom left, coverage area grey shaded), and with RDT-CW cell contours (black dashed contours)

3.3.2.4 RDT-CW discrimination using MTG-I1 0°

3.3.2.4.1 Objective validation of Yes/No convection decision

3.3.2.4.2 Test data set in September 2024

Regarding the objective validation, runs for MTG-I1 concerns a test provided by Eumetsat on 15th September 2024 the test includes the ESL correction labelled "IQT-I v4 patch#1" but not the tuning of cloud products used by RDT process. Comparisons are made with MSG3 in FDSS mission at that time. Unfortunately the new dataset is relatively poor in terms on convective cases. The synoptic-scale "Boris" thunderstorm populates the dataset but "Boris" is associated to (very) high precipitation events due to a synoptic-scale blocking. Nevertheless, some interesting convective areas can be found for the 15th of September.

Over the Météorage European domain when Meteorage lightning network is used, for the criteria "is the trajectory convective or not RDT operated with MTG/FCI exhibits POD of 24% (30% for MSG3) and a FAR of 72% (25 for MSG3). The poor performance of both RDT are explained by the choice of the Met Situation. Regarding the FAR it will be a clear objective of the next "Day-2" version to reduce it with a specific tuning.

Over the Full disk when LI data are used, for the criteria "is the trajectory convective or not RDT operated with MTG/FCI exhibits POD of 86% (76% for MSG3) and a FAR of 47% (14% for

MSG3). Scores are much better for the RDT operated with MTG/FCI, but FAR remains an issue to solve in future.

Differences in terms of performance regarding RDT operated with MSG/SEVIRI and MTG/FCI are not alarming:

- Due to the lack of stable and large sample of data, RDT operated with MTG/FCI has not been specifically tuned, it inherits from GOES-16 tuning
- On the opposite, RDT operated with SEVIRI takes benefits of many years of tuning and calibration

In the Day-1 approach of v2025, these scores are satisfying.

3.3.2.4.3 20250421 case

The continuity between the RDT product operated with MTG/FCI and the RDT operated with MSG/SEVIRI is evaluated on a more recent study case, this case take benefit of several improvement (FCI and LI input data, tuning of NWCSAF Cloud products). The objective validation is performed both over Europe with respect to the Météorage lightning network as a reference and over full-disk and -still interesting point- Africa with respect to the MTG-LI lightning sensor as a reference (See Figure 39 hereafter). Both RDT products exhibit very good scores over Europe. The FAR is below 10 %, the best product being the one operated with MSG/SEVIRI. The inland diurnal convection over Europe brings very good results for that day. MTG/LI data are used then to assess the skills of RDT over Europe and particularly Africa. The RDT operated with MSG/SEVIRI (resp. with MTG/FCI) exhibits FAR of 16 % (resp. 35%). The POD values are 100 % thanks to the use of the lightning data to drive the convective diagnosis of the RDT cells (only from “No” to Yes”). Overall, the scores are again very encouraging. What’s more, MTG/LI provides for the first time the possibility both to evaluate and then to tune in a MTG Day-2 approach the RDT products over Africa.

WWLLN is long-distance lightning network performance but it provides anyway an indication of RDT-CW performances for FCI full-disk.

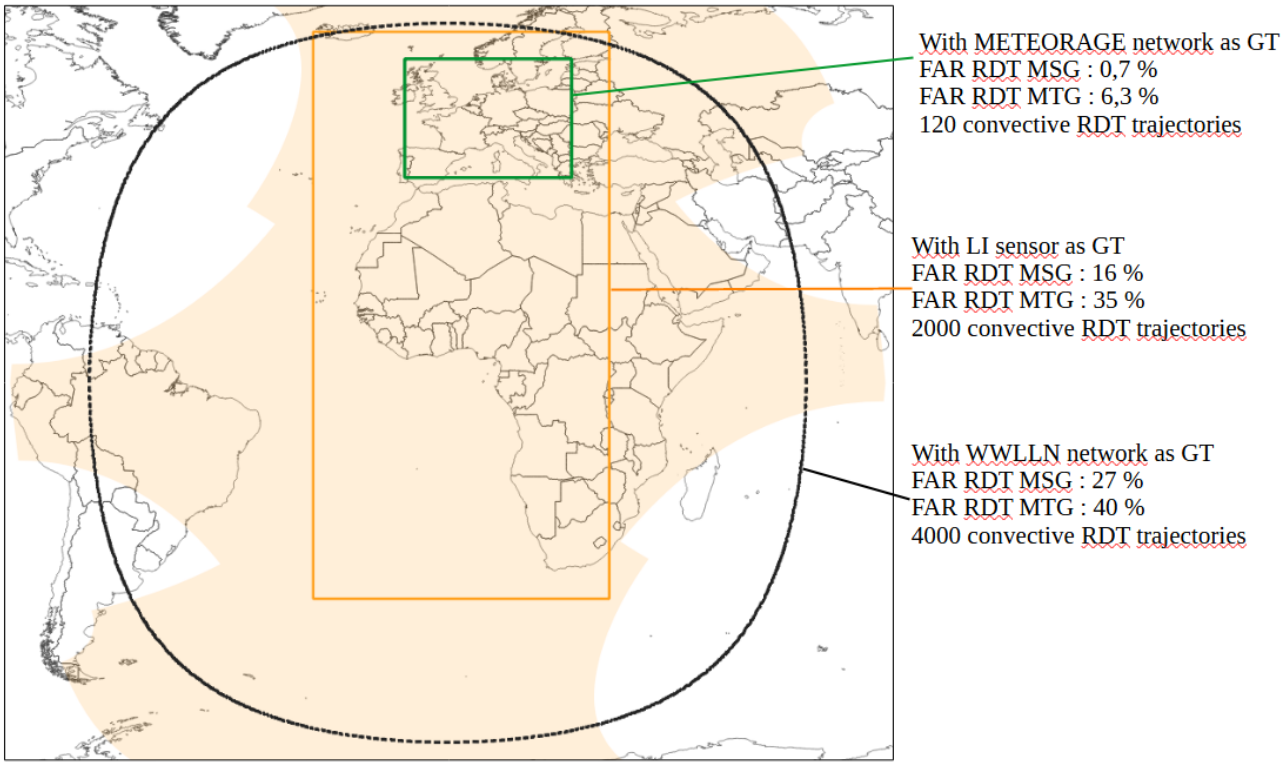

Figure 39: RDT coverage when operated on the Full Disk Scan Service (black line), MTG-LI Field-of-View (orange shading), coverage of the validation of the RDT convective trajectories with MTG-LI flashes as as reference (orange rectangle) and with EUCLID lightning network over Europe as a reference (green rectangle).

3.3.2.4.4 Case studies

3.3.2.4.4.1 The LI positive impact on RDT, Victoria Lake, 20241029

In this experience RDT is operated with two lightning sources, WWLLN and LI.

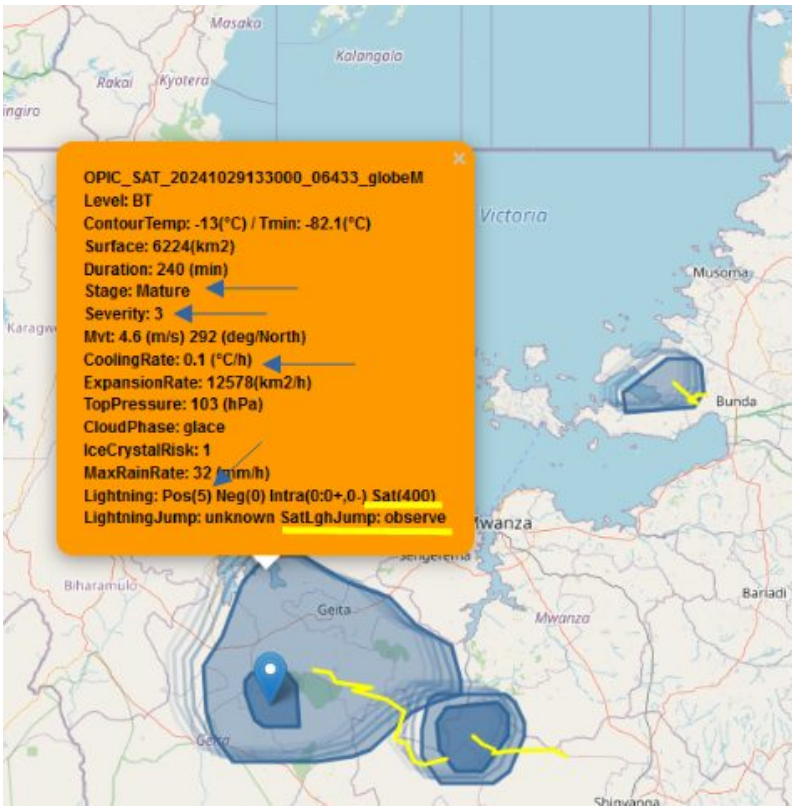

Figure 40: RDT cell South of Victoria Lake 20241029 13:30. RDT is operated with FCI, LI and WWLLN data. Trajectory in yellow, coldest region of the RDT in dark blue, overshooting top (reversed teardrop in blue/white), forecast outline (up to +1h) in grey. The gauge indicates several attributes of RDT

Few WWLLN lightning flashes (5) are paired with the main RDT cell. LI helps to pair a much more realistic number of flashes (400). A Lightning Jump (LJ) calculated with LI flashes is identified (SatLghJump: observe). This LJ contributes to severity attribute (Severity: 3, that is the maximum value in this context): the system is mature without significant cooling rate (0.1°C/h) but still dangerous! No LJ is detected with ground-based lightning network

3.3.2.4.4.2 The Valencia (Spain) MCS, 20241029

Hereafter the figure overlaying several RDT cells exhibit the accurate capture of the outline by RDT. It also illustrates the stationary behaviour of the MCS and the well established and stable convective core in the Southern part, especially for the period 1500Z-1600Z. The Northern/Western parts of the system in the divergence flux are less stable.

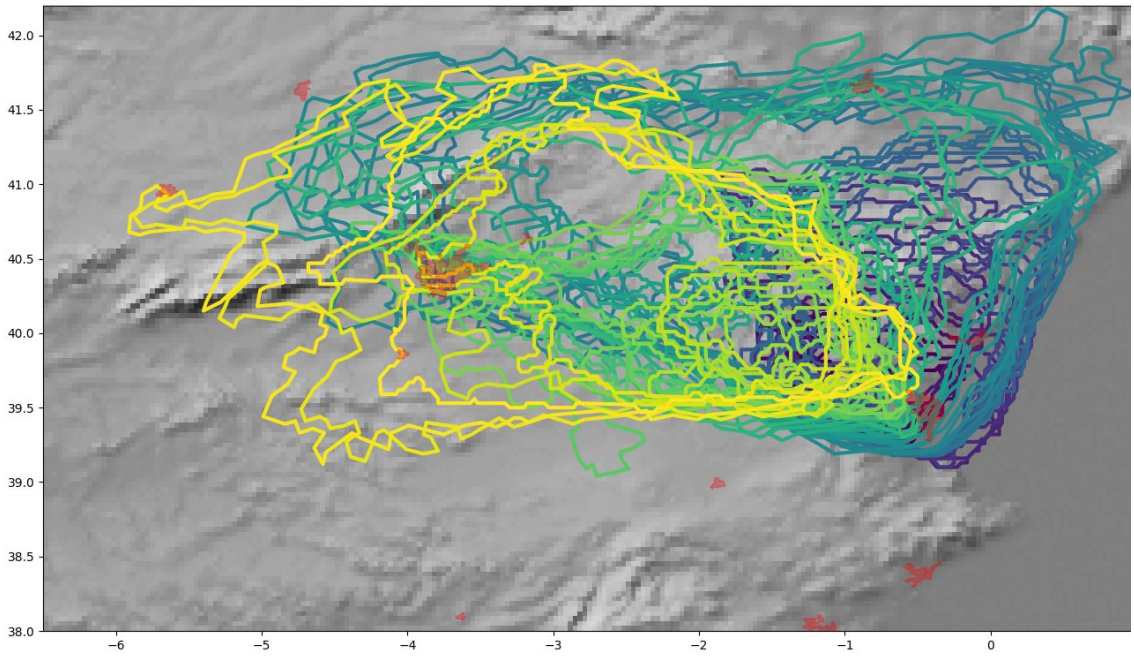

Figure 41: Un-smoothed RDT outlines during the whole Valencia (Spain) MCS trajectory (20241029). RDT operated with FCI, period 1240Z-2350Z

Regarding differences between RDT operated MSG/SEVIRI and RDT operated with MTG/FCI the behaviour are quite the same. RDT operated with FCI tends to isolate a single MCS a little bit later (two systems are identified, then one), but it is not a major issue and can be easily explained by the higher resolution that tends to isolate more towers. Time-series of attributes are quite comparable, except for the OT (see dedicated paragraph on the validation of OT).

3.3.2.5 RDT-CW applied to GOES16

NOAA has undertaken until summer 2020 a high improvement of GLM-GOES16 data, for identifying and qualifying regular and punctual artefacts of lightning data. For that reason, as mentioned in ATBD, those data have been used for a new tuning of RDT-CW discrimination scheme. Those data are also used for validation on cases study.

Following nominal configuration is chosen: 10 minutes update rate and IR10.3µm as main channel, to process RDT-CW with GOES16 ABI data.

GOES19 being committed at the beginning of April 2025, it was not possible to showcase RDT-CW applied to GOES19 ABI. Moreover, as there is no GOES19 dataset available, the GOES16 tuning scheme will first be applied to GOES19 ABI.

3.3.2.5.1 Objective validation

Runs have been undertaken for about 15 days during September 2020, in a large GOES16 sub domain including Tropical and Equatorial regions (Caribbean islands, Central America and North of South-America), continental and oceanic surfaces, as illustrated in Figure below.

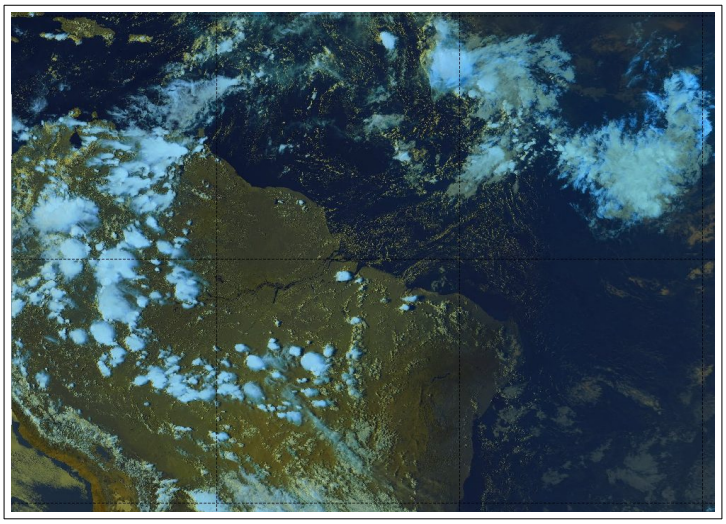

Figure 42: Sub-domain taken into account for replays and objective validation

The same methodology has been applied than for RDT-MSG4, for quantifying the results against a ground truth. But in that case GLM flash data have been taken into account. They are paired with cloud cells within a period centred on the given slot.

Scores are determined for the whole trajectory.

For the period from 20200901 to 2020929, 13 cases, POD ranges from 59,3 to 83,4% (median 73,0) and FAR ranges from 16,6 to 56,3% (median 56,3%) when moderate GT and is considered

Scores against moderate ground truth below highlight the ability of RDT-CW discrimination scheme to reach high PODs. But one can note a relative high level of false alarm ratio, with a high variability. Scores are of course dependent on the situation, generally better for most actives situations. With a modified sample of ground truth focusing on the most severe activity, average POD can rise the value of 80%.

Despite some situations with relative high false alarm ratio, those results can be generally considered as good, because catching a large amount of convective systems. Moreover, as for MSG-IODC, we face the difficulty to validate a convective characteristic with an electrical ground truth over sea surface that may lead to an apparent high level of false alarm even if some suspected features are detected on satellite images.

The possibility with GOES16 to benefit in real time from GLM data with channels from ABI imager, ensures that, with a specific active pairing (GLM data used for convection diagnosis), all convective and interesting cloud systems will be identified.

3.3.2.5.2 Case study 20200919

This situation illustrates the performances of RDT-CW over continental area, and some limitations over sea surfaces.

The overall preview in figure below in the end of afternoon highlights a very good agreement between RDT-CW cells, GLM flashes, and apparent convective clouds in RGB image. Though, oceanic surfaces are associated with RDT-CW detection but very few flashes. And one can also note some obvious misses over land.

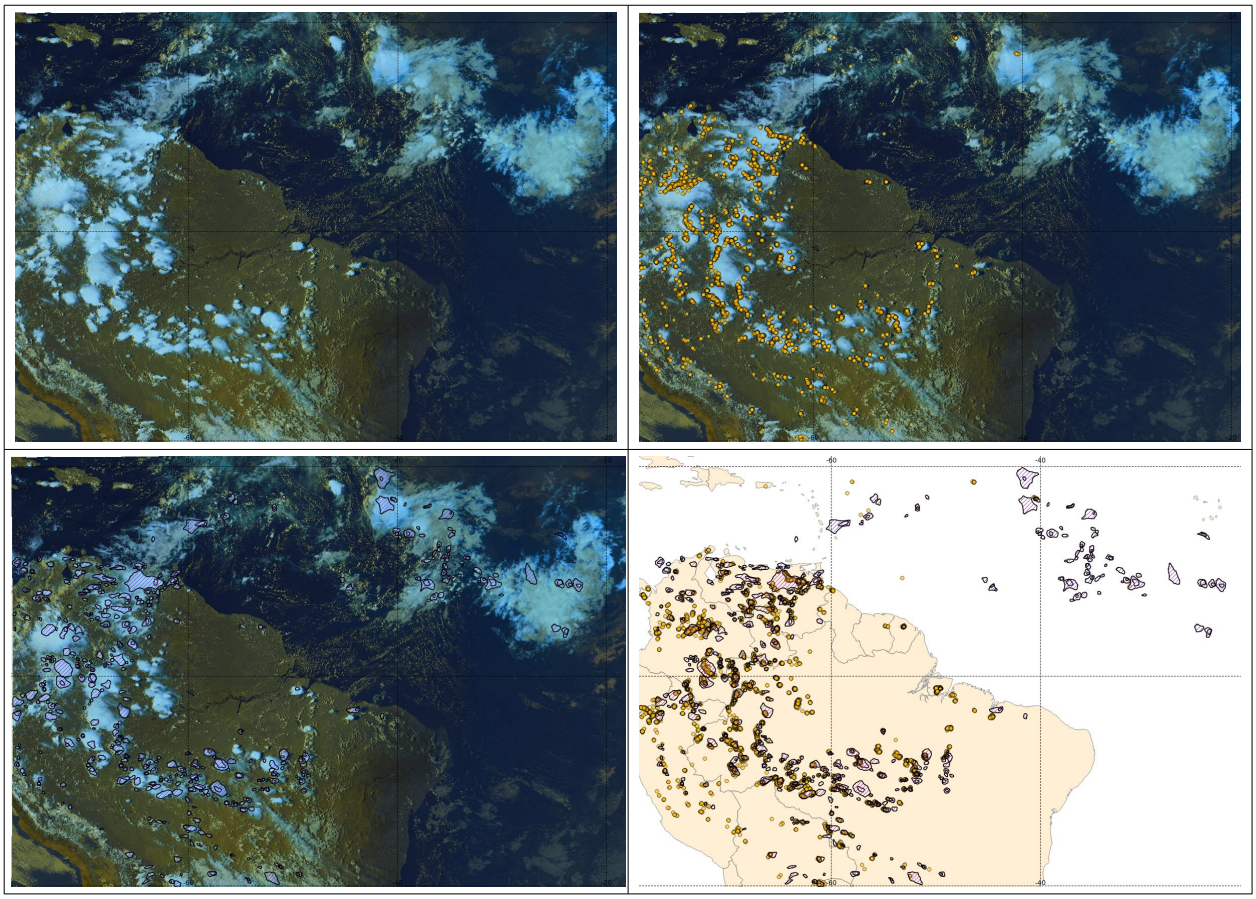

Figure 43: GOES16 case study for 20200919 at 20h00Z. RGB image (top left) overlaid with synchronous GLM (top right, orange dots), with RDT-CW (bottom left, dark shaded contours), and RDT-CW overlaid with GLM (bottom right).

Following steps focus on misses and supposed false alarms, over land and sea. With a zoom on a land area displayed in Figure 44, it appears that, even over land, it is not so easy to qualify with a high level of confidence some misses or false alarms. Some misses are obvious, but we know that the use of real-time GLM data can now compensate this weakness. Other misses are doubtful, because never caught by RDT neither GLM, but getting almost same appearance than neighbouring confirmed convective clouds. On the other hand, RDT-CW identifies clouds which never become electric, but are obviously convective and close to electrical activity.

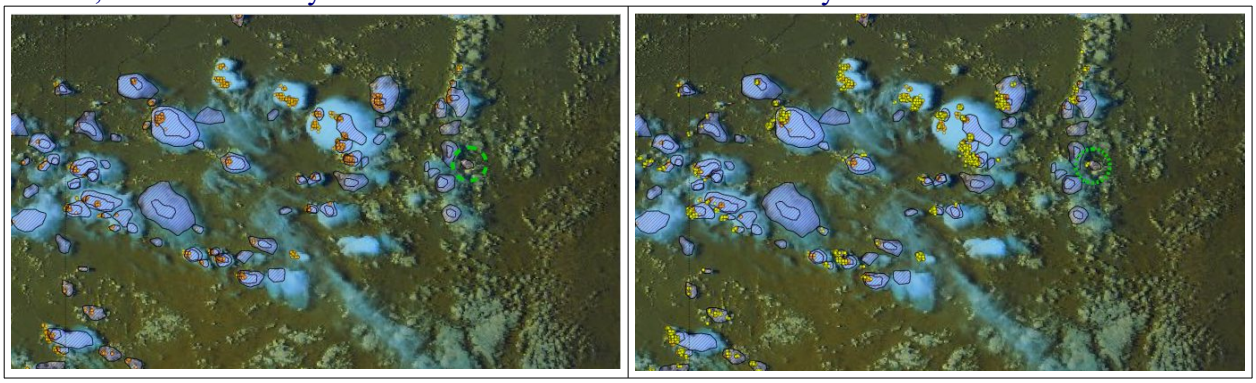

red = miss
dashed red = good non detection or double miss ?
blue = supposed false alarms
green = late hit (RDT after GLM)
dashed green = early hit (RDT before GLM)

Figure 44: GOES16 case study for 20200919 at 20h00Z, over land. RGB image overlaid with synchronous GLM (top left , orange dots), with RDT-CW + next following 30min GLM data (top right, yellow dots), then with cumulated RDT-CW+GLM between 19h50 and 20h30Z (bottom left).

Over sea surface, checking RDT-CW performances with electrical activity is difficult: weak electric signature of diurnal convection over ocean, high distance of the nearest lightning detection point for some ground-based network. With a zoom on a zone concerned by ITCZ, few electrical activity appears and RDT-CW identifies significant cloud systems. Despite some false alarms in complex embedded cloud systems, RDT-CW seems here the best tool to focus on significant phenomena, compared to lightning data only or RGB only.

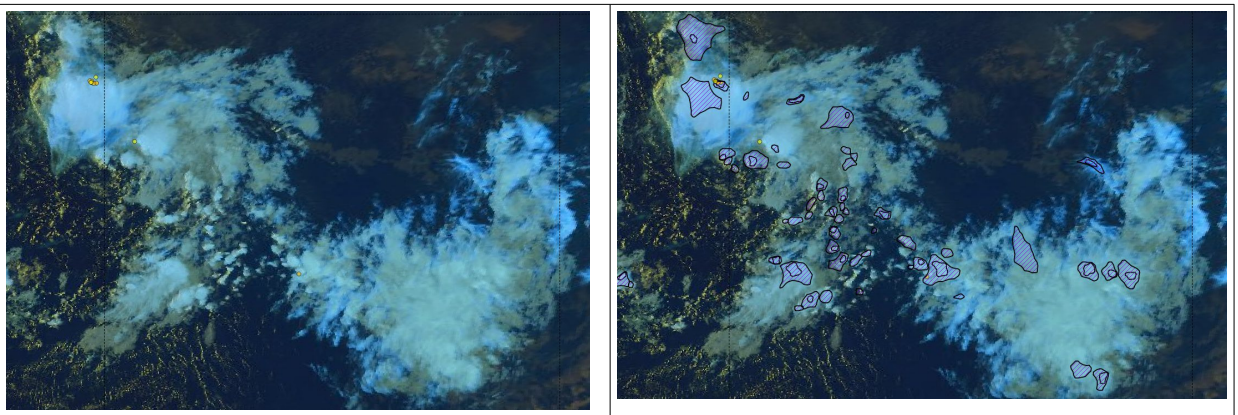

Figure 45: GOES16 case study for 20200919 at 20h00Z, over sea. RGB image overlaid with 40min cumulated GLM (left, orange/yellow dots), with RDT-CW (right).

3.3.2.5.3 Case study 20201123, Caribbean Sea

Here is presented a case study on a slightly different domain over sea surfaces, with moderate convective activity, illustrated in Figure 46 for a beginning of afternoon. Ten-minute GOES16 GLM flashes centred on 20h00Z slot are of limited extent. RGB image like RDT-CW cell contours highlight some other cloud systems obviously of interest. Very few flashes are orphans from RDT-CW cells, and RDT-CW subjectively seems to present good performances.

Supposed false alarms (blue circles) are identified in Figure 46. Moreover, if we have a look on the following electrical activity in following figure , misses (red circles) and early good detections confirmed by GLM (green circles) are highlighted.

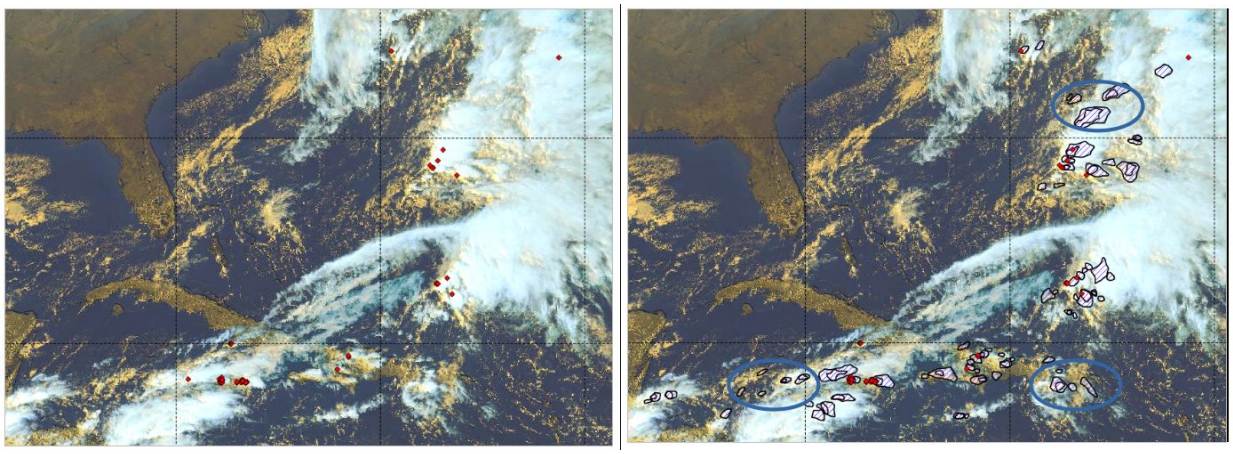

Figure 46: GOES16 case study for 20201123 at 20h00Z. RGB image superimposed with synchronous GLM (left, red diamonds), and with RDT-CW (right, dark shaded contours). Blue circles are supposed false alarms

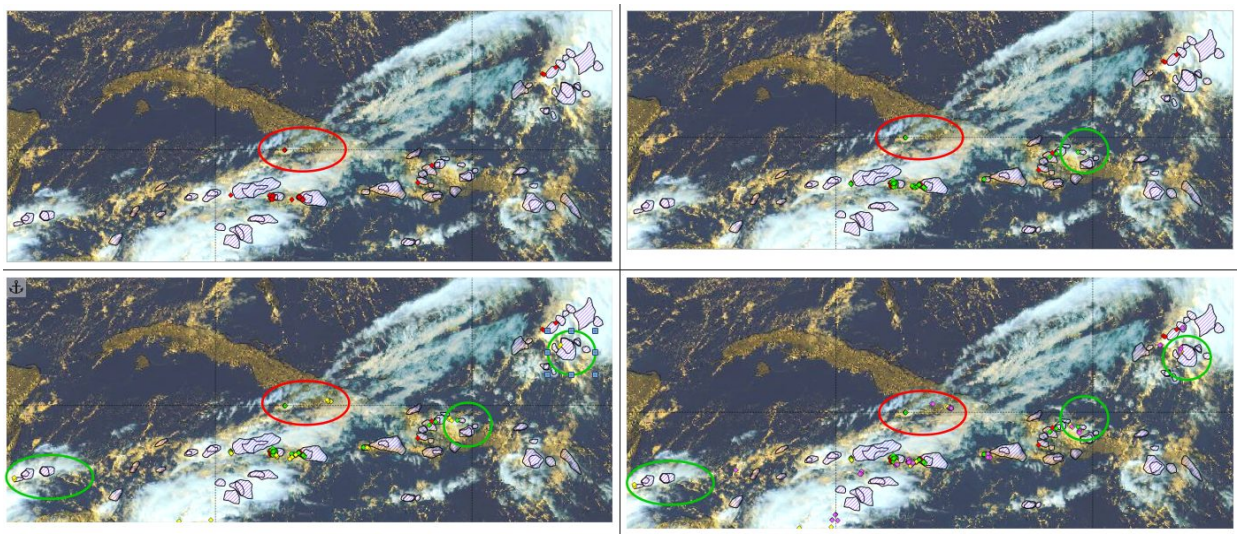

Figure 47: GOES16 case study for 20201123 at 20h00Z. RGB and RDT-CW , superimposed with synchronous GLM flashes (red diamonds), following 30 minutes GLM (green diamonds), following 60 minutes (yellow diamond) and 90 minutes (pink diamonds). Misses (red circles) and confirmed early detections (green circles) highlighted.

For this situation, on this sub-domain, RDT-CW can be considered in agreement with GLM data, keeping in mind the necessity to have a look on the temporal evolution of the activity of ground truth.

Moreover, supposed false alarms (mainly above sea surface) seem associated with cloud cells far from GLM data, but with some texture or feature specific of convective clouds.

3.3.2.6 RDT-CW discrimination using Himawari-8

Validation process for RDT-CW applied to HIMAWARI has been done subjectively, and based on limited number of cases studies. It must be recalled here that Himawari data are made available in Meteo-France for NWC SAF processing at a sub-nominal 20 minutes update rate (instead of 10 minutes). For that reason, specific tuning has not been attempted. This lead us to consider GOES16

tuning, with the necessity to switch to the use of IR10.3 as main channel (instead of 11.2 previously). Lightning data from WWLLN data will be considered as an indication of convective activity, but hardly as a fully reliable ground truth.

3.3.2.6.1 Case study 20210326 over Micronesia region

We focus here on an almost full oceanic tropical domain. Next figure illustrates a mid-day situation, with a numerous apparent convective activity. Nevertheless, this activity is poorly confirmed by the electrical data from WWLLN networks.

The comparison between v2018 and v2021 RDT-CW results show how much both the adaptation of the tuning originally developed for GOES16 and the use of IR10.3 as main channel modify the identification of convective systems. The previous release was known to over-discriminate cloud systems as convective, producing a suspected large set of false alarms. Version v2021 appears as a mitigation of this point.

This release keeps an identification of convective systems which are confirmed by electrical activity (some few misses north of Solomon islands, but already missed with v2018 results), diagnoses most obvious convective clouds and MCSs, and seems to miss only some small growing convective clouds.

For this latter case, it is likely that the 20 minutes update rate at our disposal does not allow to take full benefit from a tuning made with 10 minutes data. However, we consider this release more efficient, keeping in mind the possibility to use lightning data as a possibility to change the the convection diagnosis from “No” to “Yes”.

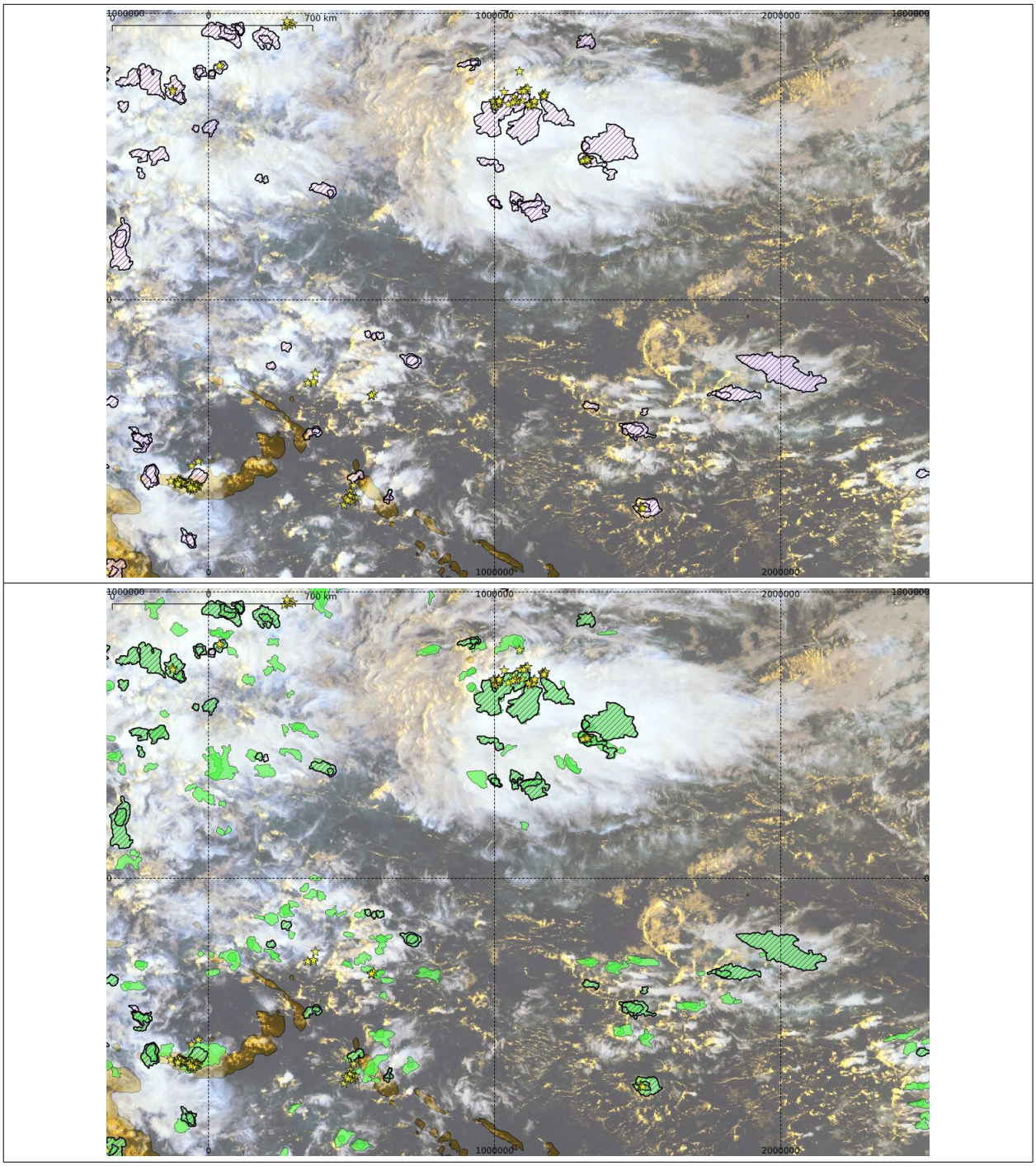

Figure 48: Himawari-8 case study for 06h00Z on 20210326. RGB image with 1h-accumulated WWLLN impacts around 06h00Z overlaid with RDT-CW v2021 black dashed contours (top), and with RDT-CW v2018 light green cells (bottom)

3.3.2.6.2 Case study 20180117 over Indonesia

Figure below illustrates with 06h00Z RGB image over Central Indonesia a large amount of convective clouds. Though, electrical activity is not so spread but rather concentrated in the South-Eastern part of the domain. The majority of RDT-CW cells for this slot are associated with WWLLN impacts and/or with suspected MCSs on RGB image. Highlighted are apparent convective systems

identified by RGB and RDT-CW without electrical activity (green circles), and low electrical activity missed by RDT-CW (red circles). One can note also some false alarms with RDT-CW (blue circles).

But with the use of IR10.3µm channel and GOES16 statistical models, those false alarms seem largely reduced when compared to previous release, and we consider this discrimination scheme brings valuable results when applied to HIMAWARI.

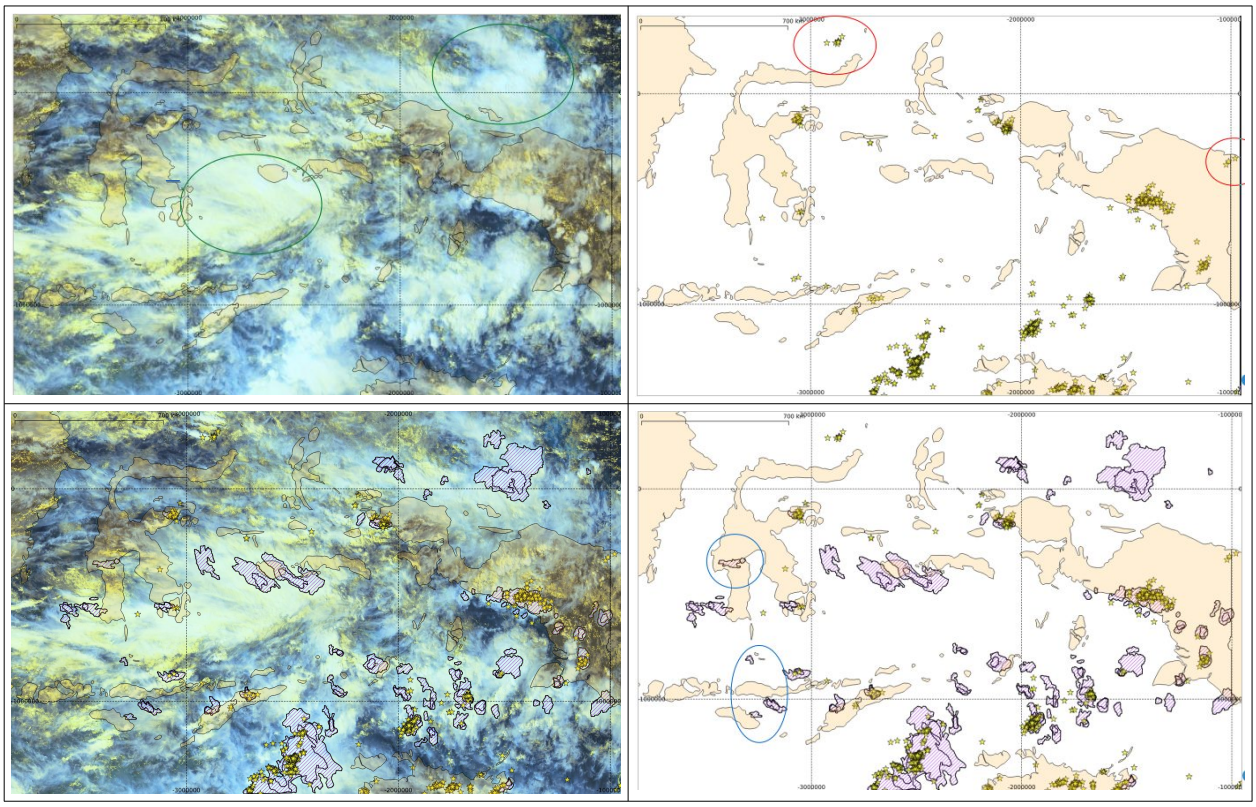

Figure 49: Himawari-8 case study for 06h00Z on 20180117. RGB image (top left), 30min-accumulated WWLLN impacts around 06h00Z (top right), RDT-CW overlaid with WWLLN (bottom right) and all data superimposed (bottom left). Supposed false alarms (blue circle), good detections (green circles), misses (red circles) are indicated

3.3.2.6.3 Case study 20180702 over East Asia

During this situation, convective cells develop over land on the Northern part of the domain, and a tropical disturbance is moving northward in the Southern part, mainly oceanic.

Next figure highlights some misses by RDT-CW, in particular over Mongolia. Even if on the edge of the domain chosen for this case study, those isolated convective clouds should have been identified by RDT-CW. We suspect here a lack due to the sub-nominal update rate at our disposal. Though, this release seems to be more efficient for focusing on convective activity, lowering the number of false alarms regarding previous v2018 product (highlighted with blue circles). This is the case for the head of the perturbation, but also for low clouds over China.

Finally, v2021 discrimination scheme for Himawari seems to help us to lower the number of false alarms, which was an issue.

Figure 51 illustrates an even better RDT-CW v2021 performance, with very few misses and false alarms, and a good identification of all obvious or apparent convective systems. Almost all WWLLN strokes are associated to or very close to a RDT-CW contour cell.

Here again, RDT-CW performs better than previous version.

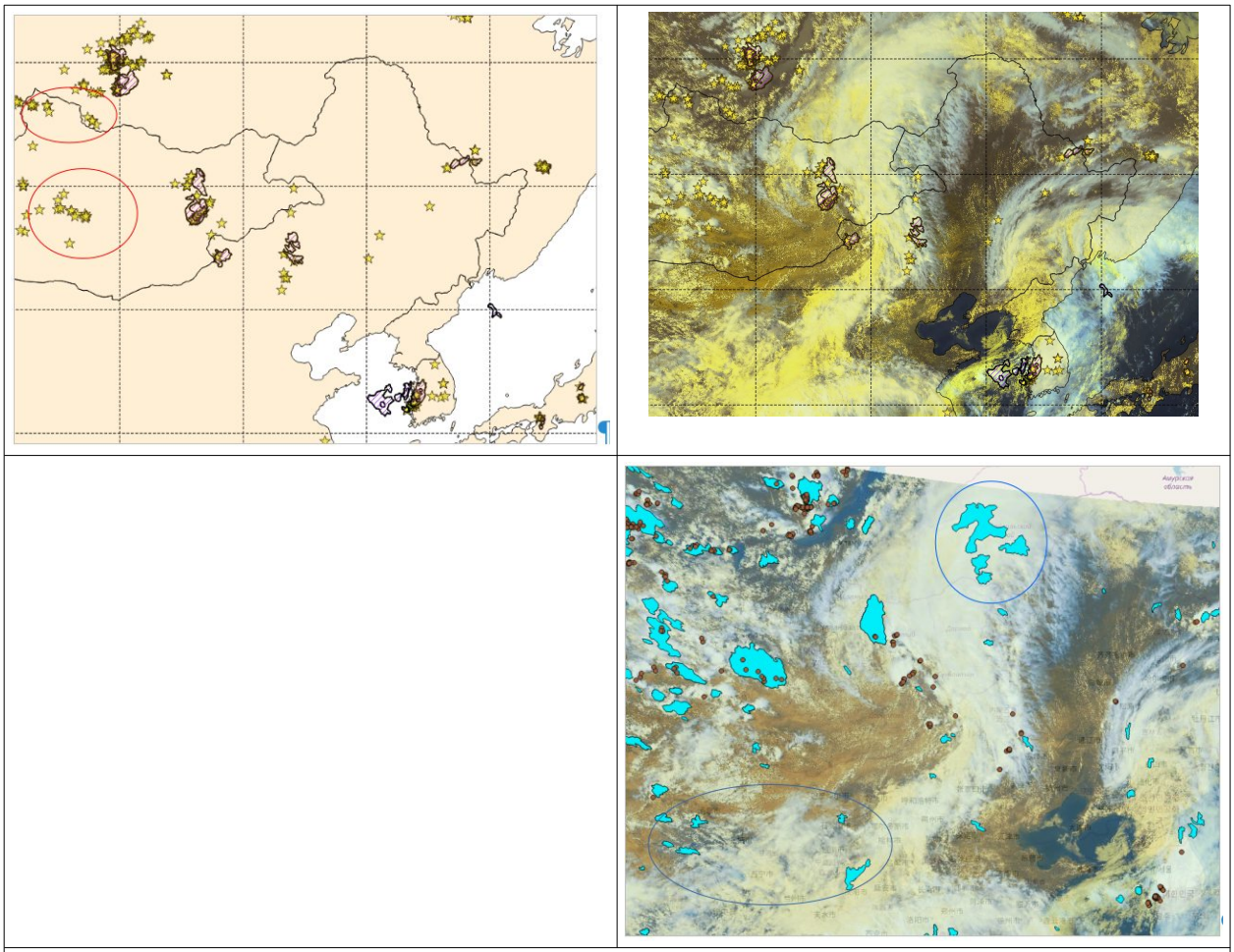

Figure 50: Himawari-8 case study for 20180702 06h00Z. Northern inner land Est Asian domain. RDT-CW v2021 black dashed contours with WWLLN strokes as yellow stars (top left), same overlaid with RGB (top right), RDT-CW v2018 blue cells (bottom right).

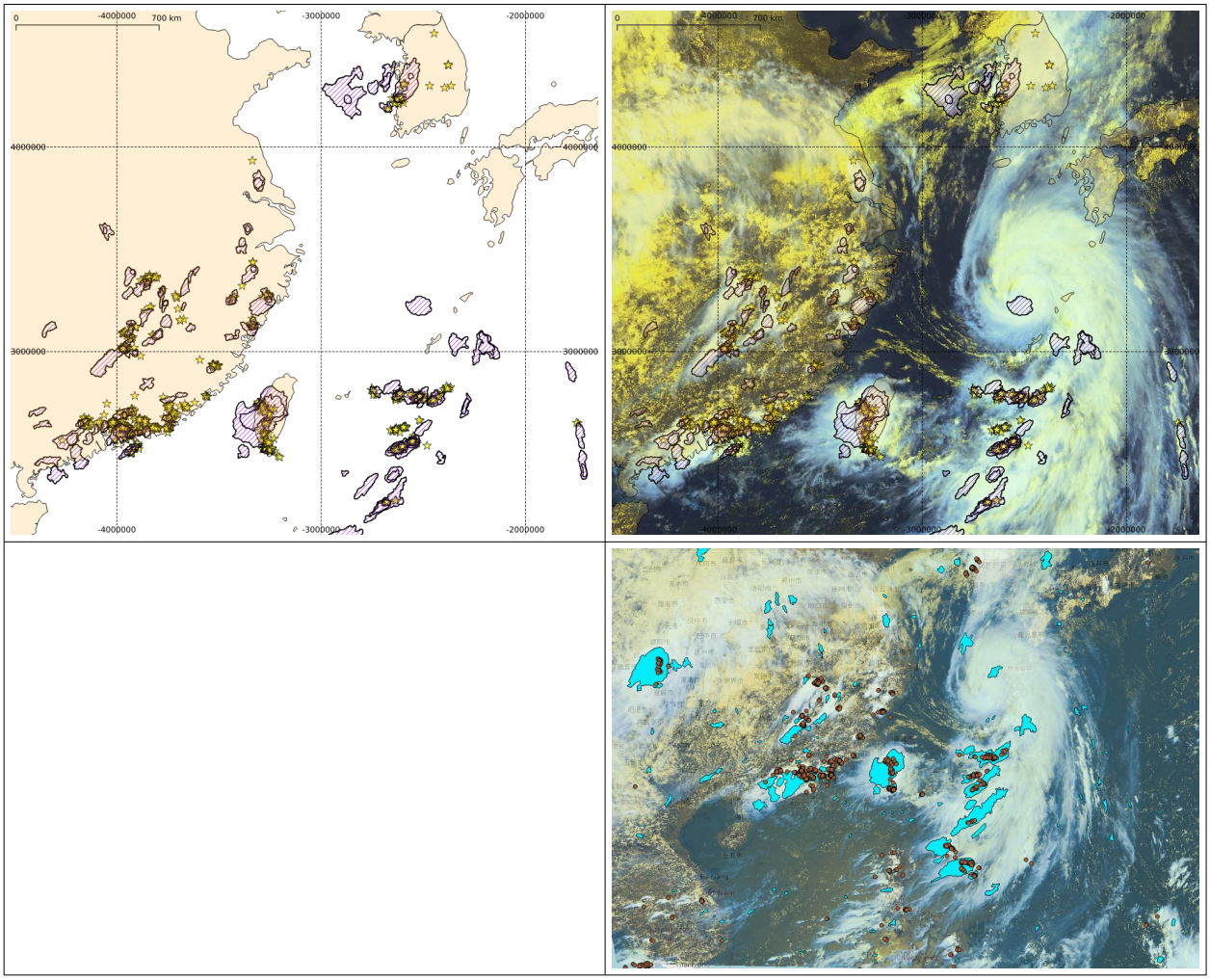

Figure 51: Himawari-8 case study for 20180702 06h00Z. Southern oceanic Est Asian domain. RDT-CW v2021 black dashed contours with WWLLN strokes as yellow stars (top left), same overlaid with RGB (top right), RDT-CW v2018 blue cells (bottom right).

3.3.2.7 RDT-CW applied to GOES17 ABI

As mentioned in ATBD, like for Himawari case, GOES17 data are taken into account at Météo-France at a sub-nominal update rate of 30min, instead of 10min. Moreover, regular ABI cooling problems with GOES17 lead us to suspend any tuning activities with this satellite. Because GOES16 and GOES17 are same generation satellites, it made sense to use GOES16 statistical models for generating RDT-CW with GOES17. For validation purposes, GLM-GOES17 data were used as ground truth for cases study when available in our production centre, WWLLN data otherwise.

With a full oceanic coverage area, difficulties were expected to formally validate RDT-CW against electrical data. Practically, whatever the source GLM or WWLLN, many RDT-CW cells are never paired with flash data, despite convective characteristics on images. Thus, many supposed “false alarms” are generated. On the other hand, one can observe that RDT-CW will highlight most supposed significant cloud systems.

Regarding the fact that now GOES-17 can be used now only for post-processing, the current validation reports only contains one case study, the most recent.

This case study (20210418) focuses on a reduced oceanic domain North of Samoa. For this situation, GLM has been used for validation. Figure hereafter highlights for 21h00Z, relatively numerous and equally-distributed flashes over the domain. Almost all flashes in the period [20h45-21h15] are associated with or close to a RDT-CW cell. Almost all RDT-CW cloud cells correspond on the RGB image to bright cold convective cloud. But not all those clouds become electric (and over oceanic areas electrical activity is lower than over terrestrial areas) . Consequently, despite an apparent very good subjective agreement between RDT-CW and RGB image, the number of false alarms remains high regarding electrical activity. One can note very few misses, all occurring with RDT-CW cloud cells in the vicinity.

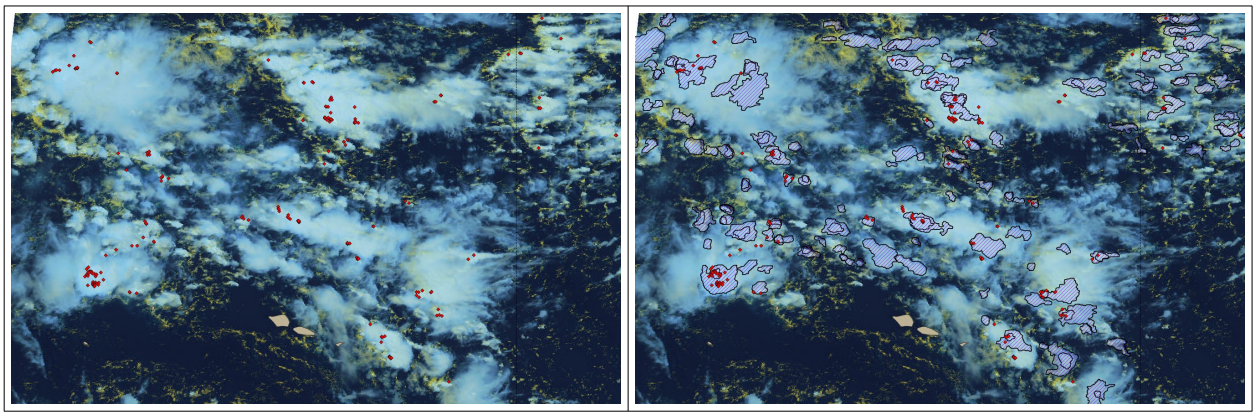

Figure 52: GOES17 case study for 20210418. RGB image with synchronous WWLLN data (left), and with RDT-CW black dashed contours (right).

3.3.2.8 RDT-CW applied to GOES-18 ABI

Like for Himawari case, GOES18 data were first taken into account at Météo-France at a sub-nominal update rate of 30min. Because GOES16 and GOES18 are satellites of the same generation, it made sense to use GOES16 statistical models for generating RDT-CW with GOES18. For validation purposes, GLM-GOES18 data were used as ground truth for cases study.

As illustrated in Figure 53 there is a good general agreement between GLM-GOES18 flashes and RDT-CW cells. Even though over ocean areas, there are less electrical activity. Few false alarms are probably detected along the equator line in the Center Pacific, while some GLM-GOES18 artefacts appear in clear-sky areas.

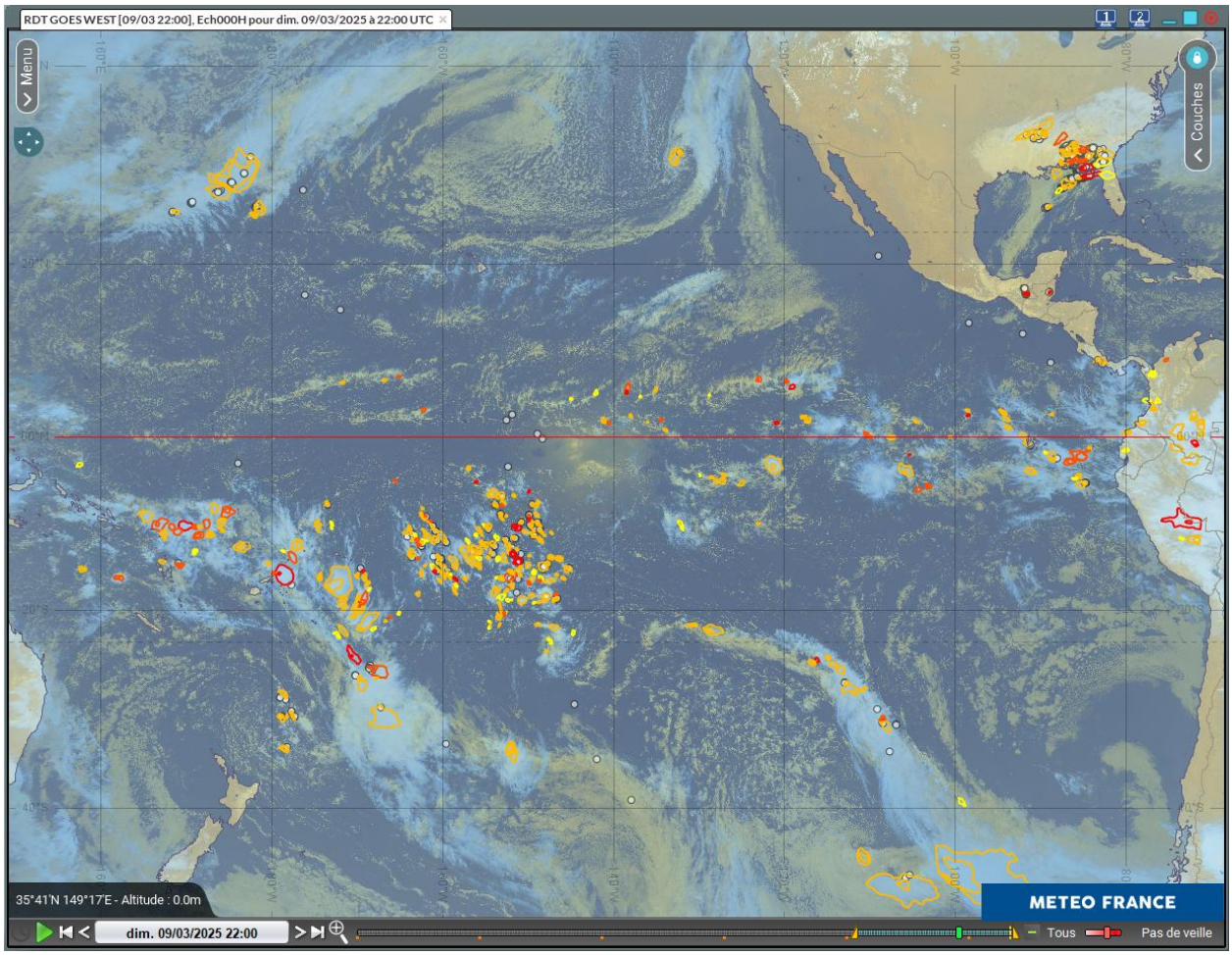

Figure 53: 20250309T220000Z. RDT-CW operated with to GOES18 ABI (colours of the RDT cells depending on the severity), GOES18 GLM (grey circles).

3.3.3 Conclusion about RDT-CW convection diagnosis validation

This validation approach, based on various situations, satellites, geographical regions, and periods, give us enough elements to consider RDT-CW v2021 discrimination scheme as relevant. Those results aren't changed by the current v2025 version dedicated to MTG-I1. Following Figure synthesizes the values. Scores over the larger domain over Indian Ocean are not shown, scores of RDT operated with GOES-18 ABI are not calculated. Scores for MTG are not shown as the RDT has to take benefit of a fine tuning.

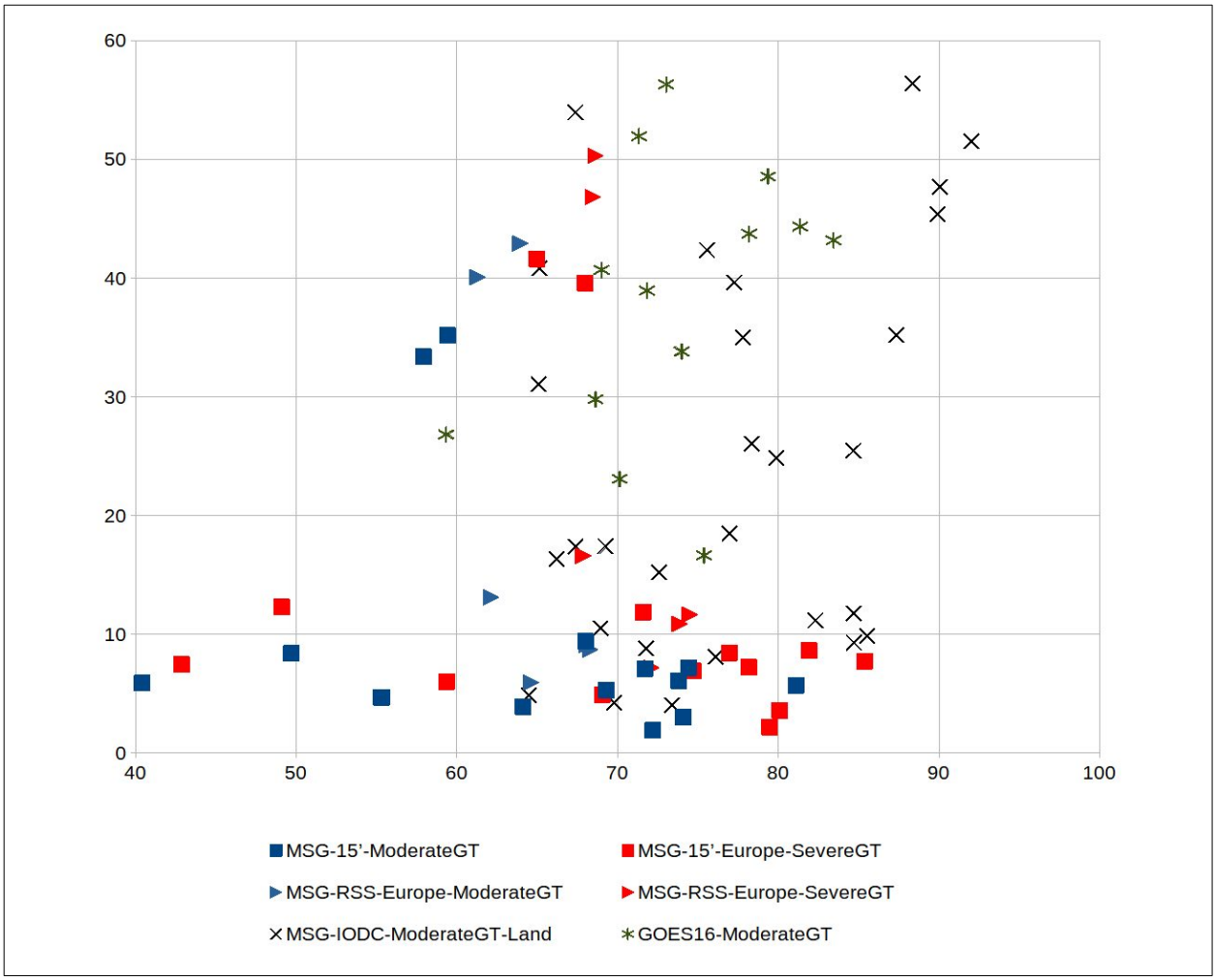

Figure 54: Synthesis of POD (X-axis) and FAR (Y-axis) values for several experiences described in previous sub-chapters. Scores with large domain over Indian Ocean are not shown. One point for one day

An objective validation provides scores reaching the requirements, especially in terms of POD. Some meteorological situations are sometimes associated with FAR under requirements, but average values remain acceptable.

It remains difficult to undertake an overall and global objective validation for all satellites, regions and seasons, regarding the methodology used. Thus a subjective analysis of various sampled situations is necessary to complete this approach.

Case studies cover several meteorological situations: land or sea surface, mid-latitudes, tropical regions, equatorial latitudes, seasons (except winter). An overview of those cases study reveals the ability of RDT-CW to identify most significant convective clouds. If some misses can be observed, the convection can be sometimes identified in the following image. In any case, theses misses would have been recovered in real-time mode if RDT-CW is operated with lightning data used for the diagnosis.

The main issue is the number of false alarms that is sometimes observed in some particular regions. This number seems difficult to lower. False alarms can be obvious or just suspected when no adapted ground truth is available. This is in particular the case for all tropical oceanic regions, where the RDT-CW seems rather adapted to identify all convective clouds, even if they don't evolute towards deep convection.

3.4 OVERSHOOTING TOP DETECTION

3.4.1 Overview

As detailed in [AD.11], Overshooting Top Detection (OTD) in RDT-CW code is undertaken in two steps.

- First, morphological analysis of cloud cells' top allows identifying cell's list of so-called "OT-candidates".
- Then, OT candidates are eliminated or confirmed considering a combination of thresholds of common BT or BTD available for all satellites (this condition has been set more restrictive in v2021), additional information from NWP (gap to tropopause), or from additional channels when available (high resolution visible, IR9.7 or IR13.4)

Criteria are inspired from existing bibliography about OTD, and have been adjusted and subjectively validated on case studies and regarding routine production. With OTD, we have the first use of visible channel in RDT algorithm (VIS 0.6), and possibly high resolution for this channel (HRV for MSG series).

3.4.2 Objective validation vs expert CHMI OT database

3.4.2.1 Context

A CHMI overshooting top database has been made available by Convection Working Group [RD.12]. This data base has been used to undertake a comparison with RDT-CW diagnosis of overshooting top detection. This database, processed on the 20th June and 29th July 2013, is issued from meteorologists' expertise with MSG1 on a 2.5 minutes super rapid-scan experiment from EUMETSAT over small regions in Central Europe.

The objective was first to assess the relevancy of RDT-CW OTD, and then to evaluate in this diagnosis the contribution of a high resolution visible channel as set in v2021 release.

3.4.2.2 Methodology

RDT-CW has been generated on those two periods with a configuration similar to v2021(input from additional optional PGEs, from lightning network and NWP), applied to MSG3 with 15min update rate and MSG2-RapidScan at 5min update rate.

As expected, for those two days, the number of expert OTD increased with diurnal convection. But, in the expert database, the benefit from a high scan rate of 2.5min, and the extended use of high resolution visible channel lead to a much higher number than with a default configuration of RDT-CW OTD in NWCSAF: about ten times more than with RDT-CW-MSG2-RapidScan mode, and almost twenty times more than with RDT-CW-MSG3 15 minutes scan. Moreover, the multiple buddings of an active convective system are all referenced in the expert database while the number of overshooting tops in a RDT cell is limited to two.

In such conditions, a quantitative comparison between expert OTs and RDT-CW OTDs will clearly lead to a huge number of misses. The quantification of RDT-CW OTDs false alarms will on the contrary be regarded with attention. For a reliable comparison, the exact SEVIRI dates have been taken into account. Regarding the mean latitude and size of the domain, we add 1 minute to expert OTs' dates, 3 minutes to RDT-CW-MSG2 OTs in RSS mode, and +11 minutes to RDT-CW-MSG3 OTs.

In the pairing process several tolerance thresholds have been tested , with following final choices:

- Temporal tolerance depending on update rate: 5 minutes for RDT-CW-MSG2 RapidScan, 15 minutes for RDT-CW-MSG3
- Spatial tolerance: 20 km

For a quantitative comparison, dataset without parallax correction have been taken into account, for experts OTs like for RDT-CW OTDs.

3.4.2.3 Example

Figure hereafter highlights the difference between an expert's analysis of OT presence (CHMI database) and an automated one (RDT process). The 16h40Z slot of MSG1 is here associated with 15 expert-assessed OT, most of them associated with obvious buddings. RDT-CW detection process of OT applied to slot 16h30Z (corrected radiometer date 16h41 for MSG FDSS over Europe) of MSG2 was able to detect one overshooting tops for each cloud system. Experts can detect several OT inside a cloud system but there is a limitation of the numbers of OT inside a RDT cell. The most spectacular case concerns the central system where experts have diagnosed eight OT while RDT has detected one.

Two RDT OT out of three are very closed to an expert-assessed OT. The third one is Southward the expert-assessed one, in the colder part of the system. The detection of relatively warm OT is difficult in a automatic process.

For other slots (not shown) conclusions remain the same: when a OT is detected by RDT this OT corresponds to a OT diagnosed by CHMI experts (given a reasonable space or time tolerance). Given the use of CHMI data base for reference, the number of misses by RDT remain significant.

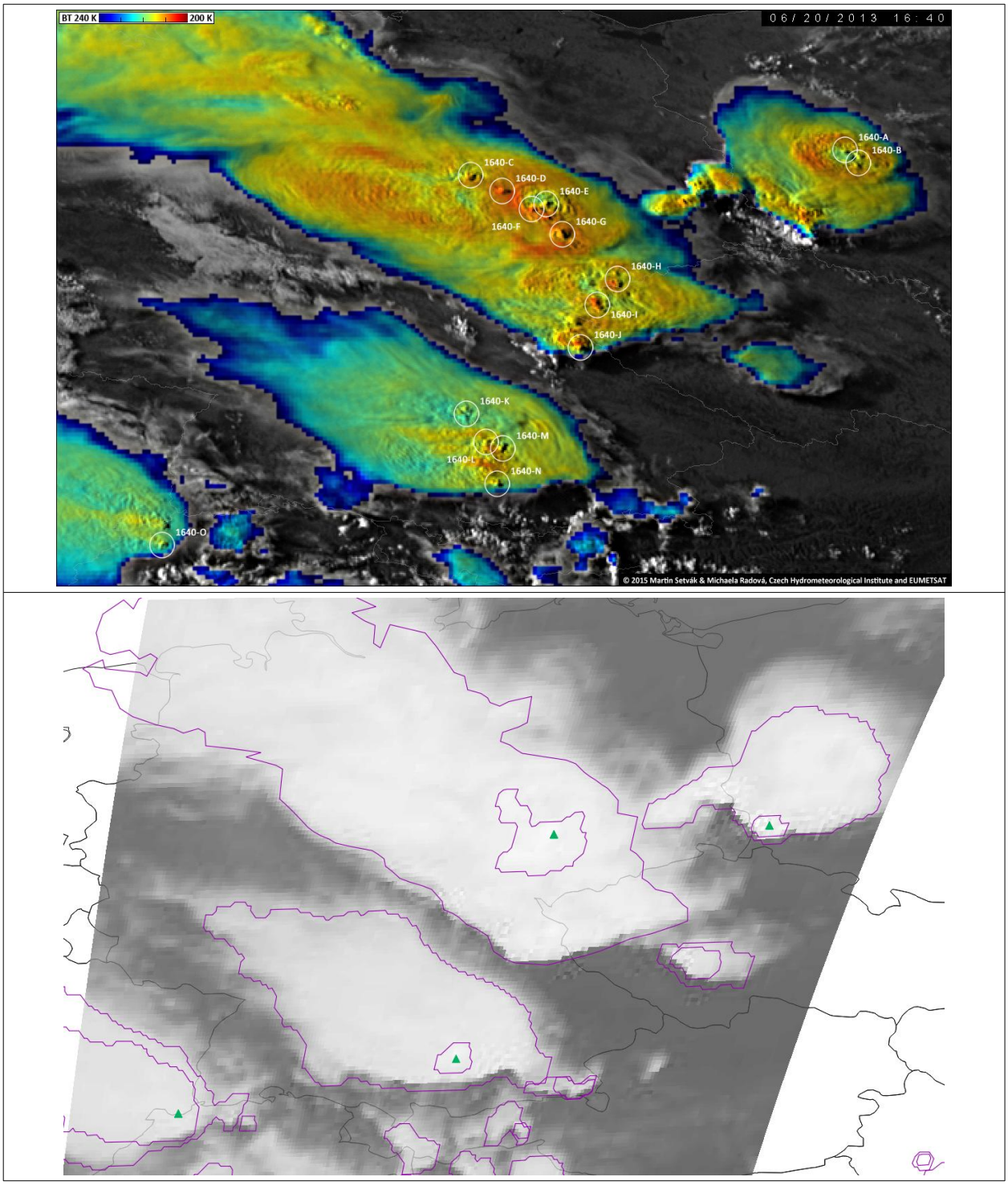

Figure 55: Sandwich image (HRV+IR10.8) with expertised OT for 16h40Z on 20/06/2013 (top). IR image with RDT-MSG cells from 16h30Z slot (+11minutes for exact radiometer date) and OTDs as green triangles (bottom)

3.4.2.4 Results of quantitative comparison

The 20130620 daytime period is much more active than for 20130729, with three times more expert-assessed areas with overshooting top. Nevertheless, the ratio between expert OTs and RDT-CW OTs remains the same. In both cases, the overshooting top activity is concentrated in the afternoon, with a high rise of cases beyond 16h00Z.

For each RDT-CW OT, expert-assessed OTs are searched given a space and time tolerance. There are thus:

- Hits: the number of pairing between an expert-assessed OT and a RDT-CW OT, knowing that a given expert-assessed OT could be paired with several RDT-CW OT
- False alarms: the number of orphans RDT-CW OTD
- Misses: the number of expert-assessed OTs paired with any RDT-CW OT

For this kind of validation, the number of true negatives is of few interest. Thus, we mainly evaluate the POD and the FAR for this comparison.

Despite the good results of the subjective analysis comparing RDT-OT and expert-assessed OT as seen in the previous paragraph, the objective scores calculated for the whole dataset exhibit low PODs and significant FAR (table hereafter). POD are between 10% and 20% and FAR between 22 and 28% with respectively MSG-FDSS and MSG-RSS. It confirms the interest of high-frequency scan for the detection of short-lived phenomena like OT.

Given the ratio between RDT-CW OT and expert-assessed OTs (between 10 and 20 %), the comparison is clearly not in favour of RDT-CW .

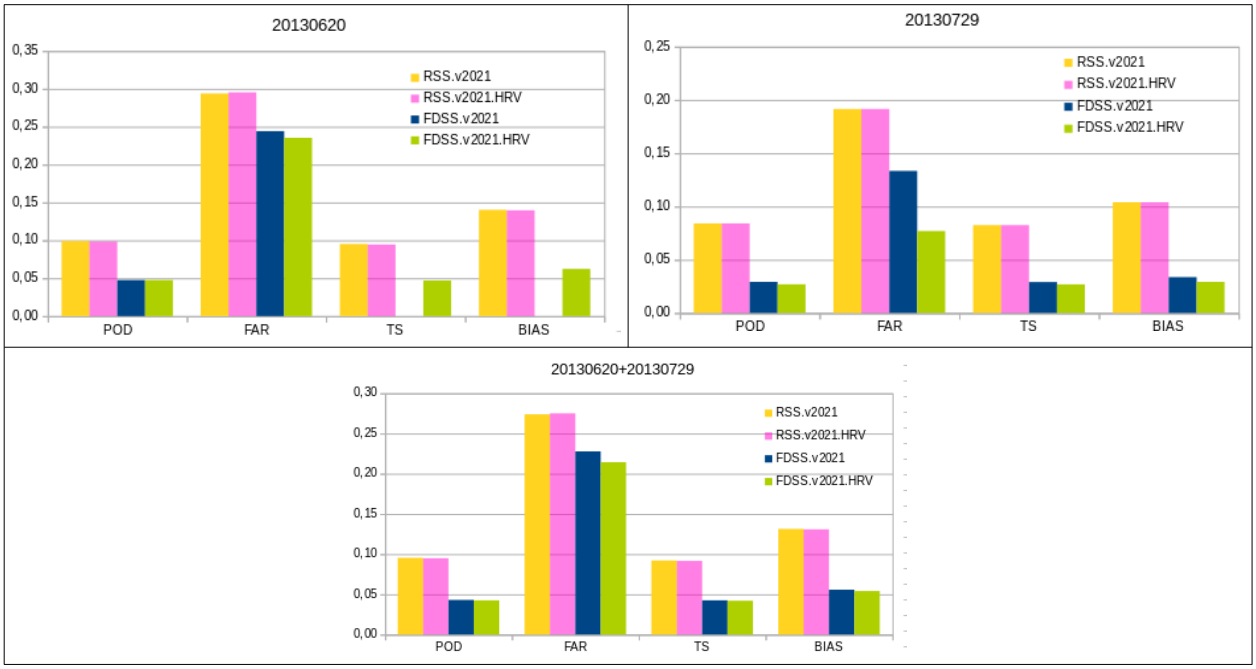

Figure 56: scores of RDT-CW OTD vs CHMI expert OTs for the two periods 20/06/2013 (top left) , 29/07/2013 (top right) and both day together (bottom)

3.4.2.5 Synthesis

The objective verification of overshooting top detection within RDT-CW revealed a significant number of false alarms compared to the number good detections. This was already suspected on operational productions with the previous release.

This release includes modifications in RDT-CW OTD algorithm, which aimed to lower those suspected false alarms, or excessive number of OTD. It appears that mechanically, the number of detections also decreased when compared to CHMI expert OTs database.

The use of high resolution for visible channel very poorly improves the scores of objective validation. Further work appears necessary to validate or improve this approach in the overshooting top detection algorithm.

3.4.2.6 MTG-I1/FCI case

Please note that the threshold concerning BT, BTD, etc. don't depend on the instrument onboard the satellite. In several studies. regarding the OT attributes, developers have noticed an under-detection with RDT operated with MTG/FCI: for example only 4 OT during the MCS of Valencia (from 20241029 mid-day to 20241030 night) and 9 with MSG3 (FDSS) and many more with MSG4 (RSS). A positive bias in BTD4 IR10,8-IR8,7 of MTG/FCI is suspected. The ESL correction implemented in March 2025 didn't improve the OT detection inside RDT cells.

The evolution of number of OT during Valencia case is shown in next figure (Figure 57). One can note that for the capture of OT there is a huge shift between both MSG satellite and also a shift between MTG and MSG. MSG_FDSS exhibits much less than a third OT than MSG_RSS. MTG capture a half of OT captured by MSG_FDSS: considering the scan MTG should have captured 50% more OT than MSG_FDSS. This gives a complex picture where the type of sensor plays a role but perhaps also the age of the sensor and the tuning of the algorithm.

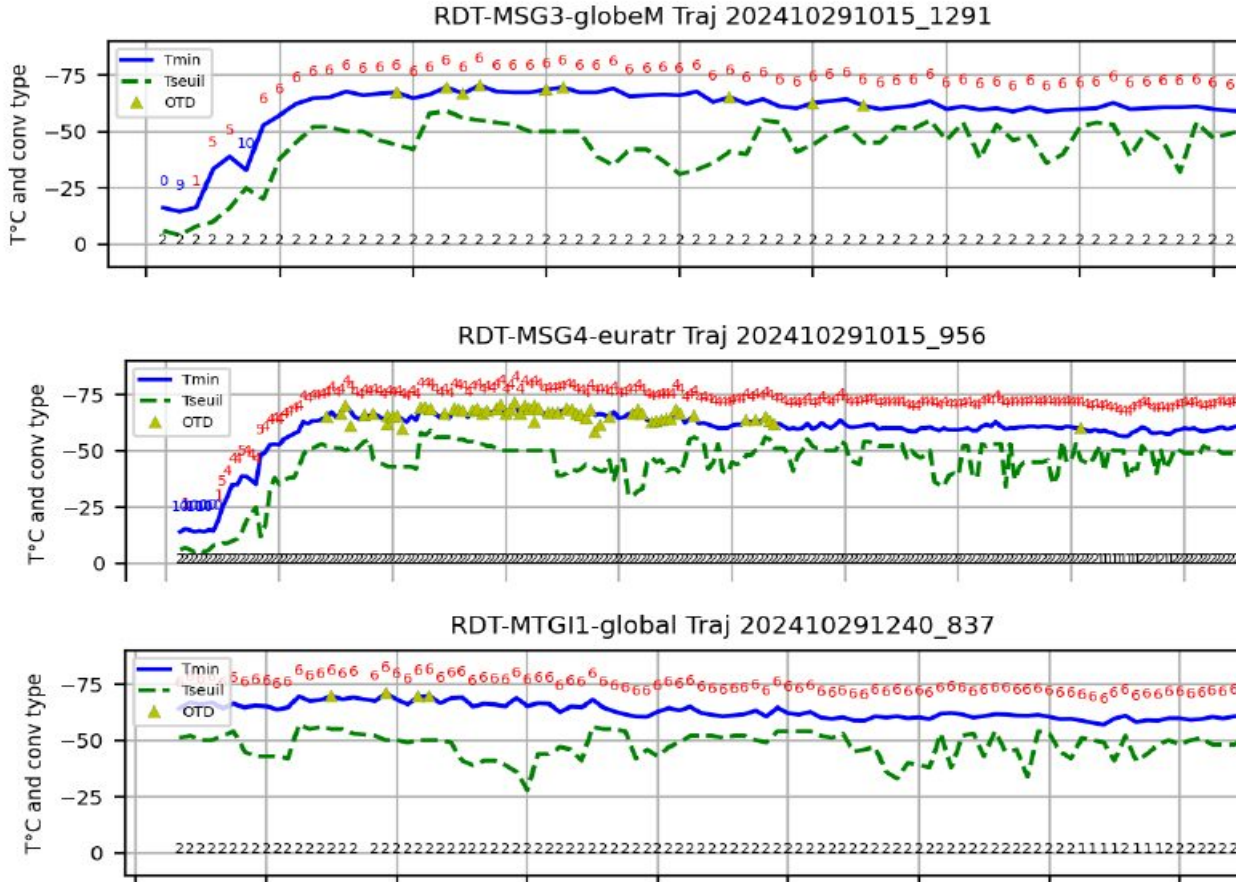

Figure 57: evolution of several RDT attributes for Valencia case (20241029, X-axis time scale relative to the lif of MCS detected by each RDT). RDT operated (from top to bottom) SEVIRI (FDSS), SEVIRI (RSS), FCI. OT in green triangles, minimum temperature of the cell in blue (Y-Axis), other curve non relevant for the analysis

Looking in detail the BTD4 (IR10.8-IR8.7) box-plot during the case of Valencia for the top of RDT cells, similar conclusions can be drawn: differences already exist between two MSG satellites, but differences with MTG are large: the BTD4 value for MTG/FCI is higher and the threshold 0,5°C for the OT confirmation is almost never reached for MTG/FCI giving RDT operated with MTG/FCI less chance to detect OT.

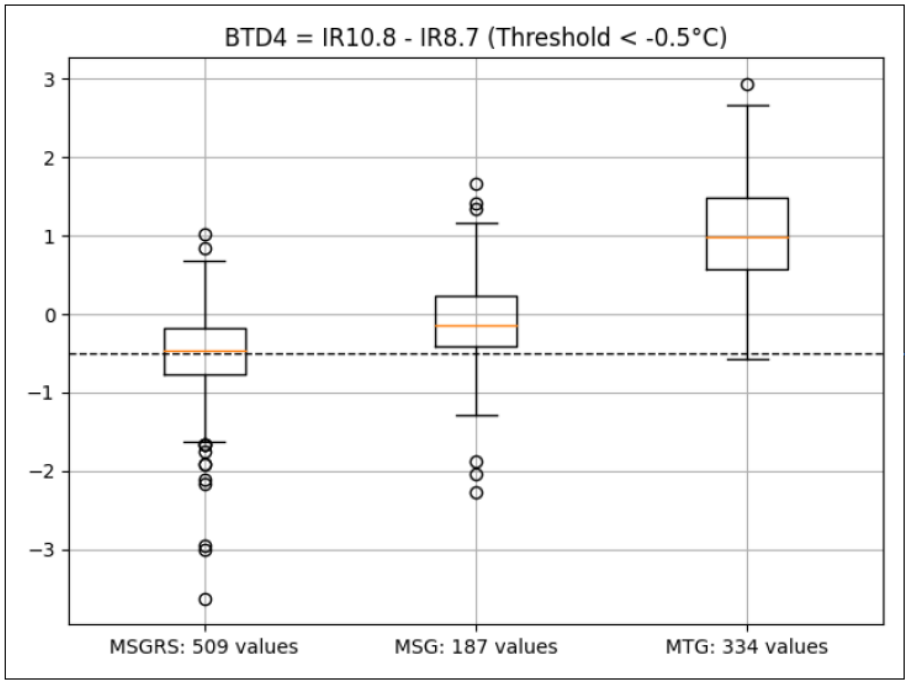

Figure 58: box-plot (median, 1st and last quartiles, first and last deciles and outliers) of BTD4 top of RDT cells during Valencia case

A new version of the OT algorithm has been proposed [RD.15] and the algorithm will be revisited in next versions. One can expect also some changes in MTG input data.

3.5 LIGHTNING JUMP DIAGNOSIS

A lightning jump detection is implemented since version 2018 of RDT-CW. The algorithm takes benefit from full lightning activity (for details see [AD.11]), and relies on minute lightning analysis inside RDT cell for a period of 12 minutes with a condition on lightning rate and lightning rate trend.

The main objectives of this diagnosis are to contribute to severity index and to be used as a precursor of hazards like hail.

The assessment of this attributes needs to access time and localisation of hail events or other strong hazards, and ensure that those events occur on the path of a RDT-CW cell after or at the same time of a Lightning Jump (LJ) LJ diagnosis. It also needs to take benefit of an efficient and reliable lightning network.

Up to now, only some subjective validations of this attribute have been attempted on cases study over France and neighbouring countries, using Meteorage lightning network for RDT-CW, and following references as ground truth for validation:

- Météo-France HYDRE product over France, which includes an Hydrometeor diagnosis thanks to data fusion with data from radar, satellite, NWP and observations. This product is updated every 5 minutes, and provides reliable diagnosis of medium/large hail
- ESSL European Severe Weather Database (ESWD) over a larger domain, with reports of severe convective weather events, like hail, wind gusts, tornadoes, lightning damages, etc.

Hereafter are presented some cases study using those ground truths.

3.5.1 Case study 20180529 over France and Benelux

Figures below highlight RDT-CW cells associated with Lightning Jumps diagnosis prior to hail events from HYDRE and/or ESWD severe weather events.

A comparison with HYDRE product shows a subjective good collocation between hail diagnosis and RDT-CW cells associated with LJs. Even if it is still to be confirmed, LJ diagnosis seem here to be sometimes precursors of hail events.

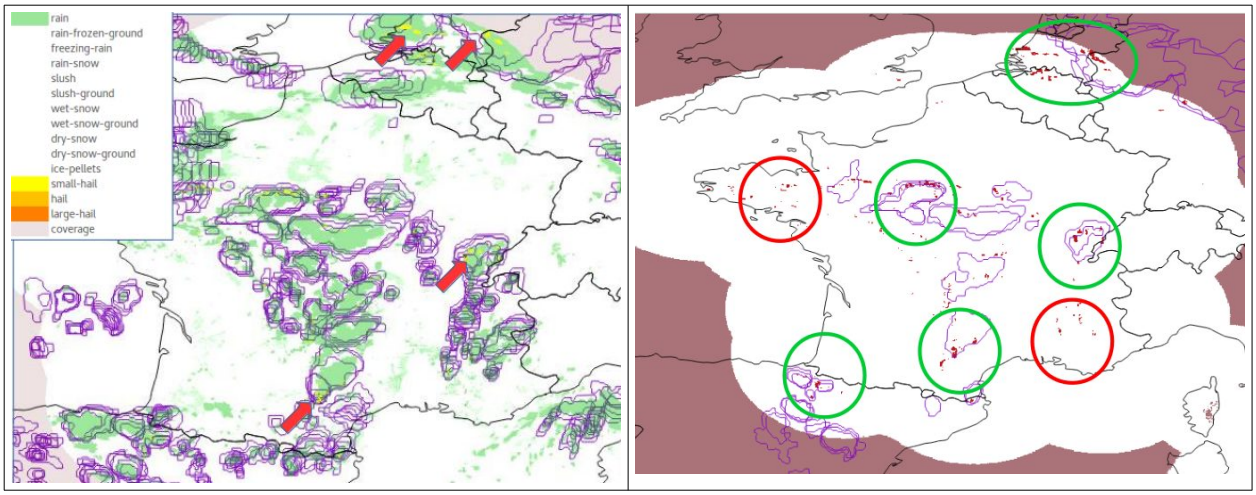

Figure 59. 20180529 Case study. Left: cumulated [15h30-16h00] RDT-CW cells overlaid with [16h00-16h15] HYDRE product. Right: filter on RDT-CW cells with LJ and on hail diagnosis with HYDRE (red pixels for small/medium/large hail classes)

The same situation is regarded below through ESWD severe weather events over Benelux.

Regarding RDT-CW cells associated with LJ vs ESWD convective reports (wind gusts, hail, lightning, tornadoes), one can estimate that most severe weather events find a correspondence with previous RDT-CW with LJ. There is a subjective good pairing, even if numerous RDT-CW cells with LJ are not paired with reports. It is however difficult to conclude if this is due to lack of observation or to RDT-CW false alarms.

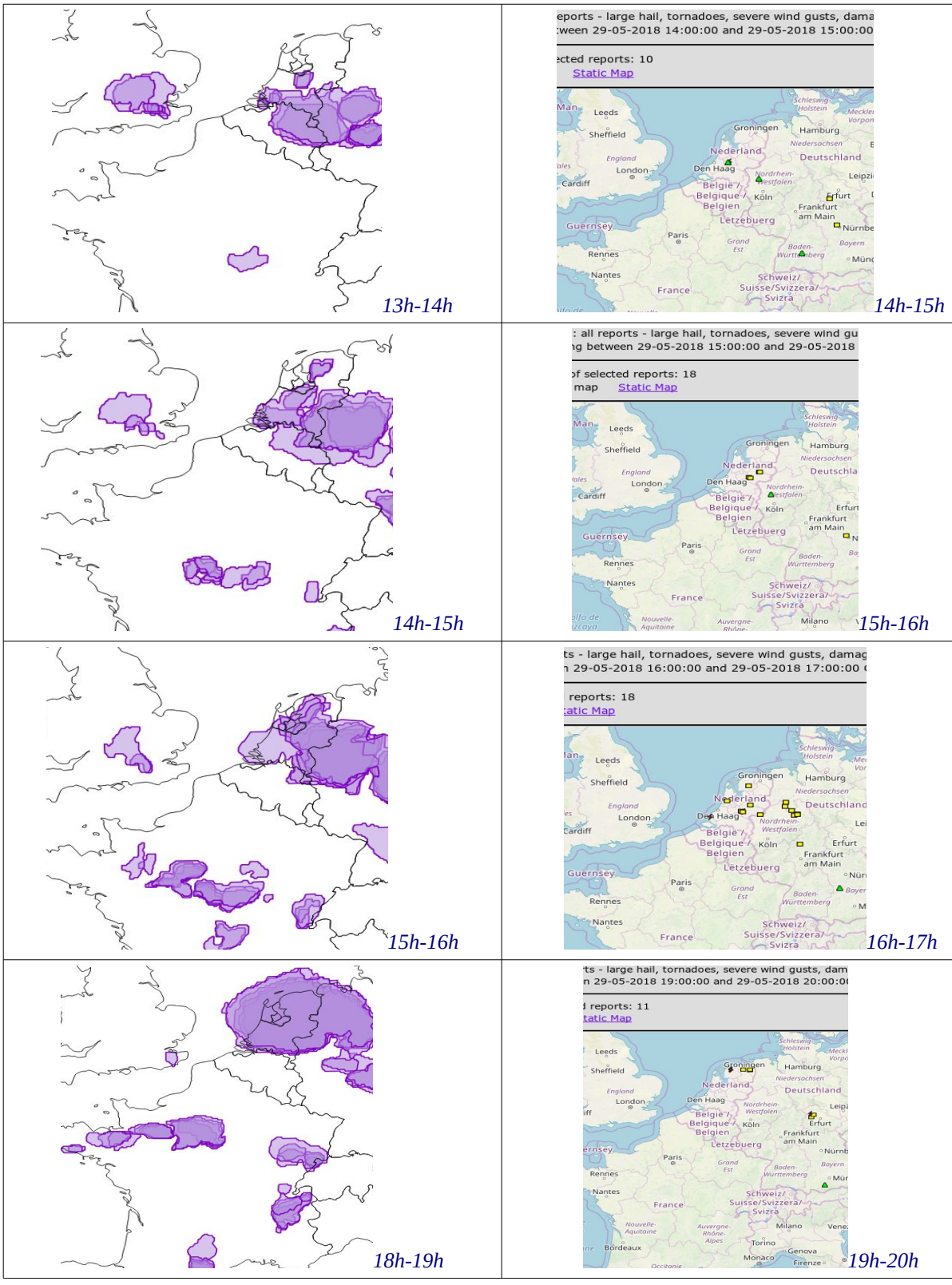

Figure 60. 20180529 Case study. RDT-CW cells with LJs (left column) , consecutive ESWD severe weather reports (right column)

3.5.2 Case study 20190809 over France

In this situation, a south-west/nord-east axis of convection is observed in the end of the afternoon. Regarding the data accumulated over a 16h00Z-19h00Z period, pairing RDT-CW cells associated with LJ and medium/large hail diagnosed with HYDRE product, we can note a high level of matching.

Here again, despite some isolated hail pixels not paired with RDT-CW cells, and suspected false alarms South of Pyrenees, the situation appears favourable for considering LigntingJump diagnosis as relevant.

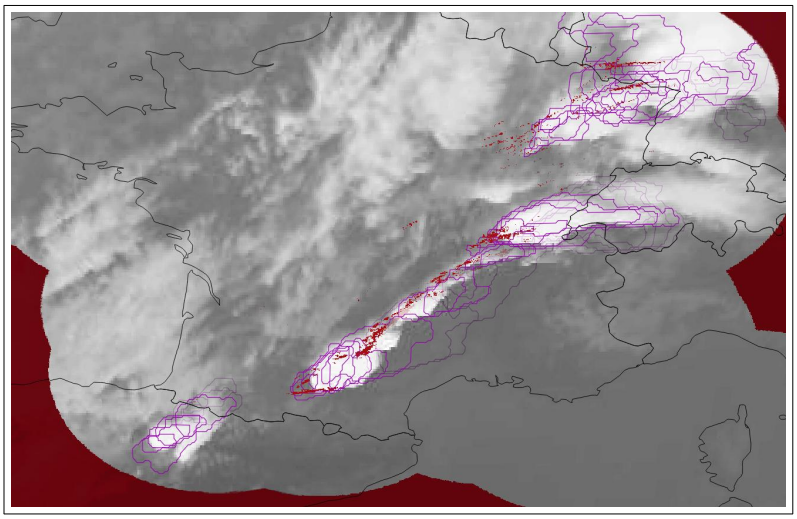

Figure 61: 20190809 16h-19hZ case study. Accumulated RDT-CW cells with LJ (magenta contours), and accumulated medium/large hail pixels from HYDRE (red pixels)

3.5.3 Applicability to GLM

Lightning sensors like GLM or LI provide a continuous and large-scale measurement of electrical activity of cloud systems. This activity is quantified in events, groups and flashes, but without discrimination of polarity.

RDT-CW is operated every 10 minutes with GOES16, with high rate netCDF GLM in input data. In order to eliminate artefacts, NOAA quality code is used for the pairing between GLM flashes and the cells. Lightning jump diagnosis is applied with the same configuration (parameters thresholds) as for ground lightning data.

In the absence of ground truth, this diagnosis with RDT-CW applied to GOES16 must be regarded with precaution. The number of co-located flashes can sometimes be very important with a lightning sensor, and the analysis of a 1minute lightning activity of a RDT-CW cell seems to provide a much larger number of lightning jumps.

In the example below, a RDT-CW cell over Bolivia lasts from 06h00Z to 16h00Z, is electrically active with multiple overshooting top detection, and many lightning jumps during its entire tracking (almost twenty).

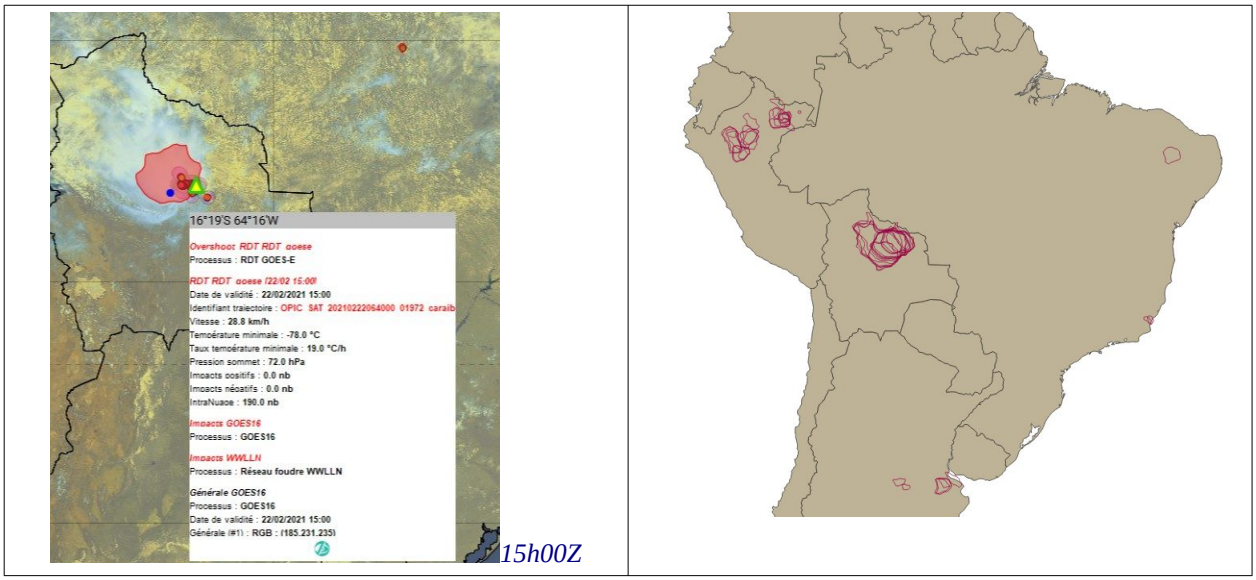

Figure 62: 20210222 case study with GOES16. RDT-CW cell over Bolivia at 15h00Z (left) with 190 paired flashes (here simulated as WWLLN) and OTD (yellow triangle). [06h30-16h00Z] cumulated RDT-CW cells with diagnosis of lightning jump during the period

The ten minutes time-series below (top graph of next Figure) shows two main peaks of increasing activity, but the RDT-CW lightning jump algorithm apparently "lights on" for more than twenty slots, almost continuously.

A deeper analysis of the 1 minute flash rate (or FR) highlights in the middle graph the necessity to adapt the configuration of the algorithm. Significant rises of electrical activity can be estimated once FR is above 20 min^{-1}, and not 10 min^{-1} as in the default configuration of the algorithm. With a stricter threshold of FR of 20 min^{-1}, the algorithm focuses on jumps which seem more relevant, as illustrated in the bottom graph.

3.5.4 Synthesis

First subjective analysis of cases study using Meteorage network has confirmed a good correlation between hail events and previous lightning jump (LJ) diagnosis in RDT-CW cells.

A wider monitoring of real-time LJ diagnosis at different periods with various couples of geostationary satellites and lightning networks (MSG-Meteorage, MSG-IODC/GLD360, GOES16/GLM) has pointed out an excessive number of diagnosis.

A look on 1 minute FR time series has confirmed this issue in the default configuration, and lead to double the FR threshold. This has been adopted for this release.

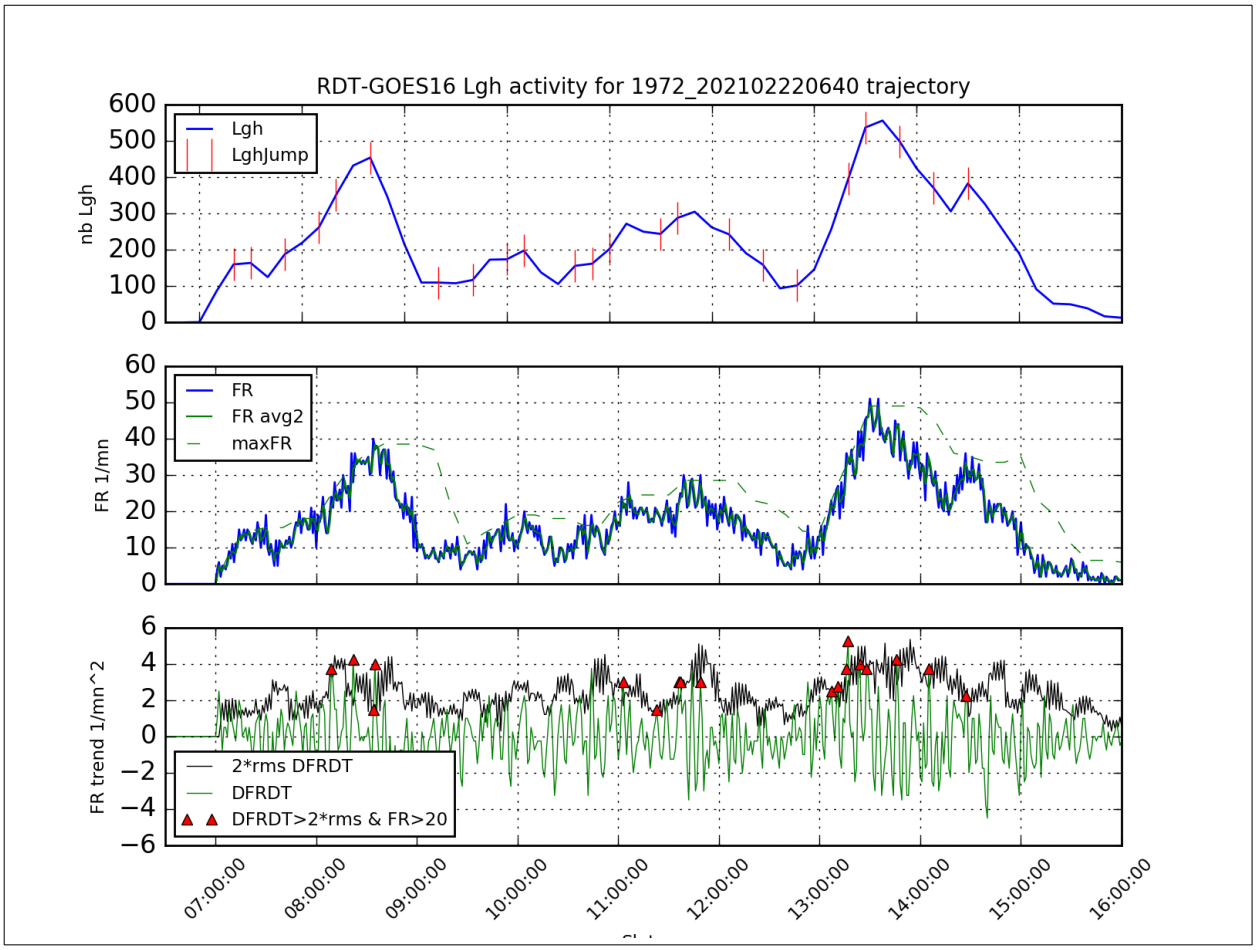

Figure 63: 20210222 case study with GOES16. [06h30-16h00Z] Time series of GLM-flashes paired with RDT-CW cell over Bolivia. Top: 10 minute flash count and diagnosed LJ with FR>10 (red bars). Middle: 1 minute FR and 2 minutes-average FR. Bottom: LJ algorithm parameters, and "corrected" LJ (red triangles) taking into account new threshold FR>20.

3.6 FORECAST OF CLOUD SYSTEMS

RDT-CW software provides the user the possibility to forecast cloud cell position using the diagnosed movement speed of the cloud cell.

Extrapolated cloud cells positions are obtained through Lagrangian forecast, i.e. the whole object is moved according to direction/speed of the diagnosed movement.

Consequently, quality of this extrapolation relies highly on the quality of movement diagnosis. The use of a pre-initialized guess of movement field from blending NWP wind data and HRW, and a final-step coherence checking has allowed to filter erratic speed and/or direction due to split/merge or to threshold temperature changes. Thus, confidence is Lagrangian extrapolation has become much higher, as illustrated in figure below.

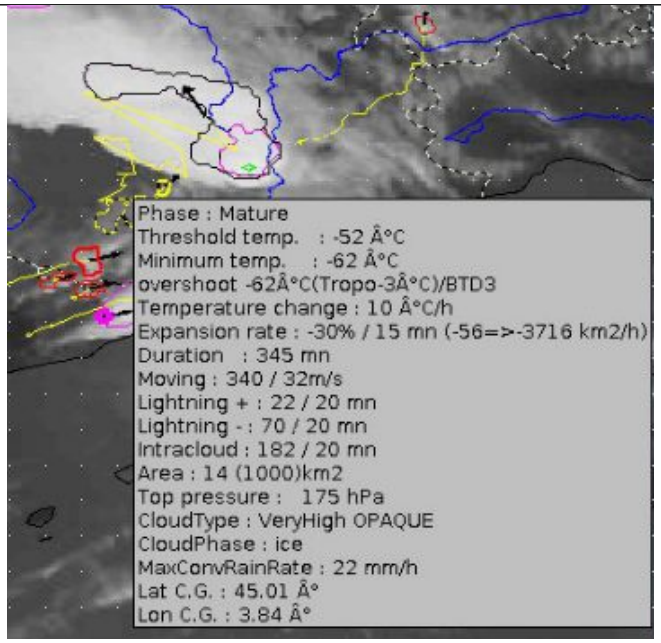

V2013 : erratic speed and direction following numerous splits/merges along trajectory

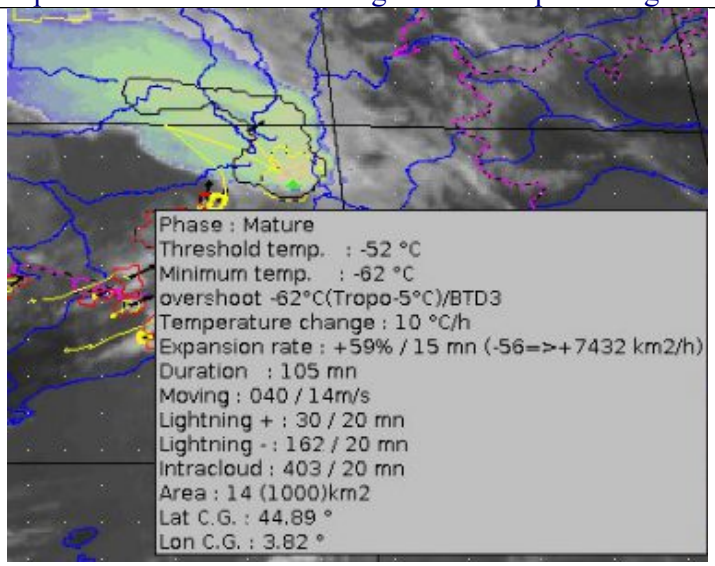

V2016 : coherent speed and direction despite numerous splits/merges along trajectory

Figure 64: v2013 vs v2016 illustration of RDT motion vectors improvement

Concerning forecast positions, it must be reminded that a cloud cell definition/contour corresponds to a given threshold temperature, and that this threshold changes dynamically/automatically from one slot to the other. ***A forecast contour remains based on the same temperature threshold than the observed/analysed object***. It will consequently be very difficult to assess the position of a forecast contour when compared to the following corresponding observed contours, because it is likely that those contours will not correspond to the same threshold temperature. Moreover, the longer the forecast ranges, the less precise the localization of forecast convective object is.

Assessment of forecast products position should ideally take into account for each cloud cell the stage of development, the morphological evolution or the expansion rate. Forecast cloud cell position can consequently only subjectively be regarded.

The objective validation of the forecast part has been carried out in a scientific report in 2018 [RD.2.], some of the results are still available for this version. Around 20% of cells are new at each

slot of MSG (15' scan) over Europe. Since the forecast scheme doesn't see these new cells, it gives the ratio of misses at step +15'. The ratio of false detection is also around 20%. Concerning the error on gravity centre position, the error value of 50 km is reached after the forecast range of 60 minutes.

Trends attributes of observed cloud cells are used to give indication of possible values changes of some parameters in the first forecast ranges (trend's values used for 15min range, half values for 30min). Here again those values can only be regarded as estimation and not pure forecast:

- Temperature change of coldest part of the cell (up to tropopause temperature limit if this value is available thanks to NWP data) and severity
- lightning trend for lightning activity and severity
- Top pressure trend for top pressure estimation
- Expansion rate for amplification or limitation of contour dilatation

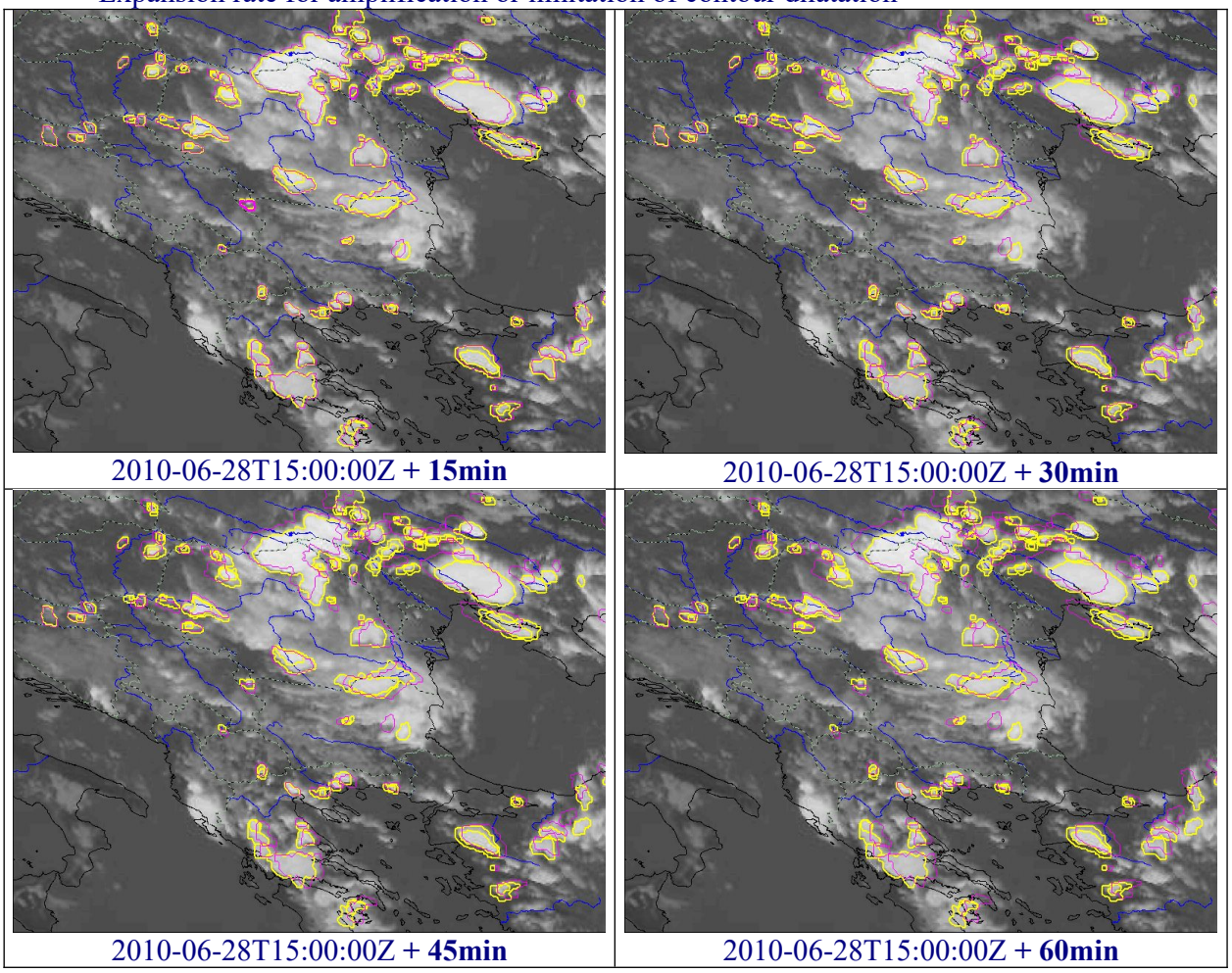

Figure 65: RDT-CW v2016 advection products (forecast contours in Magenta) from slot 2010-06-28T15:00:00Z (Observed contours in yellow).

Figure above displays forecast products (magenta contours) issued from a given slot 1500Z on the 28-06-2010. Yellow contours are observed at 1500Z. One can note very few overlap between forecast cells at various ranges, which assess a good spatial coherence of the movement speed of each cloud system.

The cyclonic movement field is very well taken into account with the forecast cloud systems.

This forecast set has been produced without smoothing neither dilation of the contours.

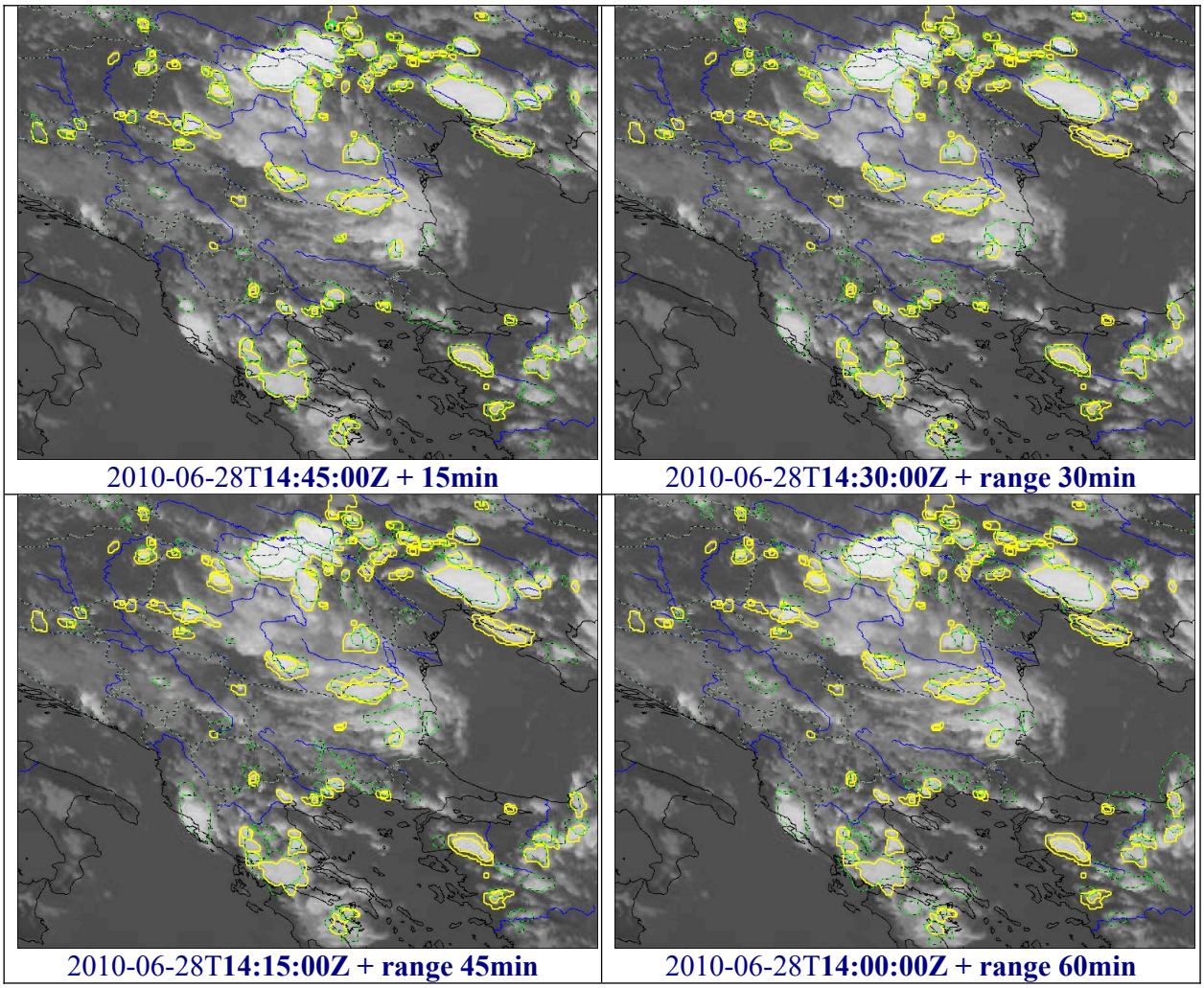

Figure 66: RDT-CW v2016 advection products (green forecast contours) from previous slots valid for slot 2010-06-28T15:00:00Z (yellow observed contours).

Figure above displays forecast products (green contours) valid for a same slot 1500Z on the 28-06-2010. Yellow contours are observed at 1500Z. The first ranges (15 and 30min) show a pretty good correspondence between previous forecast and current observation. For larger ranges, mainly large cloud systems, with longer duration, find a correspondence in the observed set.

One can note that some forecast green contours are no more valid in the analysed set, probably after declassification of the cloud system (no observed yellow contour).

On the other hand, some new cloud cells (yellow contours) appear only on the analysed set, and can not be anticipated from the previous slots.

3.7 MSG/MTG CONTINUITY, ADDITIONAL CASES AND MAIN CONCLUSION

3.7.1 20250421 over Italy

Scores are discussed in section 3.3.2.4. The objective of the chapter is to propose a visual comparison of both products. Next figure (Figure 67) illustrates that RDT operated with MTG/FCI or MSG/SEVIRI have very comparable output for one of the first 2025 deep convection case over Europe: outlines, motion vectors. There are no isolated flashes. Few warm systems aren't detected by

RDT with MTG/FCI and it will be the objective of the fine tuning of Day-2 approach to solve this issue.

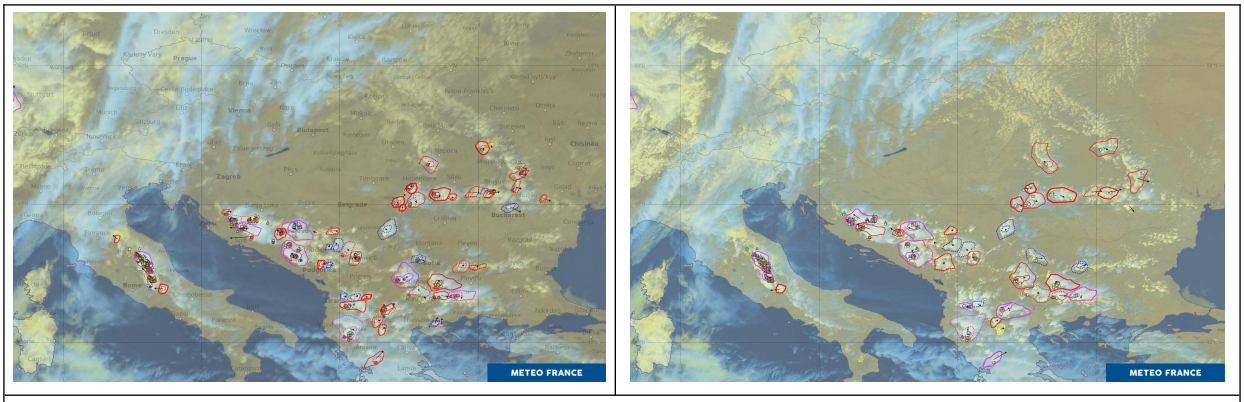

Figure 67: RDT operated with MSG/SEVIRI (left) and MTG/FCI (right) over Italy (20250421 at 1300). Style of outlines style depends of life-phase of the cell. Overlay: General RGB image, METEORAGE and LI flashes

3.7.2 20250429 over the full disk

RDT-CW can also be used as a large-scale convection monitoring tool. The figure hereafter [Figure 68] exhibits the good correspondence between a RDT operated with FCI and the one operated with SEVIRI : ZCIT, convection in the Southern part of Africa, convection associated to low pressure in South-Atlantic, frontal convection in North Atlantic, diurnal convection France/Italy, etc.

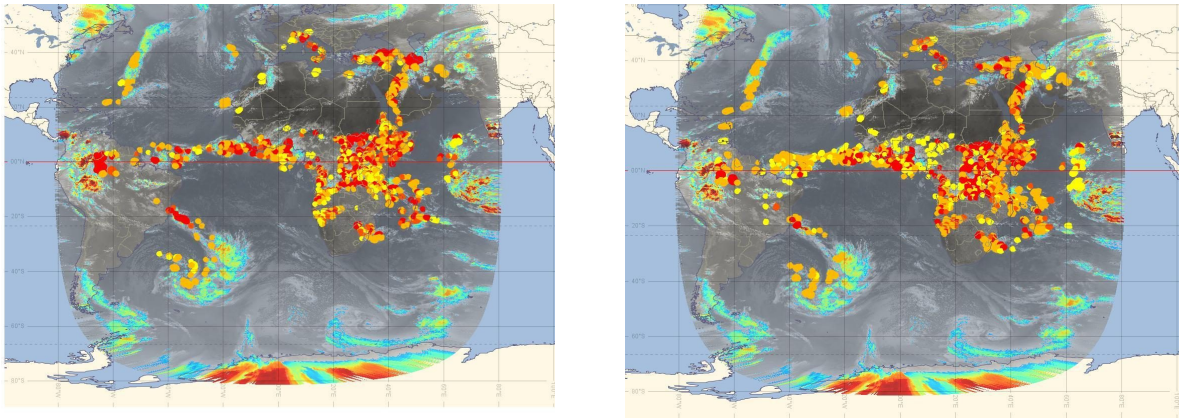

Figure 68: RDT operated with MSG/SEVIRI (left) and MTG/FCI (right) over Full-disk except Northern part (20250429 at 1230). Style of outlines style depends of severity of the cell. Overlay: thresholded 10.5 MTG channel. Outline size at a very large value

3.7.3 Conclusion about MSG/MTG continuity

Previous studies (sections 3.3.2.4, 3.7.1, 3.7.2) illustrate the good behaviour of RDT product operated with FCI compared to SEVIRI rearding detection and description of convective cells: visual continuity, higher detection. LI instrument is taken into account providing high POD of detection of electric systems and offer a complete description of convection especially over Africa. Warm systems detection (before lightning activity) is kept.

Regarding the FAR scores are correct but one can note that FAR is higher for RDT operated with MTG/FCI compared to RDT operated with MSG/SEVIRI. RDT operated with SEVIRI takes benefit

of many years of tuning while RDT operated with FCI use for the moment the tuning ogf GOES-16, another satellite of the 3rd generation. Day-2 mitigation will concern a fine tuning of RDT-CW using LI.

Regarding overshooting top detection, a attribute that impacts the severity synthesis attribute, chapter 3.4.2.6 describes the under-detection by RDT process operated with FCI data. Mitigations concern a possible improvement of input data and a revisit of the algorithm following the study [RD 15].

3.8 END-USERS FEEDBACKS

RDT, a very satisfying product widely used for Research and Operations, by Météo-France and its partners.

The use of RDT concerns for example

- Forecasters of Météo-France, in France and overseas territories (La Réunion, Antilles, Polynésie, Wallis et Futuna, Nouvelle Calédonie). RDT provides a significant help for regions not covered by radars.
- HAIC project and successive experiments (2014 and 2016 Australia, 2015 French Guyana, 2016 Darwin/La Réunion)
- RDT provided to airlines through EFB (Electronic Flight Bag)
- SESAR project and TOPMET/TOPLINK experiments
- Hymex project
- 2006 AMMA experiments (http://aoc.amma-international.org/observation/mcstracking/)
- European FlySafe Project with RDT software adapted to radar data
- NOAA for a RDT GOES (Operation + Research)
- From 2008, 2010 and 2015 Surveys distributed to SAF/NWC users, it appeared that RDT is mainly used for Research activities and operations for forecasting. New categories in 2024 survey illustrate the versatile characteristics of RDT for monitoring/warning, forecasting, research. 57,6% of the users (2024 survey) use RDT repeatedly. The judgement of usefulness of the product very satisfying (rate of 8,8/10)

Several feedback have been received during NWCSAF users' workshop in February 2025. The study by ARPA [RD.13] illustrates the benefit of RDT: "for the analysed cases, RDT-CW […] shows a good capability to […] identify […] formation before [...] lightning data are able to detect them"

RDT produced by Météo-France is downloaded by ACMAD and some African countries can visualize real-time RDT through ACMAD website (www.acmad.net).

RDT is operated by SAWS, hereafter two feedbacks

- De Coning, E., Strydom, J., Powell, C. , Gijben, M., de Beer, A., 2016, Nowcasting for aviation purposes in South Africa – a case study: Part1 – Satellite and radar based tools, WSN16 Hong-Kong, 25-29/7/2016

  "[the RDT] has provided good validation against lightning occurrence and radar reflectivities of more than 35 dBZ over South Africa"

- De Coning, E.,Gijben, M., 2017, Using Satellite and Lightning Data to Track Rapidly Developing Thunderstorms in Data Sparse Regions, Atmosphere 2017, 8 (4), 67;doi:10.3390/atmos8040067

> "The outcomes of this study are very encouraging for other countries in Africa where convection and severe convection often occur and sophisticated data sources are absent. Initial studies over East Africa indicate that the RDT product can benefit operational practices for the nowcasting of severe convection events."

RDT produced by SAWS is now available on WMO RSMC (*Regional Specialised Meteorological Center*) of Pretoria. Sixteen African countries of SWDFP (*Severe Weather Forecasting Demonstration Project*) from southern part of African continent can visualize real-time RDT.

A ESSL workshop [RD.16] exhibits in the conclusions that RDT-CW "behaves well to detect and track rapidly developing thunderstorms in the first stages of development". Limitations concern the tracking of severe systems and the jumpiness effect. This point has been imporved by developpers after the workshop.

3.9 CONCLUSION AND COMPLIANCE REQUIREMENTS

From a subjective point of view, the use of NWP data with RDT has allowed an improving gap of the discrimination efficiency. False alarms are lowered thanks to a "NWP convective mask" used as a guidance for the diagnosis, and precocity is increased with early diagnosis in warmest categories, thanks to a new tuning with NWP data and mask. The objective validation of GEN scheme over a wide region thanks to EUCLID data detailed in a previous report has confirmed this first analysis. It had been undertaken through various approaches from time step cell to the full life cycle of a cloud system, and taking into account the limitations of the ground truth. With a moderate ground truth (defined by 5 flash impacts at least during a trajectory) and non convective trajectories defined by being away from flashes of more than about 200km, satisfying skills are reached for full-trajectory approach: POD of 74% together with 2% POFD, FAR 22% and a TS of 61%. Scores are even better when considering sections of trajectories or cloud cells individually. RDT keeps good performances when taking into account intermediate season period (Spring, Autumn). Of course RDT scores are better for summer. Moreover, the skills obtained with EUCLID data over Europe are better in all configurations and for all approaches than for the previous validation. This improvement does not appear so clearly concerning the precocity of RDT GEN discrimination. It is limited to systems which are able to be early discriminated, i.e. with isolated convective system depicted from low levels. **Finally, those results fulfil the target accuracy requirements (see 1.2) over a large domain and for an extended period, i.e. 70% of detection and 25% of convective systems diagnosed before lightning activity.**

RDT-CW Calibration discrimination scheme implemented for several geostationary satellites has been tuned again for this release, over several months, taking also advantage of a stricter filter thanks to NWP data, and availability of reliable lightning data for operational runs (Meteorage network, but also GLD360 and GLM-GOES16).

Subjective cases studies have illustrated the improvement, and objective scoreshave met those from generic scheme. Moreover, those improvements are applicable to various geographical regions, and most of geostationary satellites.

We consider nevertheless that there is still room to improve the false alarms, the number of miss cases and the early diagnosis. Also, improvements remain necessary over oceanic regions, where the signature of convective systems differ from continental regions.

RDT provides an accurate depiction of convective phenomena, from triggering phase to mature stage. The RDT object allows pointing out some areas of interest of a satellite image. It provides relevant information on triggering and development clouds and on mature systems. Even if the precocity on the first lightning occurrence remains to be improved, the subjective evaluation confirmed the precocity usefulness on moderate lightning activity.

Those good results consolidate the status of RDT which had been set up to “operational” by EUMETSAT (since v2011).

Subjective validation exhibits very good results of the algorithm concerning OTD. It is a major point to improve RDT by focusing on the areas of the most severe and intense convection. This is not fully confirmed by an objective validation versus the CMHI overshooting top database made available by a Convection Working Group. Against this expert-based approach in a super rapid-scan context (2,5 minutes), RDT-CW OTD reveals as expected numerous misses, but also lower detection efficiency, and significant false alarms. A deeper use of high resolution will be necessary to improve this point.

Despite this, depending on cloud system morphology, RDT is able to present a kind of multidimensional description of convective systems.

The lightning jump algorithm, implemented in previous release, has been compared to hail and hazards detection systems on some situations. A good correlation between those events and lightning jump detection has been observed. An operational monitoring of this attribute has then led to a tightening of the criteria to limit an excessive number of diagnosis. An objective assessment is foreseen in a next scientific report.

It completes the data fusion approach with other products of NWCSAF.

4 CONCLUSION

CI and RDT-CW help to follow convection in different stage. There are compliant with MSG, MTG, GOES- 16/17/19 and Himawari-8/9 satellites.

Although there have been no major changes to the CI for v2025, it still benefits from the previous v2021 improvements: more precise use of Cloud products (cloud type and cloud top micro-physics), stricter definition of the areas of pixels of interest, day-time and night-time tunings. Extensive work on objective validation and situations conducive to the use of the CI product have resulted in scores that meet the requirements. The use of CI in conjunction with RDT-CW offer to end-users reliable tools to assess various phases of convection.

RDT-CW is a mature product with several years of continuous development and improvement and several version operational. A new tuning of the calibrated discrimination scheme confirms the operational capability of RDT-CW to generate convection warning product from geostationary satellite data whatever the geographical region. Additionally the forecast scheme takes benefit from slight improvements in the movement estimation of cloud cells such that the nowcasting capabilities of the RDT-CW up to +1 hour can be made possible.